Progress in Materials Science 106 (2019) 100570

Contents lists available at ScienceDirect

Progress in Materials Science

journal homepage: www.elsevier.com/locate/pmatsci

Flexoelectricity in solids: Progress, challenges, and perspectives

Bo Wang[a], Yijia Gu[a,b], Shujun Zhang[a,c], Long-Qing Chen[a,*]

[a] Department of Materials Science and Engineering, The Pennsylvania State University, University Park, PA 16802, USA
[b] Department of Materials Science and Engineering, Missouri University of Science and Technology, Rolla, MO 65409, USA
[c] Institute for Superconducting and Electronic Materials, Australian Institute of Innovative Materials, University of Wollongong, NSW 2500, Australia

ARTICLE INFO

Keywords:
Flexoelectricity
Ferroelectricity
Piezoelectricity

ABSTRACT

The flexoelectricity describes the contribution of the linear couplings between the electric polarization and strain gradient and between polarization gradient and strain to the thermodynamics of a solid and represents the amount of polarization change of a solid arising from a strain gradient. Although the magnitude of the flexoelectric effect is generally small, its contribution to the overall thermodynamics of a solid may become significant or even dominant at the nanometer scale. Recent experimental and computational efforts have led to significant advances in our understanding of the flexoelectric effect and its exploration of potential applications in devices such as sensors, actuators, energy harvesters, and nanoelectronics. Here we review the theoretical development and experimental progress in flexoelectricity including the types of materials systems that have been explored and their potential applications. We discuss the challenges in the experimental measurements and density functional theory computations of the flexoelectric coefficients including understanding the order of magnitude discrepancies between existing experimentally measured and computed values. Finally, we offer a perspective on the future directions for research on flexoelectricity.

1. Introduction

An important family of functional materials, the ferroelectrics, have been widely utilized in actuators, sensors, memory storage, electro-optics, microelectromechanical systems (MEMS), and others. The multifunctionality of a ferroelectric derives from the couplings among internal order parameters, such as ferroelectric polarization and spontaneous strain, and external thermodynamic variables, such as temperature, stress, and electric fields. Although the thermodynamics of such couplings has been well established at the macro-scale for homogeneous systems, the electromechanical coupling at the nano-scale for inhomogeneous systems, e.g., the flexoelectric effect, is much less well-understood.

The flexoelectric effect, or flexoelectricity, describes the coupling between the gradient of a mechanical strain and the electric polarization. Together with the well-established piezoelectricity, the dependence of the induced electric polarization upon mechanical deformation of a solid can be phenomenologically written as

$$P_i = e_{ijk}\varepsilon_{jk} + \mu_{ijkl}\frac{\partial \varepsilon_{kl}}{\partial x_j} \tag{1.1}$$

where P_i is the electric polarization component, ε_{jk} is the strain component, e_{ijk} the third-rank piezoelectric tensor, and μ_{ijkl} the fourth-rank flexoelectric tensor (flexoelectric coefficient), all defined under a zero-macroscopic electric field condition. The first term on the

* Corresponding author.
E-mail address: lqc3@psu.edu (L.-Q. Chen).

https://doi.org/10.1016/j.pmatsci.2019.05.003
Received 9 September 2018; Received in revised form 8 May 2019; Accepted 18 May 2019
Available online 31 May 2019

right-hand side of Eq. (1.1) describes the piezoelectric effect, i.e., the linear response of polarization to a homogeneous applied strain. The second term is the flexoelectric contribution to polarization from an inhomogeneous strain, i.e., the strain gradient. In this review, the Einstein summation convention is assumed with repeating indices *i*, *j*, *k*, and *l* in a term indicating summation from 1 to 3.

Although flexoelectricity is also a type of electromechanical coupling, it is not simply a higher-order extension of piezoelectricity. For example, the flexoelectric coefficient is a fourth-rank tensor, and hence in principle, it exists in all insulating materials while piezoelectricity is limited to non-centrosymmetric materials. Furthermore, as a strain gradient is inversely proportional to the spatial scale, the flexoelectric effect is size-dependent; it is small at the macro-scale, usually on the magnitude of 10^{-9} C/m^2 in terms of flexoelectric polarization and becomes increasingly prominent as the system size diminishes.

The recent interest in the flexoelectric effect in dielectric materials is partly driven by the device miniaturization and the use of nanotechnologies in which the size-dependent flexoelectric effect may play an increasingly critical role. The present review is focused on flexoelectricity in solids whereas the terminology *flexoelectric effect* is also used in areas of liquid crystals [1,2] and biological membranes [3,4]. There are several existing review articles on solid-state flexoelectricity from a number of different perspectives, including general overviews of flexoelectric effect in solids [5–7], in 2-D materials [8], and at nanoscale [9,10], fundamental physics [11], experimental progress [12,13], comparison between soft and hard materials [14], development of the first-principles theory [15], thermodynamics [16], applications [17,18], etc. Very recently, a compendium devoted to flexoelectricity in solids has also be published [19]. The present review will focus on several more recent discoveries and progress in both theory and experiments as well as a number of remaining confusions and controversies associated with the basic concepts and fundamentals of flexoelectricity in solids.

We first present the progress in the theory of flexoelectricity of solids and in the computational modeling efforts to understand the flexoelectric phenomenon at different length and time scales. Then, we survey on the experimental measurements and computational techniques of flexoelectric effects and summarize the flexoelectric coefficients of a variety of ceramics and single crystals obtained from both experiments and calculations. The common experimental methods for flexoelectricity measurement are compared. The fourth section is on the manifestation of flexoelectric effect in a number of systems, leading to modification of physical properties, new switching mechanisms, novel interfacial structures, exotic transport phenomena, etc. Section 5 is dedicated to the challenges and controversies in the study of flexoelectricity, including the ambiguities and subtleties in the definitions of flexoelectric phenomena, flexoelectric tensors, and flexoelectric fields. Especially, the discrepancies among the flexoelectric coefficients obtained from experiments and theories and among different calculation results are discussed, and the possible reasons are summarized. Section 6 presents a brief account of the emerging trends, as well as the typical flexoelectric structures, flexoelectric composites, and the applications of flexoelectricity. The review will conclude with a summary and a perspective of the flexoelectric research.

2. Progress in theories and modeling of flexoelectricity

This section provides an overview of the macroscopic and microscopic theories of solid-state flexoelectricity as well as the corresponding numerical modeling methods. We will first survey on the history and development of the theoretical aspects of flexoelectricity, followed by the macroscopic and microscopic descriptions. Numerical modeling of flexoelectric-related phenomena based on these theoretical groundworks utilizing finite element methods, phase-field simulations, and atomistic approaches will be reviewed. The theoretical evaluation of flexoelectric coefficients and possible subtleties and controversies involved in the theoretical description of flexoelectricity are deferred into Section 4 and 5, respectively.

2.1. Development of flexoelectricity theories

The earliest theoretical description of flexoelectricity in solids could be dated back to 1960s in the study of lattice dynamics [20–23], electron-phonon interactions [24], and anomalous electromechanical effects [25] in centrosymmetric ionic crystals. Initially, there was no consensus in the definition of this higher-order electrochemical coupling effect, and the direct (strain gradient induced polarization) and converse responses (field induced bending) were treated separately. It was only after more than a decade later that Indenbom et al. [26,27] firstly borrowed the terminology “flexoelectricity” from the liquid crystals community where a similar phenomenon had been more comprehensively investigated [1]. Systematic theoretical treatments on the solid-state flexoelectricity appeared in the 1980s, represented by Tagantsev’s formulation of the phenomenological and microscopic descriptions of flexoelectricity in crystalline dielectrics [28–30]. The author distinguished the flexoelectric effect from the piezoelectric effect, identified four different contributions to flexoelectric responses, and suggested the significance of flexoelectricity at the nanoscale especially in high-κ materials such as ferroelectrics. However, for a long period after that, there were limited interests in the solid-state flexoelectricity, among which only a few were relevant to ferroelectric materials [31–33]. The situation changed when the series of experiments led by Ma and Cross reported unexpectedly high flexoelectric responses in a variety of perovskite ceramics at the beginning of the 2000s [34–39]. These experimental findings, in turn, rejuvenated theoretical research on flexoelectricity, particularly in establishing a state-of-the-art first-principles framework and advancing the continuum mechanics description. To depict a big picture, we illustrate the milestones in the development of flexoelectricity theories chronologically in Fig. 2.1.

The theories of solid-state flexoelectricity include the macroscopic theory based on the continuum medium assumption and the microscopic theory accounting for the discrete nature of materials. The macroscopic theory, or the phenomenological theory of flexoelectricity within the condensed-matter community, is based on the thermodynamics of a dielectric by introducing a flexoelectric contribution into the total free energy to interpret the electric polarization induced by bending a non-piezoelectric [28,29]. The dynamic flexoelectric coupling can also be included into the kinetic energy to account for the polarization wave induced by a

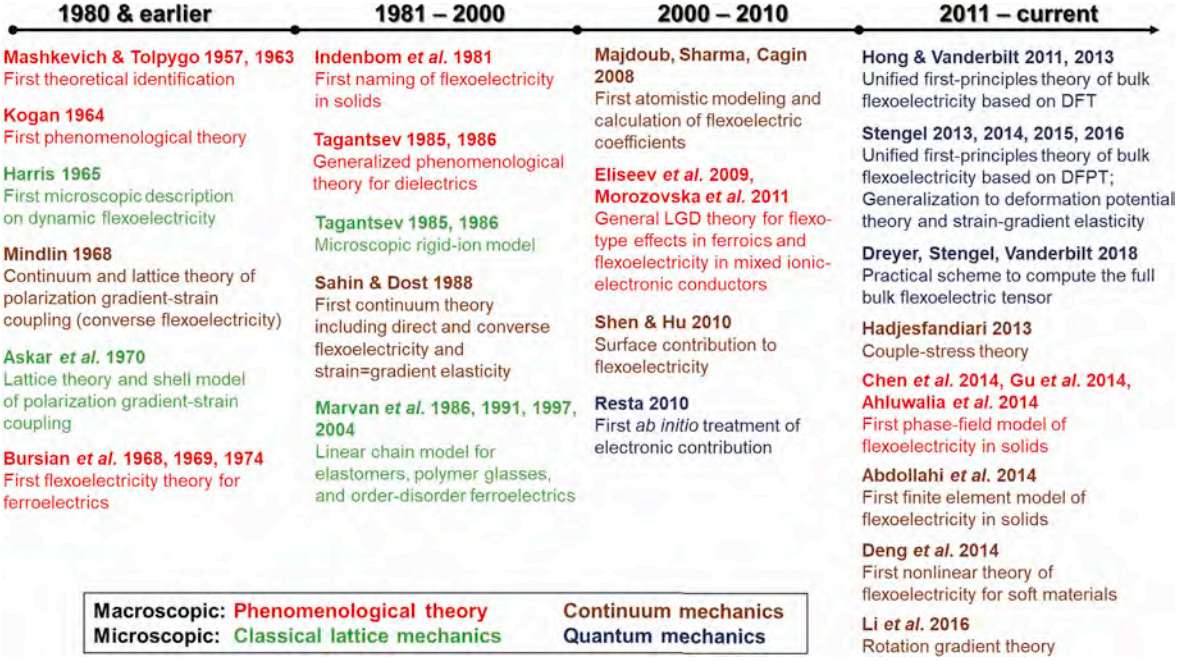

Fig. 2.1. Timeline and milestone achievements in the development of macroscopic and microscopic theories of flexoelectricity in solids. Abbreviations: Landau-Ginzburg-Devonshire (LGD), density functional theory (DFT), density functional perturbation theory (DFPT).

propagating acoustic wave [28,29]. Combined with the Landau-Ginzburg-Devonshire (LGD) theory of ferroelectrics, the phenomenological flexoelectricity theory is remarkably powerful for studying the impact of flexoelectric coupling on the static and dynamic behaviors of ferroelectrics and related materials. Recent advancement in this direction includes developing the theory for generalized flexo-type couplings [40,41], improving surface and dynamic flexoelectric contributions [42,43], and combining electrochemistry and semiconductor theories [44] to account for flexoelectric-mediated behaviors in more complex systems. In addition, the LGD-based theory is fundamental to the various numerical modeling of flexoelectric-related phenomena at a macroscopic scale, e.g., the phase-field method [45–47].

The similar macroscopic treatment on the flexoelectric effect is also recognized as the continuum theory of flexoelectricity in the mechanics community. It originates from Mindlin's seminal work on the polarization gradient-strain coupling in elastic dielectrics [22] which is known as the converse flexoelectric effect in nowadays' context. A full description of both direct and converse flexoelectric couplings was later documented by Sahin and Dost [48] to formalize the spatial and frequency dispersion effects in ferroelectrics. It was also in this work that the strain gradient-strain gradient coupling (strain gradient elasticity) and flexoelectric coupling were firstly treated in a unified continuum framework, the necessity of which has been recognized only recently [49–51]. However, the plethora of parameters used in Ref. [48] restricted its practical implementation; a modified version for isotropic dielectrics has been proposed by Maranganti et al. [52] to analytically solve continuum mechanics problems complicated by flexoelectricity. Recent advances in the continuum flexoelectricity theory are affected by the variants of gradient elasticity theory [53]. Reformulated formalism using strain-gradient theory [48,54], couple-stress theory [55,56], and rotation-gradient theory [57,58] have been promoted for more accurate and complete total energy functionals. Meanwhile, efforts towards a nonlinear flexoelectricity theory abandoning the infinitesimal strain assumption have been made [59,60], allowing for modeling the electromechanical behaviors in low-dimensional and flexural systems that can sustain large deformation. Notably, the continuum flexoelectricity theory also underpins the finite element analysis [61–63] and topology optimization [64–67], which are of critical importance in designing complex flexoelectric-based structures.

From a microscopic viewpoint, the contribution to a flexoelectric response comes from both atomic displacements and electronic charge density redistribution. Early microscopic theories of flexoelectricity tend to focus on the former, representing atoms as rigid ions with fixed point charges [29] or as polarizable core-shell pairs [68]. The first attempt toward a microscopic description of flexoelectricity was attributed to Askar et al. [68] who utilized a core-shell model, and a lattice dynamics approach to quantify the macroscopic parameters introduced by Mindlin in the polarization gradient theory of elastic dielectrics [22]. Later, Tagantsev adopted the rigid-ion approximation and established the relationship between flexoelectric responses and nonuniform atomic displacements through a longwave method [28,29]. In this context, the phenomenological flexoelectric coefficient can be expressed in terms of microscopic quantities such as dynamic matrices and effective Born charges. A comparative revisit of the core-shell and rigid-ion models of flexoelectricity has recently been given by Marangantti and Sharma [69]. In addition to lattice dynamics models, there were also simple linear chain models stemming from the study of flexoelectricity in non-crystalline polymers [70] and elastomers [71]. This linear chain model has later been extended to account for flexoelectric effects in dielectrics [72] and order-disorder ferroelectrics [73]. More recently, a 2D chain model has been proposed to examine the higher-order flexoelectric couplings [74].

The classical microscopic theories mentioned above primarily focus on the lattice aspect of flexoelectric effects. Consequently, the electronic contribution was either explicitly neglected or empirically addressed (i.e., through core-shell model) despite its critical importance. The first formal attempt toward the electronic contribution of flexoelectric response was given by Resta [75] who, inspired by Martin's quantum mechanics theory on piezoelectricity [76], examined the electronic flexoelectricity in the simple cubic lattice and questioned the conclusions drawn from classical rigid-ion models [29]. The electronic flexoelectricity in general dielectrics has later been addressed by Hong and Vanderbilt [77]. Recently, a unified first-principles theory of flexoelectricity in insulating crystalline with both ionic and electronic contributions has been formulated in the context of density-functional theory by Hong and Vanderbilt [15] and, independently, in the framework of density-functional perturbation theory by Stengel [78]. On this basis, Stengel further clarified the surface effect in flexoelectric behaviors [79] and revealed the close relations between the flexoelectric tensor and other materials physics such as absolute deformation potential [80] and strain gradient elasticity [50], all under a rigorous quantum mechanical ground. Very recently, a practical scheme to calculate the full flexoelectric tensor using a unit cell-based method built on density functional perturbation theory has been demonstrated by Dreyer, Stengel, and Vanderbilt [81].

The microscopic theory of flexoelectricity has greatly deepened the understanding of the atomic and electronic mechanisms of flexoelectric properties. Specifically, it helps establish a direct relationship between the phenomenologically induced flexoelectric parameters with the microscopically computable quantities, thereby offering a semi-empirical or *ab initio* routine for calculating the flexoelectric tensors of practical materials. The theoretical values of flexoelectric parameters can be further utilized to help eliminate other extrinsic effects in flexoelectric responses and verify the experimental measurements, to serve as inputs for higher-level numerical simulations of flexoelectric-related phenomena, and to design and screen new materials with desired flexoelectric properties through high-throughput computation and data mining techniques.

2.2. Macroscopic theories

In this subsection, we first outline the phenomenological theory of bulk static and dynamic flexoelectricity. The formulation will be framed within the LGD theory of ferroelectric materials, the applications of which to predicting and explaining flexoelectric-related behaviors in a variety of systems are reviewed. Then we summarize the general continuum mechanics theory of flexoelectricity by comparing with the phenomenological flexoelectricity theory and highlighting a few representative works. It should be noted that since these two branches of macroscopic flexoelectricity theories were independently developed in the solid-state physics and the mechanics community, they employ different terminology and expressions and have different foci. For comprehensiveness, we decide to present both of them separately in this subsection.

2.2.1. Phenomenological theory

To facilitate the discussion, we first outline here the phenomenological theory of bulk static and dynamic flexoelectricity. Notably, we formulate the thermodynamics within an LGD framework specifically for ferroelectrics since more comprehensive descriptions for general dielectrics have been exhaustively reviewed in many excellent existing articles [11,19,30]. Afterwards, the applications of the phenomenological theory to explaining and predicting flexoelectric behaviors and recent advances of the theory will be briefly reviewed.

2.2.1.1. Outline of the theory. The phenomenological thermodynamic theory of ferroelectrics, also known as Landau theory or LGD theory, lays the thermodynamic foundation for the study of ferroelectric phase transitions. According to LGD theory, the total free energy with the flexoelectric contribution can be written as a function of the spontaneous polarization P_i, strain ε_{ij}, and their spatial gradients, i.e.,

$$F = \int dV \left(\alpha_{ij} P_i P_j + \alpha_{ijkl} P_i P_j P_k P_l - q_{ijkl} \varepsilon_{ij} P_k P_l + \frac{1}{2} c_{ijkl} \varepsilon_{ij} \varepsilon_{kl} + \frac{1}{2} g_{ijkl} (P_{i,j} P_{k,l}) - P_i E_i - \frac{1}{2} \epsilon_0 \kappa_{ij}^b E_i E_j + \frac{1}{2} f_{ijkl} (P_{i,j} \varepsilon_{kl} - \varepsilon_{kl,j} P_i) \right) \tag{2.1}$$

where the α's are the Landau-Devonshire coefficients (expanded up to 4th-order for simplicity), c_{ijkl} is an elastic stiffness tensor component, q_{ijkl} is an electrostrictive tensor component, g_{ijkl} is a gradient energy coefficient of polarization, ϵ_0 is the dielectric permittivity of the vacuum, and κ_{ij}^b is the background dielectric constant. E_i is the total electric field related to the electrostatic potential ϕ via $E_i = -\phi_{,i}$. In the present paper, the comma in the subscript indicates spatial derivative, e.g., $(.)_{,i} = \partial(.)/\partial x_i$. The strain is symmetrically defined, i.e., $\varepsilon_{ij} = \frac{1}{2}(u_{i,j} + u_{j,i})$, where u_i is a mechanical displacement component. The flexoelectric contribution to the total free energy density is written as

$$f_{flexo} = \frac{1}{2} f_{ijkl} (P_{i,j} \varepsilon_{kl} - \varepsilon_{kl,j} P_i) \tag{2.2}$$

where f_{ijkl} is the so-called flexoelectric coupling tensor (flexocoupling tensor). This form of coupling term is also known as the Lifshitz invariant, which is allowed by symmetry [82].

With the total free energy functional (2.1), the equation of state is then obtained by variation in the free energy through $\frac{\delta F}{\delta P_i} = 0$ and $\frac{\delta F}{\delta \varepsilon_{ij}} = \sigma_{ij}$ where σ_{ij} is the mechanical stress. The former equation gives

$$\frac{\delta F}{\delta P_i} = 2\alpha_{ij} P_j + 4\alpha_{ijkl} P_j P_k P_l - 2q_{klij} \varepsilon_{kl} P_j - g_{ijkl} P_{k,jl} - f_{ijkl} \varepsilon_{kl,j} - E_i = 0 \tag{2.3}$$

By assuming linear dielectrics and keeping the first term in polarization, the change of polarization due to the flexoelectric coupling

and the applied electric field is

$$P_j = \epsilon_0 \chi_{ij} (E_i^f + E_i) \tag{2.4}$$

where $\chi_{ij} = (\alpha_{ij} - q_{ijkl}\varepsilon_{kl})^{-1}/2$ is the dielectric susceptibility, and E_i^f is the flexoelectric field

$$E_i^f = f_{ijkl}\varepsilon_{kl,j} \tag{2.5}$$

Thus, the net effect from the flexoelectric coupling is equivalent to the presence of an additional *electric field*, which can asymmetrically change the free energy profile of a dielectric in analogy to an electric field. Assuming zero external electric field, one can recover from (2.4) the phenomenological definition of the flexoelectric-induced polarization in (1.1). Hence, the flexoelectric tensor and the flexocoupling tensor are connected by

$$\mu_{ijkl}^E = \epsilon_0 \chi_{im} f_{mjkl} \tag{2.6}$$

where superscript E stands for the fixed electric field boundary condition. The latter equation of state gives the generalized Hooke's law, i.e.,

$$\frac{\delta F}{\delta \varepsilon_{ij}} = \sigma_{ij} = \frac{1}{2} c_{ijkl}\varepsilon_{kl} - q_{ijkl} P_k P_l + f_{klij} P_{k,l} \tag{2.7}$$

From (2.7) one can identify that an inhomogeneous polarization generates additional mechanical stress, i.e., the converse flexoelectric effect.

The above two equations of states (2.3) and (2.7) are solved in combination with the mechanical equilibrium equation (assuming no body forces),

$$\sigma_{ij,k} = 0 \tag{2.8}$$

and the Poisson equation for electrostatic equilibrium (assuming no free charge carriers),

$$\epsilon_0 \kappa_{ij}^b \phi_{,ij} = P_{i,i} \tag{2.9}$$

where ϕ stands for the electrostatic potential related to the electrical field. By solving the coupled equations (2.3), (2.7)–(2.9) with appropriate boundary conditions, one can determine the equilibrium state of a ferroelectric.

Flexoelectricity can also influence the dynamical behaviors of a dielectric, e.g., the soft-mode phonon dispersion, through a different mechanism known as the dynamic flexoelectric effect [28,29]. The dynamic flexoelectricity describes the polarization response to the accelerated motion of the medium in the time domain [5,11]. In analogous to (1.1), the dynamic flexoelectric effect can be expressed as,

$$P_i = \mu_{ij}^{dyn} \frac{\partial^2 u_i}{\partial t^2} \tag{2.10}$$

where μ_{ij}^{dyn} is the second-rank tensor of dynamic flexoelectric effect and t is time. To consider this interaction within the phenomenological theory, one needs to introduce a cross-term between polarization P_i and displacement u_i time derivatives, $M_{ij}\frac{\partial P_i}{\partial t}\frac{\partial u_j}{\partial t}$, into the kinetic energy K, i.e.,

$$K = \int dV \left(L_{ij}\left(\frac{\partial P_i}{\partial t}\right)\left(\frac{\partial P_j}{\partial t}\right) + M_{ij}\frac{\partial P_i}{\partial t}\frac{\partial u_j}{\partial t} + \frac{\rho}{2}\left(\frac{\partial u_i}{\partial t}\right)^2 \right) \tag{2.11}$$

The tensor M_{ij} is the dynamic flexoelectric coefficient (flexodynamic coefficient [83]), L_{ij} is a kinetic coefficient related to polarization dynamics, and ρ is the density of the material. Together with the total free energy (2.1), one can readily write down the Lagrangian $\mathscr{L}$ of the ferroelectric through

$$\mathscr{L} = \int dt\,(F - K) \tag{2.12}$$

Then the equation of motion can be derived by using the Euler-Lagrange equation

$$\frac{d}{dt}\left(\frac{\partial \mathcal{L}}{\partial \dot{\boldsymbol{q}}}\right) - \frac{\partial \mathcal{L}}{\partial \boldsymbol{q}} = 0 \tag{2.13}$$

where generalized coordinate $\boldsymbol{q}$ represents the displacement u_i or polarization P_i, and $\dot{\boldsymbol{q}}$ represents their corresponding time derivatives. Similar to (2.6), one can obtain the relation between μ_{ij}^{dyn} and M_{ij} as

$$\mu_{ij}^{dyn} = \chi_{is} M_{sj} \tag{2.14}$$

By solving the equation of motions with proper initial and boundary conditions, one can obtain both the static and dynamic flexoelectric effects on dynamic behaviors of a system of interest.

2.2.1.2. Applications and progress of the theory. The LGD theory with a bulk flexoelectric contribution discussed above includes the static and dynamic interactions among polarization, strain/stress, and electric fields. Though simple in its formulation, the LGD theory of flexoelectricity can explain or predict a variety of phenomena where flexoelectricity is believed to play a role. For instance, based on a simple strain relaxation model for thin films, Catalan et al. [84,85] demonstrated that the flexoelectric effect is responsible for the smearing of the dielectric constant near the Curie temperature and the thickness dependence of coercive fields and remnant polarization. Similarly, the LGD theory has also suggested the flexoelectric effect is the primary cause of built-in electric field and resulting offset of the hysteresis loop in compositionally graded ferroelectric heterostructures [86,87].

Morozovska and Eliseev et al. have extensively explored the flexoelectric effect and its interactions with other electro-mechano-chemical couplings and structural order parameters using a phenomenological framework built upon the LGD theory [44]. They have predicted a list of phenomena directly induced or indirectly mediated by flexoelectricity, including the appearance of polarization and pyroelectricity in twin domain walls, surfaces [88], and antiphase boundaries (APBs) of ferroics [89], the high conductivity at nominally neutral domain walls [90,91], the disappearance of the critical size for ferroelectric transition in nanostructures [312], and the change in kinetic behaviors of polarization reversal.

The LGD theory considering the dynamic flexoelectric effect has also led to several exciting discoveries. For example, Kvasov and Tagantsev showed a viable routine to estimate the bulk flexoelectric tensor from the phonon spectrum obtained by experimental measurement or *ab initio* calculations [83]. Morozvoksta et al. explored the modification of flexoelectricity on the soft-mode phonon dispersion [42,92,93], generalized permittivity responses [42], and the emergence of spatially modulated structures [41] in bulk ferroics. Eliseev et al. [43] predicted the existence of shear surface acoustic wave in all crystalline dielectrics enabled by bulk static and dynamic flexoelectricity, which was formerly regarded as forbidden in nonpiezoelectrics with a homogeneous flat surface. Very recently, Deng et al. studied the dynamic flexoelectric effect in nanoscale flexoelectric energy harvesters [94]. They found that the dynamic effect can be comparable to the static flexoelectric effect due to the sharp increase in the natural fequencies from the miniaturization of a sample.

The flexoelectric effect in finite samples was explored by Tagantsev and Yurkov [95,96]. They showed that the surface piezoelectricity might contribute to the flexoelectric response in a comparable extent to bulk flexoelectricity. Tagantsev and Yurkov's prediction was supported by Narvaez et al. [97] who observed a large flexoelectric anisotropy by varying the orientation of $BaTiO_3$ single crystals, which is attributed to a significant surface effect. In the same work, Tagantsev and Yurkov also explained why the application of a uniform electric field across a capacitor structure could induce bending of the plate (the flexoelectric-bending effect) [95], thus resolving the long-term debate on whether a flexoelectric sensor can act as an actuator initiated by Cross [12].

Another direction in the phenomenological theory of flexoelectricity attempts to generalize it to other flexo-type coupling effects, including flexomagnetic [40,49], flexomagnetoelectric [98–100], and flexoantiferrodistortive [41,88] couplings. A brief review of the general flexo-type effects has been given by Eliseev et al. [41]. These exploratory studies expanded our understanding of gradient-enabled effects and laid the theoretical foundation for further harnessing the related nanoscale phenomenon.

2.2.2. Continuum mechanics of flexoelectricity

The flexoelectric effect is treated in a broader context known as the extension of the classic theory of elastic dielectric in the continuum mechanics community. Comparing to the phenomenological LGD theory, the continuum theory of flexoelectricity is complicated by higher order and nonlocal mechanical and electromechanical couplings in the internal energy, multiple definitions of deformation metrics, and subsequently more comprehensive governing equations and boundary conditions. It can also be seen as an extension of gradient elasticity theory by combining the continuum electrostatics and electrodynamics with nonlocal terms.

2.2.2.1. Outline of the theory. Here, following Maranganti et al. [52], we briefly summarize the key ingredients in the continuum mechanics of flexoelectricity, including internal energy, constitutive equations, and governing equations with boundary conditions. Consider an elastic dielectric occupying a domain V bounded by a surface S, which separates V from an outer vacuum V'. In the extended linear theory of dielectrics, the internal energy density U can be expressed in a similar formulation as (2.1), i.e.,

$$U = \frac{1}{2}\alpha_{ij}P_iP_j + \frac{1}{2}g_{ijkl}P_{i,j}P_{k,l} + \frac{1}{2}c_{ijkl}\varepsilon_{ij}\varepsilon_{kl} + f^{\mathrm{I}}_{ijkl}P_iu_{j,kl} + d_{ijkl}P_{i,j}\varepsilon_{kl} + \frac{1}{2}h_{ijklmn}u_{i,jk}u_{l,mn} \tag{2.15}$$

where f^{I}_{ijkl} is the flexocoupling coefficient defined by unsymmetrized strain (type-I flexocoupling coefficient, c.f. Section 5.1), d_{ijkl} the polarization gradient-strain coupling tensor introduced by Mindlin [54], h_{ijklmn} the strain gradient elasticity tensor, and all other quantities are defined in the previous subsection. The constitutive equations are derived through thermodynamic analysis as,

$$\sigma_{ijk} = \frac{\partial U}{\partial u_{i,jk}} \tag{2.16a}$$

$$\sigma_{ij} = \frac{\partial U}{\partial \varepsilon_{ij}} \tag{2.16b}$$

$$E_i = \frac{\partial U}{\partial P_i} \tag{2.16c}$$

$$E_{ij} = \frac{\partial U}{\partial P_{i,j}} \tag{2.16d}$$

where $\sigma_{ij}$is the same as the stress tensor in classical elasticity, E_i is the local electric field, and σ_{ijl} and E_{ij} can be understood as the higher order counterparts of σ_{ij} and E_i, respectively.

The governing equations (balancing laws) can be routinely deducted through Toupin's variational principle [101] with the aid of the constitutive relations obtained from (2.16). We omit the lengthy derivation (which can be found in Ref. [52,102]) and simply present the governing equations, i.e.,

$$(\sigma_{ij} - \sigma_{ijk,k})_{,j} + b_i = 0 \tag{2.17a}$$

$$E_{ij,j} + E_i - \phi_{,i} + E_i^0 = 0 \tag{2.17b}$$

$$-\varepsilon_0 \phi_{,ii} + P_{i,i} = 0 \text{ in } V \tag{2.17c}$$

$$\phi_{,ii} = 0 \text{ in } V' \tag{2.17d}$$

where $-\phi_{,i}$ is the Maxwell self-field, b_i and E_i^0 are the external body force and electrical field, respectively. The boundary conditions on S are given by,

$$n_i(\sigma_{ij} - \sigma_{ijk,k}) = t_j \tag{2.18a}$$

$$n_i E_{ij} = 0 \tag{2.18b}$$

$$n_i([\![\epsilon_0\ \phi_{,i}]\!] + P_i) = 0 \tag{2.18c}$$

where n_i is the surface normal unit vector, t_i the surface traction, and the symbol $[\![\ ]\!]$ denotes the difference of enclosed quantity on V and V'. The governing equation (2.17) under boundary conditions (2.18) in combination with the constitutive equations (2.16) complete the continuum theory of an flexoelectric dielectric.

2.2.2.2. Application and progress of the theory. The continuum theory outlined above is a simplified version of Sahin and Dost's seminal work [48] where several other nonlocal mechanical and electromechanical couplings and kinetic energy including polarization inertia effects were included. Furthermore, Shen and Hu [102] also proposed a more comprehensive continuum framework of flexoelectricity by taking account of the surface effect. Later, Majdoub et al. [103] expanded this *static* continuum theory by incorporating the kinetic energy and employing Hamilton's principle to obtain the equations of motion. However, these continuum theories of flexoelectricity usually contain a plethora of independent material coefficients, particularly due to the use of general strain gradient theory, which restricts its implementation to model practical materials. To simplify the flexoelectricity theory formulated by the general strain gradient theory, some authors [56,57] borrowed concepts from the rotation gradient theory, couple stress theory, and general gradient elasticity [53]. Assuming a small rotation, the rotation tensor and its dual vector can be written as,

$$\omega_{ij} = \frac{1}{2}(u_{i,j} - u_{j,i}) \tag{2.19a}$$

$$\omega_i = \frac{1}{2}\,\epsilon_{ijk}\,\omega_{kj} \tag{2.19b}$$

where $\epsilon_{ijk}$is the permutation tensor. The rotation tensor ω_{ij} contains 9 independent components, in contrast to the 18 components of strain gradient, largely reducing the degrees of freedom in the gradient elastic and flexoelectric terms of the energy functional [57]. Hajesfaniari developed the couple stress theory of flexoelectricity [56], which uses the antisymmetric part of the rotation gradient, i.e., $\kappa_{ij} = \frac{1}{2}(\omega_{ij} - \omega_{ji})$, as the deformation metrics, thereby further simplifying the formulation. A systematic formulation of the couple stress-based theory of linear flexoelectricity and its comparison with strain gradient-based models are documented in a recent article by Poya et al. [104].

Recent advances in the continuum flexoelectricity theory include several aspects. First, there are attempts to generalize the treatment of flexoelectricity to a broader continuum framework with multiple physical and chemical couplings. For example, Liu et al. proposed a general theory for magneto-electro-elastic continua which may be applied to various hard and soft functional materials [105]. Ebrahimi-Nejad et al. studied the static and dynamic mechanical behaviors of piezoelectric nanobeams under magneto-thermo-electro-mechanical loads [106]. Lecoutre et al., by utilizing the principle of virtual power, theorized the continuum mechanics of deformable semiconductors with inhomogeneous strain, polarization and magnetization gradients [107]. Another route is to develop the nonlinear theory of flexoelectricity for systems with large deformation [59,108,109] and where dissipation is naturally present [60,107]. Besides, efforts have also been made to explore flexoelectric coupling in dynamic behaviors where a separate dynamic flexoelectric effect may play a role, such as the wave propagation in piezoelectrics [110], band structure of phononic crystals [111], and vibration dynamics in energy harvesters [60].

The continuum theories of flexoelectricity discussed above have been applied to analyzing the static and dynamical behaviors of a variety of systems subjected to mechanical and electrochemical loads. For certain simple structures, the closed-form solutions can be obtained. For example, Maranganti et al. have derived the Green function solution of an embedded inclusion in flexoelectric materials [52]. Mao et al. [51] derived the governing equations for a flexoelectric solid under a small deformation and provided analytical solutions to several boundary value problems. Later, they applied the same method to studying the flexoelectric effect around material defects, including point defects, edge dislocations, and cracks [112]. Analytical solutions and mechanical analyses have also been reported in classical macro-structure models such as Euler-Bernoulli beams [113–117], Timoshenko beams [118], Kirchhoff

plates [119,120], etc. On the other hand, the developed continuum mechanics frameworks also enable numerical analysis of the electromechanical fields in more complex structures. In nanostructures where the size-effect from flexoelectricity becomes dominant, for instance, extensive works have been documented to study the static and dynamic actuating behaviors (e.g., bending, buckling, and vibration) and sensing properties of nanobeams [113,115,116,119–124], nanoplates [125–127], nanorings [128–131], and other complex structures (e.g., truncated pyramids [132], shells [133–135], composite multilayers [136–138], etc.). A systematic survey in this respect has recently been published by Yan and Jiang [139]. Additionally, there is growing interest in the topology optimization of flexoelectric structures [64,67,140]. These advanced analyses based on continuum mechanics of flexoelectricity allow for designing novel flexoelectric structures for versatile applications including curvature sensors, actuators, transducers, and energy harvesters.

2.3. Microscopic theories

The microscopic origin of flexoelectricity in a solid crystal comes from the redistribution of bound and/or free charges driven by a strain gradient [11]. Roughly speaking, the microscopic flexoelectric response can be separated into a purely electronic (frozen-ion) contribution and a lattice-mediated contribution [15]. The lattice contribution is associated with the atomic displacement induced by a strain gradient, which can be described by a lattice mechanics theory. The electronic part originates from the change of electronic structure and requires a quantum-mechanics treatment. The macroscopic approaches discussed in the previous subsection cannot appropriately address the two aspects. Therefore, the microscopic theory becomes critical in understanding the atomistic and electronic mechanisms of flexoelectricity. It also offers a viable way to quantifying the intrinsic flexoelectric coefficients, which can be used to validate experimental measurements, to provide flexoelectric parameters for higher-level modeling, and to potentially design new materials with ideal flexoelectric properties.

In this subsection, we heuristically classify the microscopic theories of flexoelectricity into the classical microscopic theory, which solely focuses on the lattice-mediated response using lattice mechanics approaches, and the first-principles theories, which explicitly address the lattice and electronic contributions on a quantum-mechanics ground. For each category, we briefly touch upon the key concepts and procedures used to construct the microscopic theory and summarize the primary conclusions. We attempt to compare different works to clarify their relations. Emphasis is then placed on the recent progress in the first-principles theory of flexoelectricity. Limited by the scope of this review, we presented many equations in this subsection without resorting to a rigorous formalism; especially, we intentionally omit the sub-/superscripts of some tensor quantities wherever possible. For detailed and rigorous derivations, readers are encouraged to read the original articles and several theoretical-oriented reviews [11,19].

2.3.1. Classical microscopic theories

There are majorly three types of classical microscopic theories that have been proposed to treat flexoelectricity in solids: the shell model proposed by Askar et al. [68] for general dielectrics, the rigid-ion model established by Tagantsev [28,29] for ionic crystals, and the linear chain model developed by Marvan and coworkers for polymers [70–72] and order-disorder ferroelectrics [73]. We will focus on the rigid-ion model in this section for its profound implication in the follow-up research of flexoelectricity.

The basic assumption of the rigid-ion model approximates a crystal as a set of lattices consisting of undeformable and unpolarizable ions with fixed point charges (point-charge approximation). In other words, it models an “ideal” ionic crystal. In this sense, the polarization can be readily determined from the atomic displacements and the effective point charges. The rest of the problem reduces to developing the relation between the atomic displacements and the strain gradients.

To fully evaluate a flexoelectric response, two scenarios are often considered: the static bending of a slab and the dynamic elastic wave propagating within an infinite crystal. In the static scheme, the flexoelectric response corresponds to the average polarization driven by a homogeneous strain gradient under zero macroscopic electric field, following the definition of flexoelectricity in (1.1). In the dynamic scenario, also known as the long-wavelength analysis [141], one concerns the amplitude of the polarization wave generated by the elastic wave. For a heuristic purpose, here we simply outline the former scenario to give a sense of some basic concepts in the microscopics of flexoelectricity.

Consider a finite-sized crystal subjected to a uniform strain gradient. In general, the displacement $\boldsymbol{w}$ of an isolated atom in the deformed crystal can be written as a combination of external and internal displacements, i.e.,

$$\boldsymbol{w} = \boldsymbol{w}^{ext} + \boldsymbol{w}^{int} \tag{2.20}$$

The external displacement describes the “ideal” atomic displacement due to the unsymmetrized strain $u_{i,j}$ under the elastic medium approximation, i.e.,

$$w_i^{ext} = \int_{x_j^0}^{R_j} u_{i,j} dx_j \tag{2.21}$$

where x_j^0 is an immobile reference point and R_j the positions of the isolated atoms before the deformation. In a centrosymmetric crystal subject to a homogeneous strain, the external displacements well capture the total atomic displacements, as shown in Fig. 2.2a. However, if the applied strain is non-uniform, or if the material is non-centrosymmetric, the real atomic displacements contain an additional term known as the internal displacement (internal strain by convention) [141]. To the lowest approximation, this internal displacement can be represented as linear functions of strains and strain gradients, i.e.,

$$w_i^{int} = \Gamma_{ijk}\varepsilon_{jk} + N_{ijkl}\varepsilon_{kl,j} \tag{2.22}$$

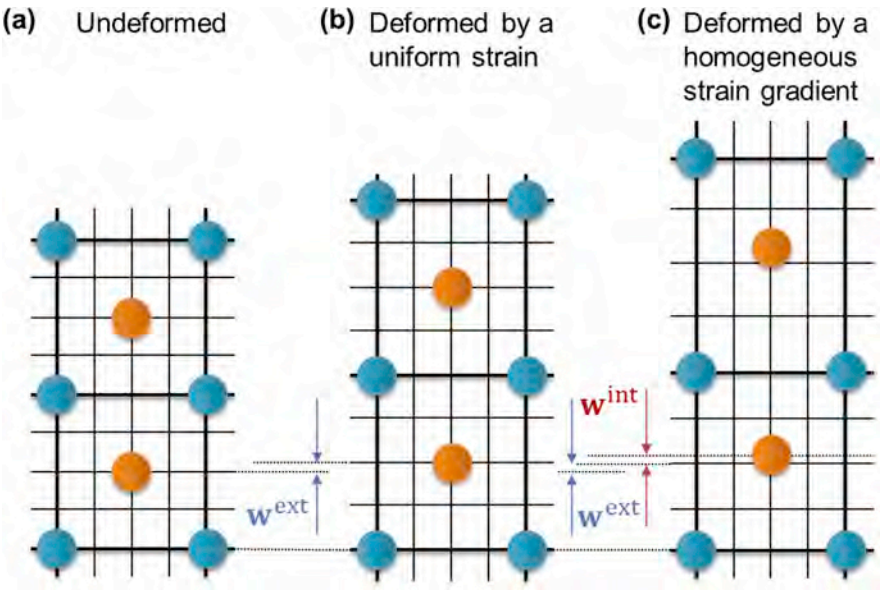

Fig. 2.2. Schematic of atomic displacements in two neighboring unit cells of a centrosymmetric crystal at pristine undeformed state (a), under a uniform macroscopic strain (b), and under a homogeneous strain gradient (c).

where $\boldsymbol{\Gamma}$ and $\mathbf{N}$ are the internal-strain tensors with respect to strains and strain gradients, respectively, which can be further expressed in terms of the dynamic matrix. Now we have established the relation between the strain gradient and the atomic displacements.

On the other hand, the point-charge approximation adopted in the rigid-ion model simplifies the expression of polarization in terms of atomic displacements and effective charges. Accordingly, the electric polarization is determined by the displacement $\mathbf{w}^n$ of the n-th atom originally located at $\mathbf{R}^n$ and associated with an effective point charge Q^n as,

$$\delta\mathbf{P} = \frac{1}{V_{fin}}\sum_n Q^n(\mathbf{R}^n + \mathbf{w}^n) - \frac{1}{V}\sum_n Q^n\mathbf{R}^n \tag{2.23}$$

where V and V_{fin} are the volumes of the crystal before and after deformation. By substituting (2.22) into (2.23) one arrives at the polarization response of a finite sample subject to a uniform strain gradient, i.e.,

$$\delta P_i = \frac{1}{V}\sum_n Q^n\Gamma^n_{ijk}\varepsilon_{jk} + \frac{1}{V}\sum_n Q^n N^n_{ijkl}\varepsilon_{kl,j} + \delta P_i^{ext} \tag{2.24}$$

The first and second terms in (2.24) are conditioned by the internal-strain tensors and control the piezoelectricity and lattice contribution of bulk flexoelectricity, respectively. By comparing (2.24) with (1.1) and assuming zero macroscopic electric field, one can readily find the flexoelectric coefficient μ_{ijkl} as,

$$\mu_{ijkl} = \frac{1}{\Omega}\sum_\kappa Q^\kappa N^\kappa_{ijkl} \tag{2.25}$$

To arrive this expression, we replace the summation over the entire crystal of volume V by over the unit cell of volume Ω wherein κ numerates on the sublattices. This formula suggests a viable way to evaluate flexoelectric coefficients by computing the dynamic matrix (thus internal-strain tensors) and Born effective charges, which has later been adopted [69,83] to calculate the full flexoelectric tensor of a variety of practical materials. Finally, the last term in (2.24), conditioned by the external strain and the volume change of the crystal, serves as a correction term and is related to *the surface flexoelectric effect*. A detailed explanation of $\delta\mathbf{P}^{\text{ext}}$ was given in Refs. [11,30].

From the static and dynamic scenarios, Tagantsev [28,29] identified four dissimilar sources that are responsible for generating flexoelectric responses, namely, the static bulk and dynamic bulk flexoelectricity, the surface flexoelectricity, and the surface piezoelectricity. The static bulk response is controlled by the flexoelectric coefficient defined in (1.1) and has a direct analog to the piezoelectric effect. The dynamic bulk flexoelectricity describes the polarization induced by the acceleration of the medium. It becomes dominant when the driving force is a propagating wave, e.g., acoustic phonons, or when the frequency of driving forces goes beyond the resonance of the sample, e.g., high-frequency vibration of a cantilever beam. Meanwhile, this dynamic effect does not have a counterpart in the piezoelectric effect. The surface flexoelectricity originates from the correction term in (2.24) and is sensitive to the surface states. The surface piezoelectricity results from the symmetry-breaking nature of surfaces; therefore, it is universal among crystals irrespective of symmetry. Interestingly, unlike other surface effects, the two surface contributions do not vanish at the bulk thermodynamic limit, i.e., when the surface-to-bulk ratio approaches zero. Consequently, they can mimic a flexoelectric response in a bending mode of a finite sample, causing non-trivial extrinsic electromechanical effects. For example, as shown by

Table 2.1
The four types of contribution to a direct flexoelectric response.

Origins	Types of contribution		Symbols	Scale with permittivity?	Vanish at infinitesimal surface/bulk ratio?	Manifestation
Flexoelectric	Bulk	Static	μ	Yes	–	Static slab bending
		Dynamic	M	Yes	–	Acoustic wave propagation high-frequency slab bending
	Surface	–	μ^{surf}	No	no	Static slab bending
Piezoelectric	Surface	–	d^{surf}	Yes	yes	Static slab bending

Tagantsev and Yurkov [95,96], the surface piezoelectricity drives the so-called flexoelectric bending, i.e., a converse flexoelectric effect induced by applying a uniform electric field across a symmetric capacitor structure. Finally, it has been shown that all four contributions except the surface flexoelectricity scale with dielectric permittivity, suggesting the latter can be safely neglected in high-κ materials. The primary features of these four contributions to a flexoelectric response are summarized in Table 2.1 for clarity. Notably, there are unsettled debates on the existence of surface flexoelectricity and on the identity of static and dynamic bulk flexoelectricity. A more comprehensive discussion on these controversies will be deferred into Section 5.3.

The rigid-ion model discussed above is based on the point-charge assumption. In this sense, the major contribution to a flexoelectric response comes from ions while the effect of electronic charge density redistribution has been generally neglected. One improvement of the rigid-ion model is to replace the rigid ion by core-shell pairs, thus enabling polarizability of the atoms. This has been adopted in Askar et al. [68], who treats an ion as a rigid core with a charged shell linked by a harmonic spring. In this sense, the shell model of flexoelectricity implicitly considers the lattice and electronic contributions in a semi-empirical way. The rigid-ion and core-shell models have recently been revisited by Marangantti and Sharma where a detailed comparison has been made [69]. Another insight to advance the rigid-ion model is to replace the point-charge approximation by a continuous-charge distribution, in a similar spirit as Martin's piezoelectricity theory [76] that built upon Born and Huang's classical theory [141]. As briefly addressed in Ref. [11], the continuous-charge model produces a formulation consistent with those derived from quantum-mechanical theories which will be discussed in the next subsection.

2.3.2. First-principles theories

The classical microscopic theories of flexoelectricity discussed above are either limited to the ionic contribution (rigid-ion model) only or implicitly treat the electronic contribution in a semi-empirical way (core-shell model). The theoretical discovery of curvature-induced polarization in covalent-bonded 2D systems, e.g., carbon nanoshells [142], graphenes [143], and boron nitrides [144], suggests a significant electronic contribution to the flexoelectric response.

Essentially, a microscopic description of flexoelectricity seeks a connection between the strain gradient and the induced polarization. To this end, one needs to find one or more intermediate physical quantities to bridge the gap. For the lattice contribution, the atomic displacement plays the central role, which can be calculated from a strain gradient via the lattice dynamics approach and, meanwhile, constitutes the polarization with effective charges. For the electronic contribution, other entities need to be defined. One immediate choice is the bound charge density $\rho(\mathbf{r})$, which relates to polarization via $\nabla\cdot\mathbf{P}(\mathbf{r}) = -\rho(\mathbf{r})$.

From a more fundamental consideration, the microscopic polarization results from the electronic cloud distortion which is adiabatically described by the quantum-mechanical probability current-density $\mathbf{J}(\mathbf{r})$. Note that in a classical picture, the current-density relates to microscopic polarization via $\mathbf{J}(\mathbf{r}) = \frac{\partial \mathbf{P}(\mathbf{r})}{\partial t}$. Indeed, there are two branches in the development of first-principles flexoelectricity theory, one utilizes charge-density response functions, and the other utilizes the current-density response functions.

Resta [75] made the first effort toward understanding the electronic contribution to flexoelectricity in bulk crystals. Based on Martin's piezoelectricity theory, the author considered the *microscopic electric field* response function as the intermediate ingredient to obtain polarization from long-wave or uniform atomic displacements. Using an elemental cubic lattice, Resta demonstrated that the longitudinal electronic flexoelectric coefficient, at least in this simplest class of dielectrics, is free of surface contribution, and the dynamic and static bulk responses are consistently described by the same flexoelectric coefficient. These conclusions contradict to the conventional recognition established from the rigid-ion models, motivating further fundamental investigations into the microscopics of flexoelectricity.

Inspired by Resta's attempts [75], Hong and Vanderbilt [77] extended the *ab initio* theory of electronic flexoelectricity into arbitrary crystalline insulators. Taking the local charge-density response as the "bridge," the authors derived the longitudinal electronic flexoelectric coefficient in terms of the third moment of the charge-density response, which is consistent with Resta's results. Afterwards, the same authors developed a comprehensive first-principles description of flexoelectricity [15] with explicit consideration of electronic and lattice-mediated contributions. They found that the flexoelectric tensor can be conveniently divided into longitudinal and transverse components. The former can be computed from the multipolar expansion of the charge-density responses to atomic displacements while the latter requires access to the current-density responses.

Independently, Stengel developed another version of the first-principles theory of flexoelectricity based on the density-functional perturbation theory (DFPT) [78]. Instead of working with the real space moments of the charge-density response of isolated atoms, the author conceives the problem in reciprocal space with the current-density responses to atomic displacements induced by a long-wavelength acoustic phonon. In this context, the full flexoelectric tensors, containing both lattice and electronic contributions and with all independent tensorial components, can be explicitly expressed in terms of well-defined linear responses. Hereafter, following Stengel [78], we briefly identify the key ingredients needed to construct the flexoelectric coefficient using the current-density

response and the force-constant matrix which are computable quantities in a DFPT framework.

Consider a crystal lattice spanned by the translation vector $\mathbf{R}_l$ and basis vector τ_κ. Then $\mathbf{R}_{l\kappa} = \mathbf{R}_l + \tau_k$ denotes the atom positions of sublattice κ and cell l. The atomic displacements associated with a long-wave acoustic phonon with wave-vector $\mathbf{q}$ is given by

$$\mathbf{u}_\kappa(l, t) = \mathbf{U}_\kappa^{\mathbf{q}} e^{i\mathbf{q}\cdot\mathbf{R}_{lk} - i\omega t} \tag{2.26}$$

where $\mathbf{U}_\kappa^{\mathbf{q}}$ is an eigenvector of the dynamical matrix at $\mathbf{q}$, and ω is the frequency. Assuming the long-range electrostatic field at zone center has been adequately screened, one can perform the Taylor expansion of $\mathbf{U}_\kappa^{\mathbf{q}}$ with respect to $\mathbf{q}$ as,

$$u_{\kappa i}^{q} = U_i(\delta_{ij} + iq_k\Gamma_{ijk}^{\kappa} - q_k q_l N_{ijkl}^{\kappa} + \cdots) \tag{2.27}$$

where $\mathbf{N}$ and $\mathbf{\Gamma}$ are internal-strain tensors which can be derived from the force-constant matrix Φ (pseudoinverse of the dynamic matrix). On the other hand, the perturbation of atomic sublattice κ along direction j, i.e., $u_{\kappa j}(l, t) = \lambda(t)e^{i\mathbf{q}\cdot\mathbf{R}_{l\kappa}}$, gives rise to a microscopic polarization response $\mathbf{P}_{\kappa j}^{\mathbf{q}}$ through the microscopic current density $\mathbf{J}$, i.e.,

$$\mathbf{P}_{\kappa j}^{\mathbf{q}}(\mathbf{r}) = \frac{\partial J_i(\mathbf{r})}{\partial \dot{\lambda}_{\kappa j}} e^{-i\mathbf{q}\cdot\mathbf{r}} \tag{2.28}$$

The cell average of $\mathbf{P}_{\kappa j}^{\mathbf{q}}$,

$$\bar{\mathbf{P}}_{\kappa j}^{\mathbf{q}} = \frac{1}{\Omega}\int_{cell} d^3r \mathbf{P}_{\kappa j}^{\mathbf{q}}(\mathbf{r}) \tag{2.29}$$

can be expanded for small-$\mathbf{q}$ as

$$\bar{\mathbf{P}}_{\kappa j}^{\mathbf{q}} = \bar{\mathbf{P}}_{\kappa j}^{(0)} - iq_k\bar{\mathbf{P}}_{\kappa j}^{(1,\mathrm{k})} - \frac{q_k q_l}{2}\bar{\mathbf{P}}_{\kappa j}^{(2,kl)} + \cdots \tag{2.30}$$

which gives the ingredients we need to construct flexoelectric coefficients. Note that zeroth-order $\bar{\mathbf{P}}_{\kappa j}^{(0)}$ corresponds to the cell-averaged Born dynamical charge tensor Z*; the remaining $\bar{\mathbf{P}}_{\kappa j}^{(\mathrm{n})}$-tensors can be regarded as its higher-order counterparts and can be further calculated from the small-$\mathbf{q}$ expansion of charge-density responses $\mathbf{J}$.

With these ingredients in hand, we can readily express the flexoelectric coefficient in terms of microscopic polarization responses $\bar{\mathbf{P}}_\kappa^{(0,1,2)}$ and the internal-strain tensors $\mathbf{N}$ and $\mathbf{\Gamma}$. For simplicity, we adopt the type-I flexoelectric coefficient, which is defined as the change of polarization by the unsymmetrized strain gradient, i.e.,

$$\mu_{ijkl}^{\mathrm{I}} = \frac{\partial P_i}{\partial \eta_{j,kl}} \tag{2.31}$$

It can be decomposed into three parts, i.e., the electronic (frozen-ion), the lattice mediated, and the mixed terms, as

$$\mu_{ijkl}^{\mathrm{I}} = \mu_{ijkl}^{\mathrm{I},elec} + \mu_{ijkl}^{\mathrm{I},mix} + \mu_{ijkl}^{\mathrm{I},latt} \tag{2.32a}$$

$$\mu_{ijkl}^{\mathrm{I},elec} = \frac{1}{2}\sum_\kappa \bar{P}_{i\kappa j}^{(2,kl)} \tag{2.32b}$$

$$\mu_{ijkl}^{\mathrm{I},latt} = \frac{Z_{\kappa,im}^*}{\Omega} N_{mjkl}^{\kappa} \tag{2.32c}$$

$$\mu_{ijkl}^{\mathrm{I},mix} = -\frac{1}{2}(\Gamma_{mjl}^{\kappa}\bar{P}_{i\kappa m}^{(1,l)} + \Gamma_{mjk}^{\kappa}\bar{P}_{i\kappa m}^{(1,k)}) \tag{2.32d}$$

For clarity, we summarize all the necessary quantities required to evaluate (2.32) and indicate their relations in Table 2.2. In fact,

Table 2.2
Equations for calculating the piezoelectric and flexoelectric coefficients using microscopic polarization responses.

	Piezoelectric tensor	Flexoelectric tensor Type-I	Flexoelectric tensor Type-II
Electromechanical tensors	$e_{ijk} = \frac{\partial P_i}{\partial \varepsilon_{ij}}$	$\mu_{ijkl}^{\mathrm{I}} = \frac{\partial P_i}{\partial \eta_{j,kl}}$	$\mu_{ijkl}^{\mathrm{II}} = \frac{\partial P_i}{\partial \varepsilon_{kl,j}}$
	$\boldsymbol{e} = \boldsymbol{e}^{\mathrm{elec}} + \boldsymbol{e}^{\mathrm{latt}}$	$\boldsymbol{\mu}^{\mathrm{I}} = \boldsymbol{\mu}^{\mathrm{I,elec}} + \boldsymbol{\mu}^{\mathrm{I,mix}} + \boldsymbol{\mu}^{\mathrm{I,latt}}$	$\boldsymbol{\mu}^{\mathrm{II}} = \boldsymbol{\mu}^{\mathrm{II,elec}} + \boldsymbol{\mu}^{\mathrm{II,mix}} + \boldsymbol{\mu}^{\mathrm{II,latt}}$
Electronic contribution	$\boldsymbol{e}^{\mathrm{elec}} \sim \bar{\mathbf{P}}^{(1,\kappa)}$	$\boldsymbol{\mu}^{\mathrm{I,elec}} \sim \bar{\mathbf{P}}^{(2,\kappa)}$	$\boldsymbol{\mu}^{\mathrm{II,elec}} \sim \bar{\mathbf{P}}^{(2,\kappa)}$
Lattice contribution	$\boldsymbol{e}^{\mathrm{latt}} \sim \mathbf{Z}^*\Gamma$	$\boldsymbol{\mu}^{\mathrm{I,latt}} \sim \frac{1}{\Omega}\mathbf{Z}^*\,\mathbf{N}$	$\boldsymbol{\mu}^{\mathrm{II,latt}} \sim \frac{1}{\Omega}\mathbf{Z}^*\,\mathbf{L}$
Mixed contribution	–	$\boldsymbol{\mu}^{\mathrm{I,mix}} \sim \Gamma\bar{\mathbf{P}}^{(1,\kappa)}$	$\boldsymbol{\mu}^{\mathrm{II,mix}} \sim \Gamma\bar{\mathbf{P}}^{(1,\kappa)}$
Force-response tensors	$\Lambda \sim \Phi$	$\mathbf{T} \sim \Phi$	$\mathbf{C} \sim \Gamma\Phi$
Internal-strain tensors	$\Gamma \sim \widetilde{\Phi\Lambda}$	$\mathbf{N} \sim \widetilde{\Phi\mathbf{T}}$	$\mathbf{L} \sim \widetilde{\Phi\mathbf{C}}$

The symbol ~ denotes a relation that the left-hand quantity can be obtained by the right-hand quantity or quantities.
The explicit expression of the products is omitted which is given in the original publications.

the formulation for the piezoelectric coefficient and for type-II flexoelectric coefficients are closely analogous to (2.32) and are also listed in Table 2.2 for comparison. Besides, we strongly refer readers to the original articles [78] and the Chapter 2 in [19] for rigorous formalism and derivations.

Based on the expression of the type-II flexoelectric coefficient listed in Table 2.2, we briefly interpret the physical meaning of each component, following Hong and Vanderbilt [15], and Stengel [78]. The electronic term $\boldsymbol{\mu}^{\mathrm{II},elec}$ is active in all insulators regardless of symmetry or composition. Numerical results from Hong and Vanderbilt [15,77] suggest that longitudinal parts of the electronic flexoelectric coefficients are negative in sign for most cubic crystals. The lattice contribution $\boldsymbol{\mu}^{\mathrm{II},latt}$ refers to the microscopic polarization due to internal atomic displacements induced by a strain gradient. It has been proven that the internal-strain tensor in $\boldsymbol{\mu}^{\mathrm{II},latt}$ is explicitly atomic mass-dependent, analogous to the dynamic flexoelectric tensor proposed by Tagantsev [11,29], suggesting that flexoelectricity is an intrinsically dynamic effect. The lattice-electronic mixed term $\boldsymbol{\mu}^{\mathrm{II},mix}$ is nonzero only in crystals characterized by Raman-active phonons, such as Si and Ge with the diamond structure. Accordingly, this term vanishes in the cubic perovskite structure. The implication of the mixed term to flexoelectricity in insulating crystals of lower symmetries is elucidated in Ref. [15,78].

Although the explicit expression of flexoelectric tensors has been rigorously derived [15,78], it is still challenging to implement the theory to computing flexoelectric properties of practical materials. The main reason is the fact that the microscopic current-density response is not accessible from public available DFPT codes and its computation involves several technical complexities. To circumvent this issue, Stengel devised a strategy based on a reformulated DFPT theory using a curvilinear coordinate system satisfying covariance requirements [145]. Instead of computing the current-density response, one can resort to the open circuit electrostatic potential built up by bending a slab structure, which directly gives access to the flexocoupling coefficients. In this finite sample method, however, the surface contribution is involved and need to be explicitly addressed. The author demonstrated this approach by computing the bulk and surface frozen-ion flexoelectric coefficients in $SrTiO_3$ slabs [79]. The finding that the magnitude and sign of flexoelectric coefficient depend on surface terminations is encouraging. It not only dispels the controversy in the existence of surface contributions to flexoelectric response, including both surface piezoelectricity and surface flexoelectricity, but also opens up new avenues for tuning flexoelectric responses via surface engineering.

Aside from this “workaround”, Dreyer et al. recently tackled the current-density response problem based on DFPT by carefully determining a form of the current-density operator that is valid for nonlocal pseudopotentials and long-wavelength phonon perturbations [81]. The calculated bulk frozen-ion flexoelectric tensor of $SrTiO_3$ perfectly matches those obtained from Stengel’s slab method [79]. Moreover, Dreyer’s methodology outperforms other supercell-based methods in that it allows for the calculation of flexoelectric property from a single unit cell, which is conceived to be more computationally efficient.

More recent advances in the first principle theory of flexoelectricity are concerned with clarifying the relations of the flexoelectric tensor with other physical properties. Stengel argued that flexoelectricity is closely related to two other effects, namely, the absolute deformation potential [80] and the strain-gradient elasticity [50]. The absolute deformation potential describes the change of electronic energy levels due to a strain field. It suffers from the same arbitrariness as does the flexoelectric effect due to the band-energy dependence which can only be rationalized through a unified formalism of both effects. The strain-gradient elasticity serves as a nonlocal correction to the classical elasticity, describing the energy contribution from the square of strain gradients. The energies associated with the strain-gradient elasticity and flexoelectricity follow a gauge invariance whereby their respective reference-dependence can be canceled out only by summing up, thus obtaining physically well-defined tensor properties. Stengel also advocates the necessity to simultaneously include flexoelectricity and nonlocal elasticity when constructing a thermodynamic function for systems where flexoelectricity and ferroelectricity coexist [50], as recently proposed by several works based on the continuum description of flexoelectricity, e.g., Ref. [51].

Although the first-principles theories of flexoelectricity have been formulated within both density-functional theory (DFT) and density-functional perturbation theory (DFPT) frameworks, their implementation for computing the flexoelectric tensors of practical materials is still computationally laborious and not yet available in publicly available *ab initio* packages. Other theoretical approaches to the first-principles calculation of flexoelectricity are under development, including the cyclic DFT [146] and geodynamical method [147], which may improve our ability to compute the flexoelectric properties from *ab initio*.

2.4. Continuum and atomistic modeling of flexoelectric effects

The macroscopic and microscopic flexoelectric theories summarized above have established the foundation for developing multiscale numerical models to study flexoelectric behaviors at the continuum, meso, and atomic scales. For example, finite element analyses based on the continuum theory of flexoelectricity has been employed to determine the electromechanical field distributions and describe the stationary and dynamical mechanical behaviors of flexoelectric structures under various mechanical loading conditions. The mesoscale phase-field method based on the LGD theory allows one to systematically investigate contributions of flexoelectricity to the static domain and domain wall structures of ferroic materials and their dynamic evolution under external fields. Atomistic modeling techniques, such as molecular dynamics and Monte Carlo simulation based on *ab initio* constructed effective Hamiltonian energy potentials can be used to understand and quantify the flexoelectric properties at the atomic scale.

2.4.1. Continuum mechanics modeling

The mechanics community uses extensively the finite element method to model the static and dynamic electromechanical responses in active materials. A finite element framework can be formulated based on the continuum mechanics theory of flexoelectricity discussed above. However, the fourth order nature of these partial differential equations poses challenges to the finite element

implementation using the C^0-continuous basis function (which is continuous itself but not its derivatives) through a direct Galerkin method. Abdollahi et al. [61] firstly circumvented this difficulty by applying a meshfree technique. This approach allows them to interpret the flexoelectric responses in the cantilever bending and pyramid compression—two schemes extensively used for flexoelectricity measurement—with higher accuracy. Alternatively, Mao et al. [62] developed a mixed finite element formulation for both piezoelectric and flexoelectric effects, which offers a more convenient implementation into public available finite-element packages. Based on a continuum theory with rotation gradients, mixed element techniques suitable for C^0-continuous elements have been put forward in 2D [63] and 3D systems [148]. Another strategy is to use the isogeometric analysis [149](IGA), which fulfills the C^1-continuity requirement and is thus suitable for flexoelectric-related problems. The IGA approach has been integrated with phase-field simulations to account for the flexoelectricity in ferroelectrics with an arbitrary geometry [150]; it has been adopted to identify the full flexoelectric properties from electrical impedance curves [151]; and it has been formulated to solve flexoelectric problems in nanoscale systems under large deformation [152]. Besides, a decoupled finite element analysis has also been adopted to simplify the calculation of piezoelectricity and flexoelectricity in nanowire beams [153].

Using the finite element implementation in Ref. [61], Abdollahi et al. explored the effect of flexoelectricity on mechanical and electromechanical properties in several complex structures [138,154,155]. In the presence of a stationary fracture in a dielectric [155], they found the flexoelectric coupling leads to a size-dependent fracture toughening, i.e., increasing resistance to fracture as the structural size decreases, and asymmetric toughness depending on the direction of polarization. This theoretical prediction has recent been observed in experiments [156]. In a piezoelectric bimorph structure for actuating/sensing applications [138], they identified that flexoelectricity can either enhance or suppress the piezoelectric effect at the nanometer scale depending on the device configuration. This prediction was recently confirmed experimentally by Bhaskar et al. [157]. By performing three-dimensional finite element simulations, Abdollahi et al. [154] further revisited the truncated pyramid compression method, a paradigm setup for measuring the flexoelectric coefficients. They demonstrated the compression field is complicated by the structure and, consequently, the effective flexoelectric constant depends strongly on the pyramid area ratio and the inclination angle. We will elaborate more on the outcome of these findings in Section 5.2.

2.4.2. Phase-field method

The phase-field model of ferroelectrics is a well-established mesoscale method for modeling, understanding, and predicting the microstructure evolution in materials (see, e.g., brief reviews [158,159]). It has been widely used to analyze the stabilities of various ferroelectric phases and domain states under different electromechanical boundary conditions, investigate the domain structure evolution induced by external electric and mechanical fields, and calculate the electromechanical responses and other physical properties. It employs a set of order parameter fields to describe the states of heterogeneous systems. For example, the inhomogeneous distribution of the spontaneous polarization is employed as the order parameter field to monitor the spatial and temporal evolution of polarization domain states by solving the time-dependent Ginzburg-Landau (TDGL) equation, i.e.,

$$\frac{\partial \boldsymbol{P}}{\partial t} = -L\frac{\delta F(\boldsymbol{P})}{\delta \boldsymbol{P}} \tag{2.33}$$

where L is the kinetic coefficient related to the domain wall mobility, and F is the total free energy of the ferroelectric given by the LGD theory (Eq. (2.1)).

The study on flexoelectricity using phase-field methods emerges quite recently [45–47,160]. To incorporate flexoelectricity, the phase-field method of ferroelectrics was extended by introducing new flexoelectric coupling terms in the thermodynamic potentials and driving forces for polarization evolution [161]. Compared with finite element-based mechanics modeling, the phase-field method can better capture the inhomogeneous microstructure evolution in a more efficient way. Compared with atomistic simulation techniques, the phase-field simulation is computationally less costly and is applicable to larger spatial and temporal scales. Moreover, using a phase-field model allows one to conveniently separate the flexoelectric contribution from other relevant effects, e.g., piezoelectricity, which is critical to understanding the primary mechanism underlying the emergent phenomena. Below, we discuss a few examples of phase-field simulations of flexoelectric effects in ferroelectric materials.

(1) Domain structures modified by flexoelectricity

Chen et al. first employ the phase-field method to study the impact of flexoelectric coupling on domain structure properties in ferroelectric thin films [47] and ordinary dielectrics [162]. Ahluwalia et al. explored the influence of flexoelectric coupling on domain patterns in bulk ferroelectrics using 2D phase-field simulations [46]. It was found a fine structure forms when the coupling strength exceeds a critical value and is related to a local transition into an incommensurate phase. Similar modulated domain structure formation has later been simulated by Jiang et al. [163,164], who proposed a phase-field model with finite element implementation considering both flexoelectricity and strain gradient elasticity. Cao et al. compared the effect of flexoelectric tensor components on polarization rotation at a/c domain walls in $Pb(Zr_{0.2}Ti_{0.8})O_3$ thin films [165], which was also observed by TEM [166,167] and is attributed to the flexoelectricity enabled by local strain gradients.

(2) Domain wall structures complicated by flexoelectricity

Gu et al. studied the domain wall structures of $BaTiO_3$ and found the 180-degree ferroelectric domain walls have mixed Bloch-Neél-Ising feature due to the flexoelectric effect [45,168]. Complexity in the 180-degree domain wall has also been documented using

a similar model [169]. In a following phase-field study on $CaTiO_3$ domain walls, Gu et al. showed that the domain wall polar order is likely induced by the flexoelectric effect [170]. The flexoelectric effect on domain walls will be further discussed in Section 4.

(3) Mechanical switching of ferroelectric polarization enabled by flexoelectricity

The mechanical switching of polarization induced by atomic force microscopy (AFM) probe was first theoretically explored by Gu et al. using phase-field simulations [171]. The flexoelectric effect and piezoelectric effect were separated and compared. The influences of the AFM tip geometry, the applied force strength, and the film thickness on the mechanical switching were also discussed. Cao et al. simulated the polarization switching of $Pb(Zr_{0.2}Ti_{0.8})O_3$ thin films under concurrent electric and strain fields created via a piezoresponse force microscopy (PFM) probe [172]. By separating the effects from an electric field, a homogeneous strain, and a strain gradient, they revealed that the homogeneous strain increases the coercive field, and the strain gradient causes a lateral offset of the hysteresis loop. Jiang et al. studied the switching behavior of incommensurate phases induced by the flexoelectric coupling in ferroelectric thin films [163]. They found that the transverse flexoelectric coupling introduces antiferroelectric-like double hysteresis loops, while the longitudinal coupling component gives rise to a imprint-like hysteresis loop. Chen et al. systematically studied the domain switching of $PbTiO_3$ nano-films subjected to cylindrical bending by 3D phase-field simulations [173]. It was demonstrated that the domain patterns can be significantly modified by the mechanical loads and the related flexoelectric field. They further explored the possibility of mechanical erasing by virtue of different loading schemes [160]. Effects of domain size, film thickness, temperature and different mechanical loads, including uniform strain, cylindrical bending, and wavy bending, were investigated.

Recently, advances have been made in the phase-field model of flexoelectricity to be applied to more intriguing problems. For example, Chen et al. included the surface contribution to the total free energy and studied the surface screening effect on the mechanical domain switching [174]. They found that the surface effect is more efficient than the flexoelectric effect, which can introduce upward domain switching and even ripple-like propagating domain switching. Xu et al. coupled the phase-field model with the transport of electrons and holes to study the leakage current of ferroelectric thin films subjected to a mechanical load [175]. They showed that local compressive force can increase the hole current while reducing the electron current via flexoelectric interactions. Further experiments are needed to validate their predictions.

2.4.3. Atomistic modeling

There are also a few efforts to model flexoelectric effects utilizing atomic-level simulation techniques such as molecular dynamics [65,122,176,177] and the effective Hamiltonian method [178]. Majdoub et al. firstly applied molecular dynamics to simulate the effective piezoelectric responses generated by bending a nanocantilever [122]. It is shown flexoelectricity interacts with piezoelectricity in $BaTiO_3$ nanocantilevers leading to a strong size-dependent enhancement of the overall piezoelectric property comparing to the bulk value. Molecular dynamics also enables the calculations of the full flexoelectric coefficients and its temperature dependence using a finite size model [177]. The finite-temperature flexoelectric behaviors can also be modeled using Monte Carlo simulations based on an effective Hamiltonian energy potential where the ground state flexocoupling tensor needs to be calculated *ab initio*. Based on this technique, Ponomareva et al. examined the temperature dependence of flexoelectric properties in $Ba_{0.5}Sr_{0.5}TiO_3$ [178] which substantiates the phenomenological argument that flexoelectricity scales with temperature in parallel with the dielectric permittivity [29]. Notably, the accuracy of capturing flexoelectric responses by molecular dynamics or effective Hamiltonian simulations highly relies on the parameters used to construct the corresponding interatomic force field or the Hamiltonians.

3. Progress in the quantification of flexoelectricity

To understand and further utilize flexoelectricity, it is critical to quantitatively measure the flexoelectric effect and compute flexoelectric coefficients of a material. From the experimental end, the magnitude of flexoelectricity is fundamental to the materials design of flexoelectric-based devices. It is of equal importance to seek for materials with reduced flexoelectricity to minimize undesired flexoelectric-induced outcomes. From the computational end, an efficient way to calculate flexoelectric tensor serves as an effective validation of experimental measurements and helps to distinguish the intrinsic and extrinsic contributions. Moreover, advances in computational methods for flexoelectric effects may provide guidance to the development of new flexoelectric materials with desirable performance. In this section, we provide a brief update on recent progress made in quantifying flexoelectricity in solid materials by both experiments and theoretical computations.

3.1. Experimental measurement of flexoelectric coefficients

3.1.1. Experimental methods

Although a few experimental observation indicated the existence of flexoelectric effect in solids as early as 1960s [25], a systematical measurement of flexoelectricity was not performed until early 2000s by Ma and Cross at Penn State. In their seminal works [34–39], three experimental schemes were established to measure the flexoelectric tensor of several ceramic oxides, as schematically illustrated in Fig. 3.1a–c. The dynamic cantilever bending [CB, Fig. 3.1a] and quasi-static four-point bending [4PB, Fig. 3.1c] methods are designed for the transverse flexoelectric coefficient, $\widetilde{\mu}_{12}$ ($\sim$indicates effective), while the pyramid compression [PC, Fig. 3.1b] method is used for the longitudinal flexoelectric coefficient, $\widetilde{\mu}_{11}$. For these two flexural bending methods, keeping the neutral line within the sample helps eliminate the residual piezoelectric response. Moreover, 4PB bending can generate a much larger

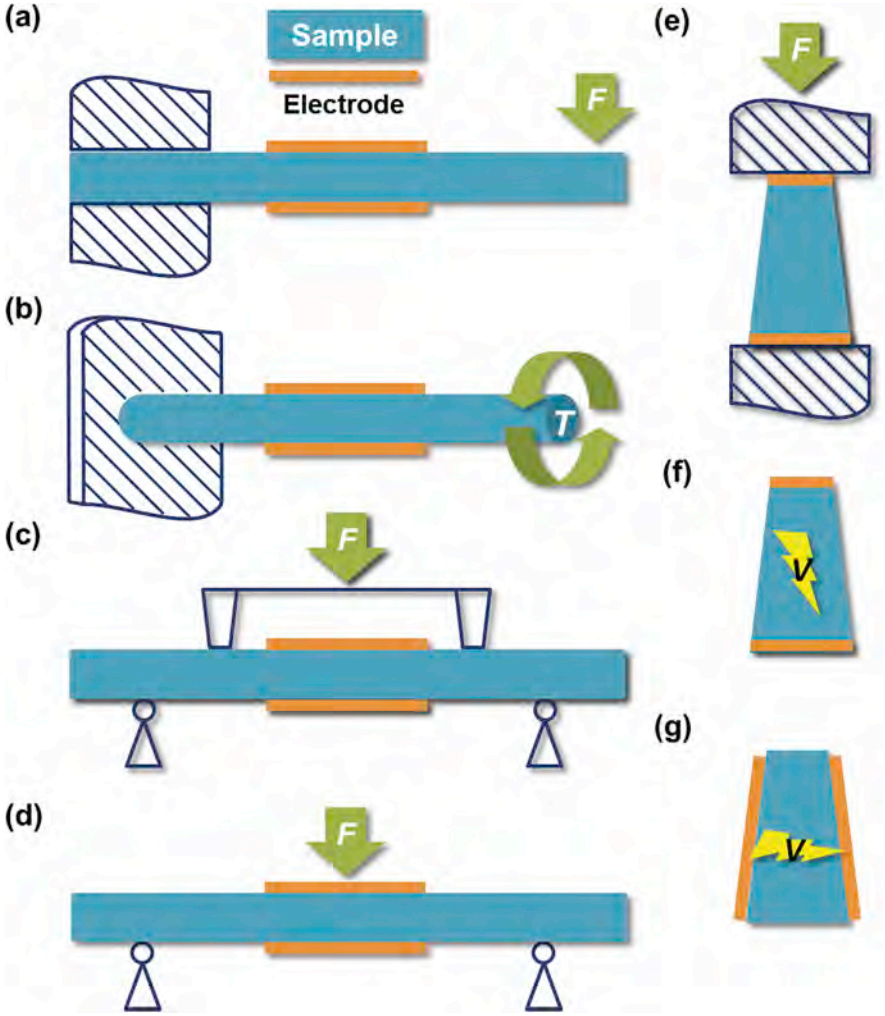

Fig. 3.1. Schematics of flexoelectric experimental setups for direct mesurements of flexoelectric constants: (a) Cantilever bending (CB), (b) cylinder twisting (CT), (c) four-point bending (4PB), (d) three-point bending (3PB), and (e) pyramid compression (PC), and for converse flexoelectric constant measurement: (f) normal-electrode pyramid (NEP) and (g) side-electrode pyramid (SEP).

strain gradient ($\sim 1\ m^{-1}$) in the sample than CB, thus allowing for the examination of nonlinear flexoelectric behaviors at a large load. Aside from measuring the direct flexoelectric tensor, Cross and coworkers [179] also proposed a practical approach to measuring the flexoelectric property by utilizing the converse flexoelectric effect. By applying a graded electric field across a pyramid sample, the induced surface displacement can be captured via high-resolution optical approaches and the flexoelectric coefficient is thereby obtained. To accurately extract the converse flexoelectric coefficient using this approach, however, a careful exclusion of the electrostrictive responses and other spurious charge generations is necessary [12].

The pioneering experiments led by Cross and his coworkers inspired further flexoelectricity measurements. Besides the aforementioned three experimental schemes, a three-point bending [3PB, Fig. 3.1d] scheme was developed by Zubko et al. based on the earlier work of Kityk et al. [180] to measure the full flexoelectric tensor in single crystal $SrTiO_3$. The same technique has later been applied to examine the temperature dependence, chemical composition dependence, and anisotropy of flexoelectricity in other ferroelectric single crystals [97,181]. A systematic comparison of the three bending methods in measuring transverse flexoelectric coefficients has recently been conducted [182]. Alternatively, as an extension of CB method, the cantilever twisting [CT, Fig. 3.1e] approach was devised to measure the shear flexoelectric component and has been implemented in various ferroelectric polymers. Utilizing the converse flexoelectric effect, Shu et al. [183] also measured the shear flexoelectricity of $(Ba,Sr)TiO_3$ (BST) ceramics using a pyramid sample with electrodes on the two sloping sides. In principle, the full flexoelectric tensors of a cubic-symmetric insulator can be determined efficiently owing to the development of well-designed experimental frameworks. Nevertheless, most of the flexoelectric coefficients measured using these macroscopic methods are only effective properties which may consist of various flexoelectric contributions and combine multiple flexoelectric tensor components. Therefore, a direct comparison between experimental results and theoretical calculations should be made with care.

Table 3.1
Direct and indirect experimental techniques to measure flexoelectric tensors.

Direct/indirect	Methods	Direct/converse effects	Flexoelectric tensor	Static/dynamic measurement	Features/Limitations	References
Direct	Cantilever bending (CB)	Direct	Transverse (effective)	Quasi-static	Easy setup	[34–36,39,196,197,203–208]
	Four-point bending (4PB) three-point bending (3PB)	Direct	Transverse (effective)	Static	High strain gradient	[37,97,181,198]
	Pyramid compression/stretching (PB/PS)	Direct	Longitudinal	Quasi-static	Spurious charge response	[12,71,209]
	Cylinder torsion (CT)	Direct	Shear	Static	Shear component	[210]
	Normal electrode pyramid (NEP)	Converse	Longitudinal	Static	Electrostriction influence	[179,211]
	side electrode pyramid (SEP)	Converse	Shear	Static	Shear component	[183]
Indirect	Phonon spectra	Direct	All	Dynamic	Surface effect-free; mixed static and dynamic contribution	[83]
	Nanocompression (NC)	Direct	Longitudinal	Static	Voltage-free	[189–192]
	Photorefractive response (NR)	Converse	Longitudinal	Dynamic	–	[188]
	Split Hopkinson pressure bar	Direct	Longitudinal	Dynamic	–	[212]

Aside from these direct methods, which are directly based on the constitutive equation of flexoelectricity (Eq. (1.1)), indirect techniques to estimate flexoelectricity have also been proposed. Representative works in this respect are listed in Table 3.1. The indirect techniques measure material properties and phenomena mediated by flexoelectricity from which the flexoelectric coefficient can be deducted. For example, it is known the flexoelectric interaction gives rise to the repulsion between transverse acoustic and transverse soft-mode optic phonons of ferroelectrics [11]. Therefore, the phonon dispersion of a ferroelectric single crystal, which can be accurately measured by using neutron inelastic scattering or Brillouin scattering [184–187], provides information on the bulk static and dynamic flexoelectric responses. Estimated flexoelectric coefficients based on phonon spectra, however, are semi-quantitative because the sign of each component is difficult to be unambiguously determined, and the static and dynamic flexoelectric effects coexist in this context. Another indirect approach makes use of the contribution of inverse flexoelectricity on the photorefractive response in single crystals, leading to the estimation of a longitudinal converse flexoelectric constant in $Bi_{12}TiO_{20}$ [188]. Implementation of this optical approach to examine flexoelectricity of more well-studied perovskites is still missing. In addition, since flexoelectricity is related to the indentation size effect in dielectrics [189], a nano-compression method [190] has been proposed to extract the longitudinal flexoelectric components at the nanoscale and applied to quartz [189], $BaTiO_3$,[191] and $SrTiO_3$ single crystals [192]. These indirect measurements exhibit advantages over the direct measurements in serval aspects. The phonon spectrum-based method enables the assessment of the dynamic flexoelectric effect while eliminating side effects from the surface. The nano-indentation approach is voltage-free, and it generates large and localized strain gradients, thus allowing for studying nonlinear flexoelectric behaviors under large stimuli [193]. Notably, using indirect approaches on known flexoelectric materials can serve as mutual corroboration for the flexoelectric coefficients measured by direct methods.

3.1.2. Flexoelectric materials

For high flexoelectricity, one of the prime candidate materials is the ferroelectrics since the flexoelectric property scales with the dielectric permittivity [28,29]. Cross et al. investigated the strength of flexoelectricity in $Pb(Mg,Nb)O_3$ (PMN) [34], $BaTiO_3$ [35], BST [39], $(Pb,Sr)TiO_3$ [12], and $Pb(Zr,Ti)O_3$(PZT) [36,37] ceramics and highlighted the exclusively enhanced flexoelectricity in BST, which is two order-of-magnitude larger than the other Pb-containing polycrystalline ferroelectrics. The Pb-free nature of BST complies with the ecological concerns of next-generation electronic devices, generating considerable research interests into the BST-based systems. In contrast, the lead-containing oxide ceramics generally show much smaller flexoelectric responses, the chemical and physical origins of which is yet elusive.

The magnitude of flexoelectric coefficients and its temperature dependence can be tuned through doping extrinsic elements or forming composites with other ceramics. For example, Shu et al. reported that the room-temperature transverse flexoelectric coefficient of BTS ceramics can be doubled by doping 0.5 wt% Al_2O_3 [194,195]. Li et al. demonstrated the existence of flexoelectricity in non-ferroelectric $(Bi_{1.5}Zn_{0.5})(Zn0_{.5}Nb_{1.5})O_7$(BZN) by forming a 3–3 composite with Ag powders [196]. The same authors also reported enhanced flexoelectricity in BST by creating 3–3 $Ba_{0.6}Sr_{0.4}TiO_3/Ni_{0.8}Zn_{0.2}Fe_2O_4$ (BST/NZO) composites [197]. We provide a comprehensive survey on the low-frequency room-temperature flexoelectric coefficients of ceramics, ceramics composites, and single crystals measured from experiments, as listed in Table 3.2. It appears that the BST-based ceramics has the record-high room-temperature flexoelectric coefficient ($\sim$120 μC/m) among others. For the intrinsic flexoelectricity of single crystals, the highest value is attributed to $BaTiO_3$ ($\sim$100 μC/m) at Curie temperature, the enhancement of which may be relevant to remnant polar nanoregions [97]. The experimental measurement of $BaTiO_3$ single crystals of various crystallographic orientations also reveals large anisotropy in the flexoelectric effect, indicating a strong surface contribution [97]. To further increase the flexoelectric strength, joint efforts from experiment and computation are required to systematically understand the physical and chemical mechanisms of doping, compositing, and microstructure effects on flexoelectricity in solids.

Apart from seeking for high flexoelectric constants, it is also desirable to develop materials with an excellent linearity of flexoelectric responses with respect to applied loads and with a controlled dependence of flexoelectricity on temperature and loading frequency. Earlier studies on ceramics have revealed remarkable linearity of flexoelectric polarization to applied strain gradient-induced polarization up to $\sim 0.3\,m^{-1}$ in almost all perovskite oxides investigated, as shown in Fig. 3.2a. Nonlinear behaviors in ceramics [37], as well as single crystals [198], were observed only at large mechanical loads [37] ($\sim 1.0\,m^{-1}$), indicating the ferroelectric contribution from domain wall motion and possibly flexoelectric poling. As for the converse flexoelectricity, good linearity between mechanical deformation and electrical field-gradient up to 10^7 V/m^2 has been reported [199]. Notably, even though the validity of linear flexoelectricity has not been unambiguously demonstrated, the presumption of linear dependence down to the nanoscale where the gradient term becomes enormously large (10^6–10^8 m^{-1}) has been widely adopted. Very recently, nonlinear flexoelectric behaviors have been observed [200] and theoretically examined [74].

The temperature dependence of the flexoelectric coefficient is believed to be similar to that of the dielectric permittivity due to the proportional relationship between flexoelectric coefficients and dielectric constants. However, measurements of various oxides showed that this relationship reasonably holds only at small and intermediate permittivity (Fig. 3.2b). For example, a sublinear drop at low permittivity and a superlinear increase of flexoelectricity near the transition temperature are commonly observed, suggesting an extrinsic mechanism of induced polarization. Notably, in relaxor-based ferroelectrics, such as PMN-28PT single crystals, the relaxor-like broadening of the permittivity peak is also captured in the flexoelectricity. Another interesting behavior of flexoelectricity is the thermal hysteresis: the flexoelectric polarization measured upon heating is large than that upon cooling until up to a temperature T*, as seen in PMN-PT and $BaTiO_3$ single crystals [97,181]. In PMN-28PT and PMN-30PT, T* coincides with the onset of the anelastic softening measured by resonant ultrasound spectroscopy [201], indicating the extrinsic contribution to flexoelectric response by the reorientation of short-range polar nanodomains remnant above T_c. Additionally, the high anisotropy of the flexoelectric coefficient observed in the high-temperature paraelectric phase of $BaTiO_3$ indicates the existence of surface piezoelectricity [97].

Table 3.2
Flexoelectric constants of various ferroelectric materials measured by experiments.

Materials	Materials type	Longitudinal μ_{1111} (μC/m)	Transverse μ_{1122} (μC/m)	Shear μ_{1212} (μC/m)	Direct/converse	Methods
$Ba_{0.7}Sr_{0.3}TiO_3$ [208]	Polycrystal thin film		24.5		Direct	Film cantilever bending
$Ba_{0.67}Sr_{0.33}TiO_3$ [39]	Ceramics		100		Direct	Cantilever bending
$Ba_{0.67}Sr_{0.33}TiO_3$ [179]	Ceramics	120			Converse	Trapezoid sample
$Ba_{0.67}Sr_{0.33}TiO_3$ [12]	Ceramics	150			Direct	Pyramid compression
$Ba_{0.67}Sr_{0.33}TiO_3$ [183]	Ceramics			124	Converse	Trapezoid sample (side electrodes)
$Ba_{0.67}Sr_{0.33}TiO_3$ [205]	Ceramics		8.5		Direct	Cantilever bending
$Ba_{0.67}Sr_{0.33}TiO_3$ [212]	Ceramics	47.6			Indirect	Split Hopkinson pressure bar
$BaTiO_3$ [35]	Ceramics		50		Direct	Cantilever bending
$BaTi_{0.87}Sn_{0.13}O_3$ [206]	Ceramics		53		Direct	Cantilever bending
PMN [34,38]	Ceramics		4		Direct	Cantilever bending
PMN-10PT [211]	Ceramics	~1000			Converse	Conical sample
PMN-10PT [209]	Ceramics	6.2–12.3			Converse	Conical sample
PZT-5H (unpoled) [37]	Ceramics		1.5		Direct	Four-point bending
PZT-5H (unpoled)[36]	Ceramics		1.4		Direct	Cantilever bending
$Pb_{0.3}Sr_{0.7}TiO_3$ [12]	Ceramics	20			Direct	Pyramid compression
$Ba_{0.6}Sr_{0.4}TiO_3/Ni_{0.8}Zn_{0.2}Fe_2O_4$ [197]	Ceramics composite		128.6		Direct	Cantilever bending
$(Bi_{1.5}Zn_{0.5})(Zn0_{.5}Nb_{1.5})O_7$ [196]/Ag	Ceramics composite		0.17		Direct	Cantilever bending
$BaTiO_3$ [97]	(0 0 1) single crystal		0.2		Direct	Three-point bending
	(1 1 0) single crystal		−0.05			
	(1 1 1) single crystal		−0.01			
$Bi_{12}TiO_{20}$ [188]	Single crystal	5.3			Converse	Photorefractive response
$SrTiO_3$ [198]	Single crystal	0.0002	0.007	0.0058	Direct	Three-point bending
PMN-34PT [181]	Single crystal		38		Direct	Three-point bending
$BaTiO_3$ [192]	Single crystal		4		Direct	Nanoindentation
Materials	Materials type	Longitudinal – transverse $\lvert f_{1111} - f_{1122}\rvert$ (V)		Shear f_{1212} (V)	Direct/converse	Methods
$SrTiO_3$ [213–215]	Single crystal	1.2–1.4		1.2–2.4	Direct	Phonon spectra
$KaTiO_3$ [184,216]	Single crystal	0–1.8		2.5–2.9	Direct	Phonon spectra
$BaTiO_3$ [186]	Single crystal	< 7.8		< 0.15	Direct	Phonon spectra
$BaTiO_3$ [217]	Single crystal	< 7		< 3.3	Direct	Phonon spectra
$SrTiO_3$ [217]	Single crystal	< 10		< 2.4	Direct	Phonon spectra

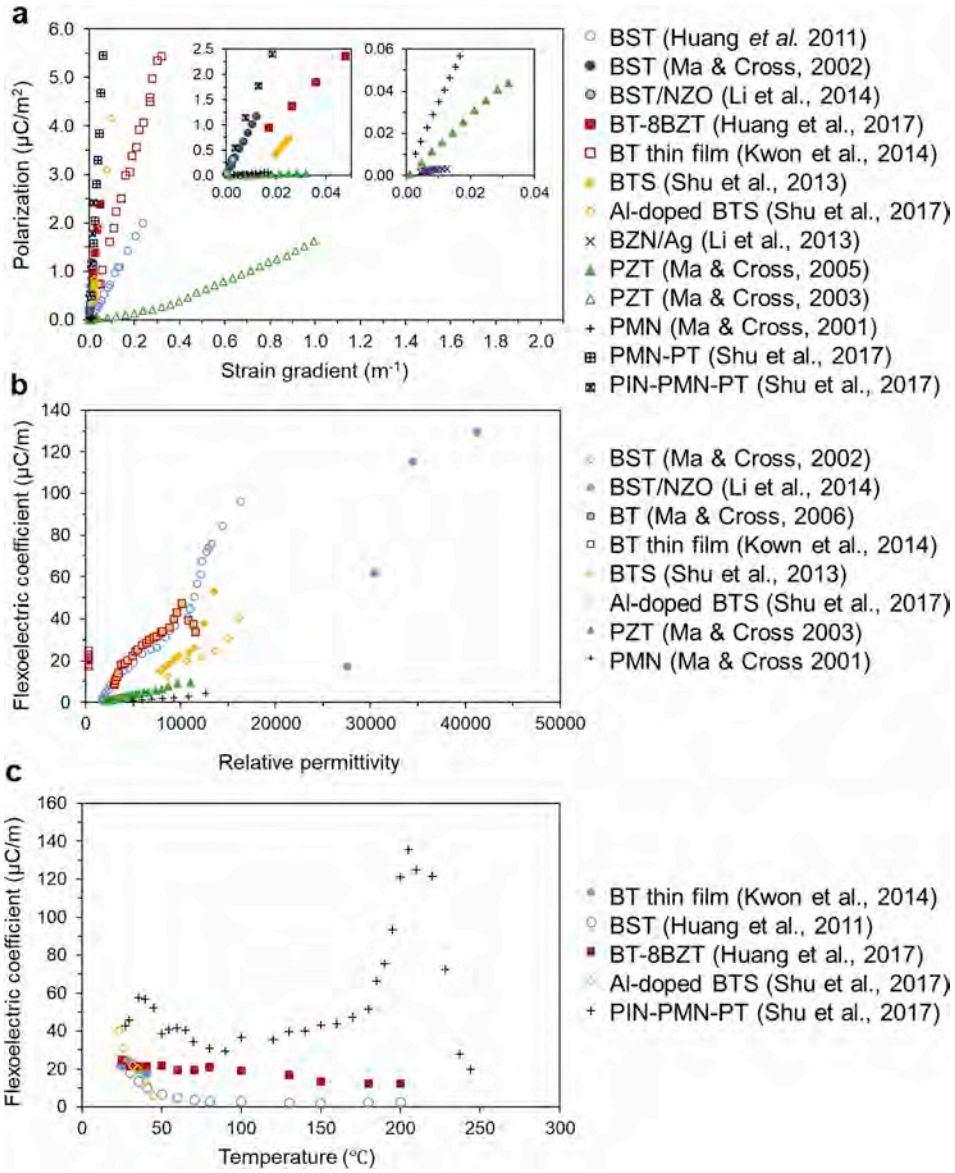

Fig. 3.2. Features of flexoelectric properties of various materials measured by experiments. (a) The linearity of flexoelectric polarization with respect to strain gradient. Insets show the zoom-in regions. (b) Scaling of the flexoelectric coefficient with respect to relative permittivity. (c) Temperature dependence of flexoelectric coefficients. Abbreviations: (Ba,Sr)TiO_3(BST), $Ni_{0.8}Zn_{0.2}FeO_4$(NZO), $BaTiO_3$(BT), $Ba(Zn_{0.5}Ti_{0.5})O_3$(BZT), $Ba(Ti,Sn)O_3$ (BTS), $(Bi_{1.5}Zn_{0.5})(Zn_{0.5}Nb_{1.5})O_7$(BZN), $Pb(Zr,Ti)O_3$(PZT), $Pb(Mg_{0.33}Nb_{0.67})O_3$(PMN), $PbTiO_3$(PT), $Pb(In0.5Nb_{0.5})O_3$(PIN).

The frequency dependence of flexoelectricity is of critical importance but remains understudied. A small dispersion is beneficial for the reliability of flexoelectric-based devices under varying loading conditions while a frequency-sensitive flexoelectricity indicates good tunability. Shu et al. [202] have shown a nearly 50% enhancement of effective flexoelectric coefficient in PMN-PT single crystals by slightly increasing the mechanical load from 3 Hz to 12 Hz, suggesting a tunability on the flexoelectricity in relaxor-based oxides. However, an opposite trend of loading frequency on flexoelectric responses has also been reported elsewhere [197]. Apparently, more exploration on the frequency dependence of flexoelectricity is desirable for a fundamental understanding of its the microscopic and macroscopic mechanisms.

3.2. Atomistic computation of flexoelectric coefficients

As early as the 1960s, Kogan estimated the flexocoupling constants of ionic crystals to be of 1–10 V [24] using a simple phenomenological model. [15]. With the establishment of the microscopic theory of flexoelectricity, it is possible to calculate the flexoelectric coefficient of a number of crystals using semi-empirical techniques and state-of-the-art first-principles methods. For

instance, the flexoelectric constants for rocksalts, binary semiconductors, and perovskites have been calculated by Marangantti and Sharma [69] based on Tagantsev's rigid-ion [29] and Askar's core-shell [68] models. The *ab initio* computation of the longitudinal component of a flexoelectric tensor was firstly performed by Hong et al. through a supercell-based direct method [218]. More recent advances allow one to obtain the full flexoelectric tensor of arbitrary solid crystals [15,78,79], which confirms Kogan's pioneering result in terms of the magnitude of intrinsic flexoelectricity. This subsection summarizes the recent *ab initio* and semi-empirical calculation results of the flexoelectric constants of solid crystals, especially, ferroelectric perovskites.

3.2.1. First-principles calculations

There are mainly two approaches to evaluate flexoelectric constants from first-principles density-functional theory calculations. The direct approach follows the definition of the flexoelectric coefficient in (1.1) and directly evaluate the polarization induced by an applied strain gradient. Since the strain gradient needs to be compatible with the periodical boundary condition, it is achieved by imposing a sinusoidal atomic displacement to the supercell. The induced polarization is calculated by fixing one sublattice while relaxing the rests. Finally, the flexoelectric component is obtained by dividing the local polarization over the applied strain gradient. Hong et al. firstly utilized this direct method to calculate the longitudinal component for $BaTiO_3$ and $SrTiO_3$ [219]. Later, it has been extended by Xu et al. to evaluate the transverse and shear flexoelectric components [220]. Although the direct method is straightforward to implement, the results are sensitive to the choice of constrained sublattice (force-pattern, c.f. Section 5.3) and the size of the supercell. Furthermore, it implicitly assumes an open circuit (fixed-D) boundary condition, making it difficult to compare with experimental values which are usually performed under the short-circuit (fixed-E) boundary condition. Additionally, the calculated flexoelectric constants inherently contain the lattice and electronic contributions, making it difficult to elucidate the microscopic origins of flexoelectricity.

The indirect method is based on the first-principles theory of flexoelectricity. In this context, the flexoelectric tensor can be decomposed into the lattice-mediated, the frozen-ion (electronic), and the mixed contributions (c.f. Section 2.3 and Table 2.2). By computing each component within a consistent quantum mechanics framework, one can finally obtain the full flexoelectric tensor which can be separated into its lattice and electronic contributions. Following this philosophy, Hong and Vanderbilt have provided a supercell-based method and performed systematic computations of the full flexoelectric tensors for a number of elementary, binary, and perovskite crystals with cubic symmetry. For all materials computed, their flexoelectric coefficients under fixed-D condition are on the order of -0.1 nC/m and the corresponding flexocoupling coefficients are within the range of -10 to -20 V. Note that the flexoelectric tensor components are identically negative in stark contrast to the positive values from experimental measurements. Also, this *ab initio* estimated values are two orders of magnitude smaller than common experimental results, which is believed to be related to surface contributions [15]. Besides, it is still challenging to obtain the full flexoelectric tensor without invoking the current-density response formulation which is complicated to implement.

Evaluating the surface contribution to a flexoelectric response is later made possible by Stengel. The author devised an alternative strategy to circumvent the difficulty in calculating the microscopic current-density responses by reformulating the density functional perturbation theory (DFPT) onto a curvilinear coordinate system [145]. Stengel showed that total (bulk and surface) flexocoupling coefficient is equivalent to the open circuit voltage ΔV induced across a bent slab in the limit of large thickness t, i.e.,

$$f_{xijk} = \lim\left(\frac{1}{t}\frac{\partial \Delta V}{\partial \varepsilon_{jk,i}}\right) \tag{3.1}$$

where $\varepsilon_{jk,i}$is the gradient of symmetrized strain, f_{xijk} is the sum of bulk flexocoupling tensor f_{xijk}^{bulk} and surface contribution f_{xijk}^{surf}, and the subscript x denotes the direction normal to the slab surface. In this sense, rather than seeking for the polarization response of a bulk, one can instead resort to the electric field response of a slab. To obtain f_{xijk} with both electronic and ionic contributions, one needs to first perform a slab calculation in a "truncate-bulk" scheme to obtain the frozen-ion contribution, and then relax the slab for the lattice-mediated response. Meanwhile, to access the full tensor f_{ijkl} with cubic symmetry, slabs with three independent crystallographic orientations should be consistently evaluated. Following this procedure, Stengel obtained the surface and bulk flexoelectric constants for $SrTiO_3$ including frozen-ion and lattice-mediated contributions [78]. The overall relaxed lattice flexoelectric constants exhibit an interesting surface state-dependence which signifies the surface contribution to the flexoelectricity.

More recent efforts focus on refining the calculation to further rationalize the discrepancy in the sign and the magnitude of flexoelectric tensors with experimental values. To this end, many subtleties and ambiguities in the theoretical calculations of the flexoelectricity have been revealed. These issues include the choice of reference energy and subsequent ambiguity in defining the electric field under a structural gradient [80], the pseudopotential dependence of microscopic response functions [15,77], the necessity to unify the theory of the flexoelectricity with other effects [50,80], etc. We will turn back to discuss these issues in Section 5.3.

3.2.2. Semi-empirical calculations

In addition to pure *ab initio* attempts, semi-empirical methods have also been utilized to quantify flexoelectric coefficients combining first-principles calculations with higher-level computation techniques. These semi-empirical techniques include lattice dynamics [69,83], molecular dynamics [103,176,177], and effective Hamiltonian methods [178]. In each approach, experimental parametrization and/or DFT-based first-principles calculations have been used to obtain the essential ingredients of the model, such as the dynamic matrices and phonon spectra [83], empirical interatomic potentials [177], and flexocoupling coefficients in energy functionals [178,221].

Maranganti and Sharma [69] firstly implemented Tagantsev's classic microscopic theory of flexoelectricity [29] and computed the flexoelectric tensors of various cubic crystals in the context of classic lattice dynamics. The DFT calculation is used to compute the dynamic matrices and Born effective charges which are then used to obtain the flexoelectric coefficients. Kvasov and Tagantsev [83] recently applied similar strategies to study the dynamic flexoelectric (flexodynamic) coefficient in $SrTiO_3$ through dynamic matrices, Born effective charges, and phonon spectra obtained from DFPT. They argued that the dynamic flexoelectricity is comparable to or even stronger than the static bulk part under certain conditions. However, it remains controversial whether the dynamic and static bulk flexoelectric are intrinsically equivalent or not.

Molecular dynamics simulations have been utilized to compute the flexoelectric tensors through a direct method. The full flexoelectric tensor can be readily obtained using three independent schemes of longitudinal, transversal, and shear strain gradients in a periodical system. Chatpoulus reported the flexoelectric tensor of MgO [177], which shows a much smaller order of magnitude than those of ferroelectric materials. This result is expected considering the large difference in dielectric permittivity. A similar technique has also been utilized to study the temperature dependence of the flexoelectric constant in a $BaTiO_3$ pyramid sample built by a molecular dynamics simulation [176]. The temperature-behavior is however opposite to those obtained by experiments [35]. Very recently, Zhuang et al. performed molecular dynamics simulations to evaluate the flexoelectric constants of several representative 2D materials, providing an effective approach to explore the flexoelectricity in low-dimensional materials [222]. Notably, the accuracy of the flexoelectric coefficient evaluated by molecular dynamics highly relies on the choice of the atomistic model and the effective interatomic potentials.

Another *ab initio*-based method is employed by Ponomerava et al. [178] The flexocoupling tensor is first computed using a supercell-based direct method and then utilized to construct an effective Hamiltonian for the finite temperature simulation of a slab model. Accordingly, the finite temperature flexoelectric tensor of a paraelectric $Ba_{0.5}Sr_{0.5}TiO_3$ film and its dependence on temperature and film thickness are examined. Their results demonstrate that the flexocoupling coefficient is nearly independent of temperature while the flexoelectric coefficient scales with temperature approximately by the dielectric permittivity, consistent with the conclusion from early phenomenological prediction [29]. The enhancement of the flexoelectric response in thinner films also highlights the importance of surface contributions.

3.2.3. Other computational methods

Recently, the advancement and popularity of machine learning techniques have brought new insights to materials design. Li et al. demonstrated a unique approach [223] to statistically estimate the flexoelectric constant by learning from experimental measurement. He performed data mining on a set of HRTEM images of the ferroelectric polarization distribution in the $PbTiO_3/SrTiO_3$ superlattice [224] to obtain the statistical features of a vortex nanodomain. Meanwhile, the authors conducted high-throughput phase-field simulations with parameterized flexoelectric constant to "fit" the machine-learned statistical features. In this sense, it is implicitly assumed that flexoelectricity, other than extrinsic defect-related factors, is the primary contributor to the variation of vorticity at the core of polarization vortex arrays in the $PbTiO_3/SrTiO_3$ superlattice. The estimated flexocoupling coefficients for both $PbTiO_3$ and $SrTiO_3$ agree well with theoretical values to the order of several volts. This work highlights the power of integrating big data and machine learning techniques to resolve controversies for flexoelectric-related phenomena.

Recently, large-scale simulations have been employed to study the flexoelectricity based on the second-principles theory incorporating both electronic and lattice degrees of freedom [225]. Comparing to the conventional density functional theory, it has the advantage of being able to handle larger systems with 100,000+ atoms, while comparing to semi-empirical methods, it contains the information about the electronic degrees of freedom. Considering the importance of both electronic and ionic contributions to flexoelectricity (Section 5.3), we expect the second-principles theory will serve as a promising, additional computational technique for understanding the flexoelectric-related phenomena and evaluating flexoelectric properties in the future.

A comparison of various methods mentioned in this subsection is summarized in Table 3.3. The flexoelectric and flexocoupling coefficients of several perovskite oxide crystals evaluated by these approaches are listed in Table 3.4.

The advances in the first-principles calculations and atomistic models allow us to quantify the full flexoelectric tensors of various crystal materials from *ab initio*. Both bulk and surface flexoelectric effects, as well as a static and dynamic contributions, can be appropriately identified with an organic combination of various techniques. We expect these advances would further deepen the microscopic understanding of flexoelectric phenomena and facilitate the computational design of novel flexoelectric materials.

4. Progress in the manifestation of flexoelectric effects

The flexoelectric effect manifests itself when the intrinsic flexoelectric coupling is high, e.g., in ferroelectric materials, and/or when the structural or field gradient is significant. As the material aspect has been elaborated in the previous section, we focus on the latter aspect in this section about where to find and how to generate large gradients for the manifestation of flexoelectricity.

There are a few points need to be emphasized. First, the origin of a gradient can be directly or indirectly related to the definition of flexoelectricity. Strain/stress gradients may directly arise from inhomogeneous structural deformation while electric field/polarization gradients may arise from the nonuniformity of polarization or electric fields. These mechanical and electrical gradients may also be indirectly induced via chemical inhomogeneity, thermal gradients, and variation of other structural orderings due to the omnipresent coupling between multiple state variables. Second, strain gradients may be spontaneous, such as due to the spontaneous polarization change across a ferroelastic domain wall, or can be generated by external stimuli, such as by the local stress field created by SPM tip pressing. Furthermore, for dynamic flexoelectric effects, even the temporal variation of atomic displacements or polarization contributes to the flexoelectric response. The diverse types of gradients in practical materials provide a rich playground to

Table 3.3
Theoretical methods to calculate flexoelectric constants.

Type	Method		Strengths	Drawbacks	Reference
First-principles	Direct		Straightforward to implement; all tensor components	Supercell size dependent; mixed lattice and electronic contribution; uncontrolled electrical boundary conditions	[218,220]
	Indirect	Longwave method	Separate lattice and electronic contributions	Complex to implement; only longitudinal component	[15,77]
			Separate lattice and electronic contributions; unit-cell based; all tensor component	Complex to implement	[81]
		Slab model	Surface contribution; all tensor component	Supercell-based; complicated to implement (curvilinear coordinate)	[79]
Semi-empirical	Molecular dynamics		Temperature and geometry factors; straightforward to implement; all tensor component	Effective potential dependent	[176,177]
	Effective Hamiltonian		Temperature and geometry factors; all tensor component	Flexocoupling coefficients dependent	[178]
	Lattice dynamical	Shell model	Inverse flexoelectric coefficient	Rely on phonon spectra data; sensitive to core-shell interaction	[68]
		ab initio	Bulk dynamic contribution; straightforward to implement	Rely on phonon spectra data; ignore electronic contribution	[69,83]

Table 3.4
Theoretical calculated flexoelectric constants of perovskite crystals.

Materials	Type of tensors and Units	SI units	Longitudinal f_{1111} or μ_{1111}	Transverse f_{1122} or μ_{1122}	Shear f_{1221} or μ_{1221}	Methods	Reference
$BaTiO_3$	FEC type-I	nC/m	0.15	−5.5	−1.9	Rigid-ion model	[69]
	FEC type-II		−0.37			Direct, DFT	[218]
	FEC type-II		−0.36	1.6	−1.5		[220]
	FEC type-I		−0.16	$\mu_{1122} + 2\mu_{1221} = -0.21$*		Indirect, DFT	[15]
	FEC type-I		(−370.8)**	$\mu_{1122} + 2\mu_{1221} = (-481)$*			
	FEC type-I		μ_{eff} = 0.1–0.6			MD	[176]
	FCC	V	−18.2	−23.6*		Indirect, DFT	[15]
$SrTiO_3$	FEC type-II	nC/m	−1.4			Direct, DFT	[218]
	FEC type-I		−0.16	$\mu_{1122} + 2\mu_{1221} = -0.17$*		Indirect, DFT	[15]
	FEC type-I		(−48.4)	$\mu_{1122} + 2\mu_{1221} = (-53.5)$			
	FEC type-II		−0.89	2.3	−6.6	Direct, DFT	[220]
	FEC type-I		−0.26	−3.7	−3.6	Rigid-ion model	[69]
	FEC type-II		−0.87	−0.84	−0.08	Indirect, DFPT	[81]
	FCC	V	−17.7	$\mu_{1122} + 2\mu_{1221} = -19.5$*		Indirect, DFT	[15]
	FCC		−16.2	−15.1	−1.5	Indirect, DFPT	[79]
	FCC		−2.1	−2.5	−1.5	Rigid-ion model	[83]
	FCC		$\lvert f_{1111} - f_{1122}\rvert < 0.5$		$\lvert f_{1221}\rvert = 1.5$	Phonon spectra, DFPT	
$Ba_{0.5}Sr_{0.5}TiO_3$	FCC	V	5.1	3.3	0.045	Effective Hamiltonian	[178]
$BaZrO_3$	FEC type-I	nC/m	−0.19	$\mu_{1122} + 2\,\mu_{1221} = -0.21$*		Indirect, DFT	[15]
	FEC type-I		(−2.8)	$\mu_{1122} + 2\,\mu_{1221} = (-3.2)$			
	FCC	V	−21.8	$\mu_{1122} + 2\,\mu_{1221} = -24.4$*			
$PbTiO_3$	FEC type-I	nC/m	−0.2	$\mu_{1122} + 2\,\mu_{1221} = -0.25$*		Indirect, DFT	[15]
	FEC type-I		(−26.4)	$\mu_{1122} + 2\,\mu_{1221} = (-34)$			
	FCC	V	−22.4	$\mu_{1122} + 2\,\mu_{1221} = -28.9$*			
	FCC	V	$\lvert f_{1111} - f_{1122}\rvert < 3$	$\lvert f_{1221}\rvert \sim 2$		Indirect, ML	[223]

* Values in parenthesis indicates they are under short circuit boundary condition at room temperature.
** Abbreviations: FEC – flexoelectric coefficient; FCC – flexocoupling coefficient; MD – molecular dynamics; ML – machine learning.

explore flexoelectric-related phenomena.

In this section, we highlight three scenarios at the micro/nanoscale where appreciable strain, stress, and other gradients can be present, and the role of flexoelectricity becomes significant.

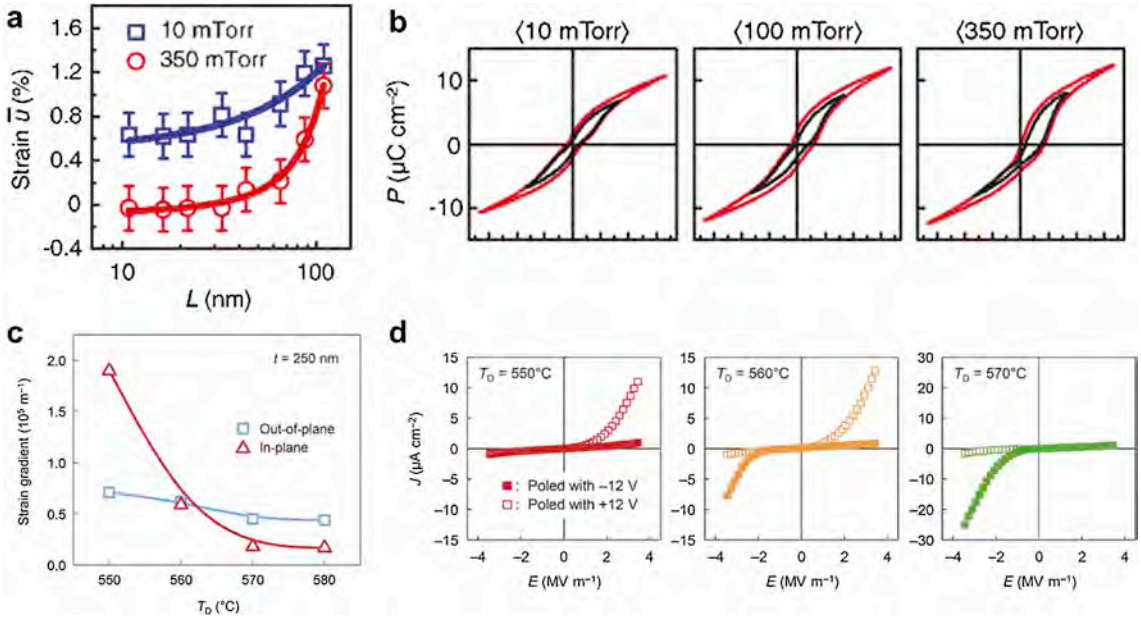

Fig. 4.1. Strain gradients and its influence on ferroelectric and electrical properties in ferroelectric thin films. (a) Variation of the average in-plane strain as a function of penetration depth in $HoMnO_3$ thin films deposited at different oxygen partial pressure P_{O2}. (b) Corresponding polarization hysteresis loops varying from double loops to biased single loops for different P_{O2} during the growth process. (c) Measured out-of-plane and in-plane strain gradients in 200 nm $BiFeO_3$ films deposited at different temperature T_D. (d) Corresponding current density-electric field curves measured in $BiFeO_3$ films at different T_D. (a, b) Adapted with permission from [226] Copyright © 2011, American Physical Society. (c, d) Adapted with permission from [228] Copyright © 2014, John Wiley and Sons.

4.1. Manifestation by strain gradient engineering

Fabrication of epitaxial oxide thin films may unintentionally induce strain gradients along the out-of-plane direction. This unwanted structural nonuniformity is believed to be detrimental to the dielectric properties of ferroelectric films [84,85]. However, a strain gradient can be deliberately engineered in ferroelectric nanostructures to realize desired functions, a process known as the strain-gradient engineering. Typical examples of strain-gradient engineering in thin film ferroelectrics and the impact on ferroelectric and transport properties are shown in Fig. 4.1. For instance, Noh's group demonstrated that the strain relaxation behaviors can be tuned by adjusting the oxygen partial pressure [226] and/or the deposition temperature [227,228] during the film growth. As a result, a giant strain gradient of 10^5–10^6 m^{-1} can be built into epitaxial ferroelectric thin films [226,228]. The resulting built-in field aligns the dipole defects during the cooling process and consequently modifies the domain configurations and the corresponding hysteresis loops [226,228]. Along with controlling the film thickness, the self-poling direction of epitaxial $BiFeO_3$ [227] and $BaTiO_3$ [229] films can be altered, and the resultant rectifying diode behaviors have been explored [227,228,230]. These studies have expanded the strain engineering of functional oxides [231] into the heterogeneous strain regime where the flexoelectric effect may dominate.

Aside from generating gradients by strain relaxation, there are other strategies to bring strain gradients into nanostructured ferroelectrics. For example, compositionally graded PZT and BST thin films have shown significant chemical and structural gradients, leading to modified ferroelectric and dielectric properties [86,87,232]. An extreme example utilizing the chemical inhomogeneity to create strain gradients may be the recent work by Wu et al. where a *digitized* nanofilm with a layer-varying composition of $SrTiO_3$ and $LaAlO_3$ demonstrates a flexoelectric polarization [233]. The flexoelectricity enabled by chemical gradients has also been realized in core-shell dielectric nanoparticles at temperatures as high as 800 °C [234]. Moreover, high-quality multilayered heterogeneous oxides bring a new dimension of materials design and, concomitantly, emergent phenomena such as new topological phases in ferroelectric superlattices [224]. The large strain gradient from a single layer can be continuously transferred into multilayer heterostructures, as demonstrated by Tang et al. [235]. With large and continuous strain gradients across the layers, it is interesting to explore how the flexoelectric coupling plays a role in these heterostructures. A very recent work has revealed that a strain gradient coupled with the composition gradient is able to control the disorder dynamics in $KTa_{1-x}Nb_xO_3$ single crystals [236]. Additionally, localized strain doping by helium implementation [237–239] and dynamical optical enhancement of long-range strain gradients [240] also open new perspectives in the strain gradient engineering for enhanced flexoelectricity.

4.2. Manifestation by stress gradients at the nanoscale

Although the aforementioned strain gradient engineering provides a viable way to tune long-range or local structural inhomogeneity, it is challenging to dynamically and locally modulate the introduced strain gradients. In contrast, it is more flexible to activate flexoelectric-related phenomena via external mechanical stress rather than built-in strains.

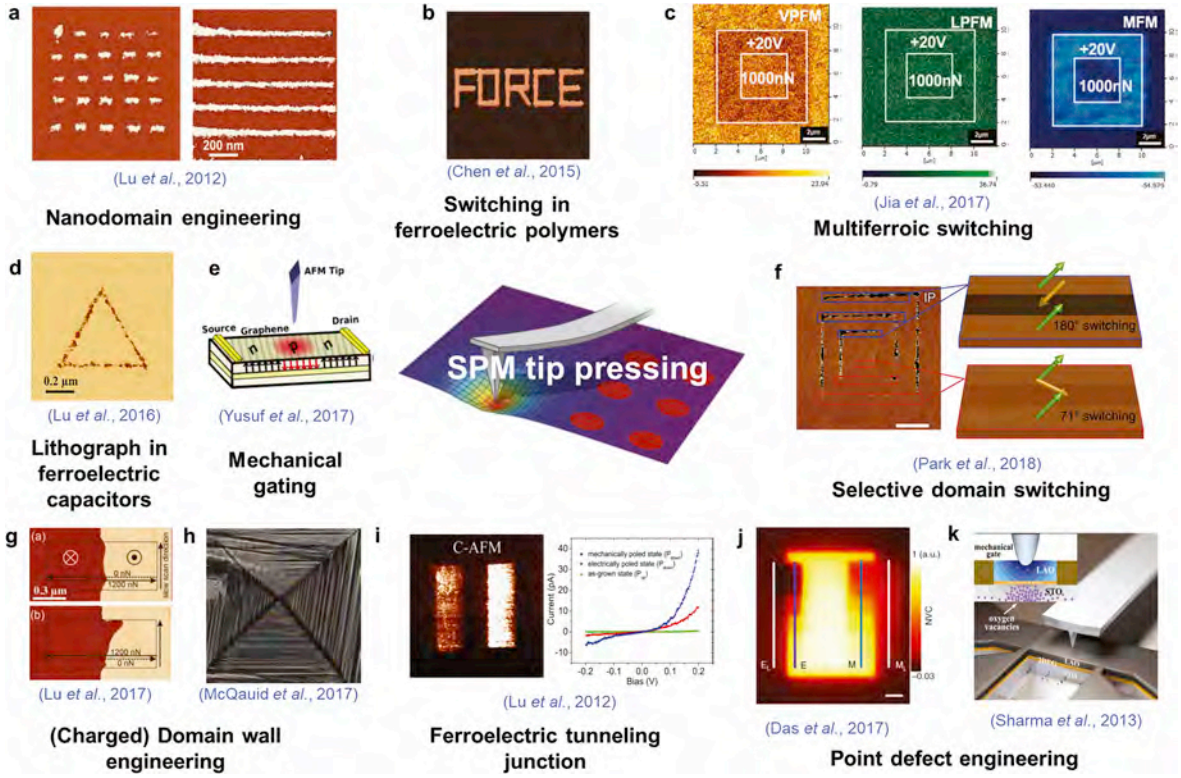

Fig. 4.2. Mechanical control of multifunctionalities in ferroelectric and multiferroic nanostructures by using SPM tips. Detailed descriptions and reference of each figure are given in the text. (a) Adapted with permission from [241] Copyright © 2012 The American Association for the Advancement of Science. (b) Adapted with permission from [249] © 2015 AIP Publishing. (c) Adapted with permission from [253] Copyright © 2017 Springer Nature. (d) Adapted with permission from [256] Copyright © 2016 American Chemical Society. (e) Adapted with permission from [257] Copyright © 2017 IOP Publishing. (f) Adapted with permission from [251] Copyright © 2018 Springer Nature. (g) Adapted with permission from [244] Copyright © 2017 AIP Publishing. (h) Adapted with permission from [262] Copyright © 2013 American Chemical Society. (i) Adapted with permission from [259] Copyright © 2012 American Chemical Society. (j) Adapted with permission from [263] © 2017 CC BY license. (k) Adapted with permission from [258] Copyright © 2017 CC BY license.

The advancement of scanning probe microscopy (SPM) techniques offers such a mechanical control. A crude estimation shows that, by applying a few μN force through a rigid, sharp probe onto an oxide surface, one can generate stress of several GPa, which decays in tens of nanometers from the center of the contact area. The created highly-concentrated stress field can directly interact with the ferroelectric polarization through both piezoelectric and flexoelectric effects. For example, it is conventionally believed that a mechanical force can only induce non-180-degree ferroelastic switching via piezoelectricity. However, Lu et al. demonstrated that, due to the flexoelectric effect, the ferroelectric polarization in ultrathin $BaTiO_3$ films can be reversed by 180-degree through a ~1 μN mechanical load from an SPM tip (Fig. 4.2a) [241]. Similar mechanical switching of ferroelectric domain has been realized in a wide spectrum of ferroelectric thin films, such as $BaTiO_3$ [242,243], $PbTiO_3$ [244], $PbZr_{0.2}Ti_{0.8}O_3$ [245], nanopolar regions in $SrTiO_3$ [246], Al-doped HfO_2 [247], bismuth-layered $K_{0.5}Bi_{4.5}Ti_4O_{15}$ [248], ferroelectric polymers PVDF-TrFE (Fig. 4.2b) [249], and multiferroics such as $BiFeO_3$ [250,251], $TbMnO_3$ [252] and $Bi_5Ti_3FeO_{15}$ (Fig. 4.2c) [253]. These findings demonstrate the universal existence of strong flexoelectricity in ferroelectrics. Theoretical studies of mechanical switching have highlighted the role of flexoelectricity over piezoelectricity in unbalancing the free energy landscape [171] and creating polarity, while a few recent studies have also examined alternative mechanisms for the observed mechanical switching, such as bulk chemical transport and surface effects [174,254].

The mechanical approach to switching ferroelectric domains circumvents voltage-induced side effects, such as leakage, charge injection, and dielectric breakdown. Moreover, mechanically-written nanodomain arrays are spatially denser than the electrically-induced counterparts [249,255] while exhibiting comparable response time and retention properties [249]. These features of mechanical switching offer a new perspective for designing low-energy ultrahigh-density memories. Furthermore, attempts have been made to utilize mechanical control of polarization for ferroelectric nanodomain lithography in capacitors (Fig. 4.2d) [256], gating ferroelectric field-effect transistors (Fig. 4.2e) [257], controlled selection of switching paths (Fig. 4.2f) [251], domain wall engineering (Fig. 4.2g and h) [244,258], and switching electroresistivity for ferroelectric tunneling junctions (Fig. 4.2i) [259]. Although mechanical switching by SPM pressing is limited to the unidirectional polarization reversal, recent theoretical [174,260] and experimental explorations [251,261] have attempted to go beyond this limit.

Aside from polarization switching, many other mechanically-mediated phenomena have been reported where flexoelectricity is directly or indirectly involved. For example, Das et al. applied a mechanical scanning probe to dynamically reconfigure the surface oxygen vacancy distribution in a nonferroelectric $SrTiO_3$ thin film (Fig. 4.2j) [263]. The depolarization field generated by flexoelectricity is attributed to be the main driving force. Similar pressure-induced migration of charged defects in oxides has also been evident in tuning the $LaAlO_3/SrTiO_3$ interface conductivity (Fig. 4.2k) [262] and switching the electroresistance in non-stoichiometric NiO films [264,265]. In addition, a reversible super tetragonal-to-rhombohedral phase transition in highly-strained $BiFeO_3$ films can be modulated by a mechanical scanning probe [266–269] whereas the role of flexoelectricity in this stress-induced transition has not yet been explored. Besides, ferromagnetic switching accompanied by ferroelectric switching in response to a mechanical load has been reported recently in multiferroic $Bi_5Ti_3FeO_{15}$ thin films [253], yet whether the flexomagnetic effect or a flexoelectric-mediated magnetoelectric coupling is responsible for the phenomena remains an open question.

Flexoelectricity also plays a significant role in nanoindentation, where an irreversible deformation on a bulk single crystal sample is created by a relatively large indenting force. The size-dependent hardening effect has been measured in $BaTiO_3$ [189] and $SrTiO_3$ single crystals [191] and is attributed to the flexoelectric effect [192]. It is interesting to note that this elastic stiffening in nanoindentation has enlightened a viable method to quantify flexoelectric coefficient [164] and to mechanically identify the polarization directions in single crystal ferroelectrics [270].

4.3. Spontaneous flexoelectricity at general interfaces

Interfaces in materials are characterized by structural and property changes from the adjacent regions. In a chemically homogeneous mono-phase single crystal, twin walls and APBs are typical types of homogeneous interfaces. Phase boundaries appear in multiphase materials and the grain boundaries in polycrystals. Heterogeneous interfaces represent the boundary where two different materials conjunct and the structures and properties can be distinct than the two neighbors. Finally, surface as one special interface has unique properties dissimilar to corresponding bulk. In principle, flexoelectricity exists in all these general interfaces. In this subsection, we provide a few examples to illustrate the spontaneous appearance of flexoelectricity at general interfaces.

4.3.1. Domain walls

Ferroic transitions often lead to the formation of domains separated by domain walls. The overall responses of a ferroic solid to external fields are often strongly influenced by the behavior of domain walls. Interestingly, domain walls also possess intriguing properties, for instance, high electronic conductivity [90,271–273], chirality [274,275], and oxygen vacancy segregation [276,277] in ferroelectric domain walls and polar domain wall arising from incipient ferroelectrics [201,278–282]. It was suggested that the domain walls of ferroelectrics might even be treated as a new engineering element in multifunctional materials [283]. Due to the experimental difficulty of separating flexoelectric contribution from the piezoelectric effect, most existing efforts studying the influence of flexoelectric effect on domain wall structures have been based on the phenomenological LGD theory. The flexoelectric-induced behaviors of domain walls can be classified into the following three categories.

(1) Polar domain walls in nonpolar paraelectric phases

By introducing the flexoelectric coupling terms to the LGD free energy, Tagantsev et al. [284] demonstrated that the flexoelectricity can introduce polar instabilities at the APBs of $SrTiO_3$. Morozovska et al. [88,89] systematically studied the so-called *roto-flexo* effect, i.e., the appearance of electric fields proportional to polarization and structural order parameter gradients across a domain wall. They demonstrated that the flexoelectric effect can induce polarization as high as several $\mu C/m^2$ in both the APBs and the twin walls of $SrTiO_3$. Employing the phase-field method, Gu et al. [170] also demonstrated that the flexoelectric effect is the most likely origin of the polar domain walls in $CaTiO_3$.

(2) Domain wall structures complicated by the flexoelectric effect

The 180-degree domain walls of tetragonal ferroelectric phases (with out-of-plane polarization) have long been believed Ising-like, i.e., with no in-plane component associated with polarization rotation. Yudin et al. [275] revisited the 180-degree domain wall of $BaTiO_3$ and showed that the conventionally-believed Ising walls are complicated by a Bloch component and become bichiral due to the flexoelectric effect. The polarization component perpendicular to the domain wall (Neél component), which may also be introduced by the flexoelectric effect, is however ignored in this work. Based on phase-field modeling [45] and DFT calculations [168], it was shown that the 180-degree domain wall of tetragonal $BaTiO_3$ exhibits both Bloch and Neél characteristics in addition to the Ising feature. As shown in Fig. 4.3, the additional two features are complicated by the domain wall orientation which is related to the flexoelectric effect [45].

(3) Flexoelectric-mediated domain wall conduction

Domain wall conduction has been extensively observed and investigated in ferroelectric materials. Apart from charged domain walls, uncharged domain walls have also shown appreciable conductivity due to carrier accumulation around wall regions in ferroelastics, multiferroics, and semiconducting ferroelectrics. The flexoelectricity induced by the strain and structural gradient across the domain walls is believed to be responsible for or at least contribute to some of these phenomena. For example, Eliseev et al. [285]

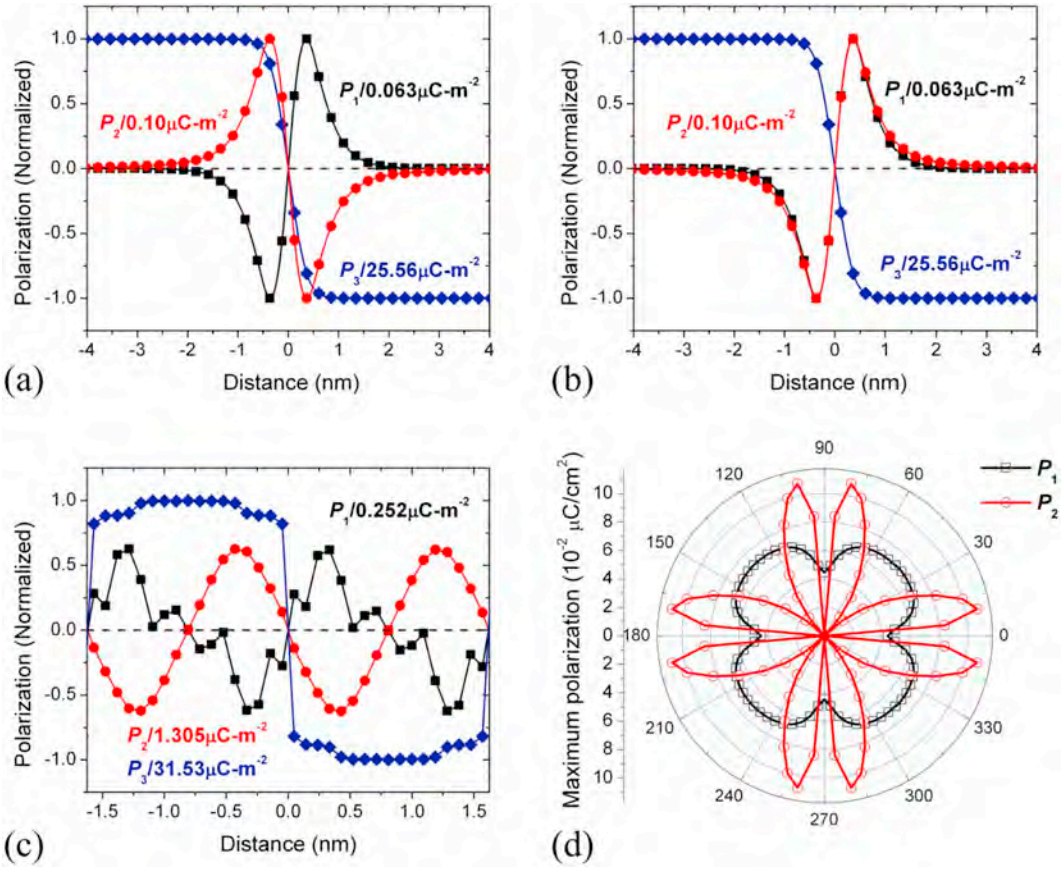

Fig. 4.3. Polarization profiles of 180° domain walls. (a) P_1 and P_2 distribution at $\theta = 5\pi/12$ and (b) at $\theta = \pi/12$ from the phase-field method. (c) P_1 and P_2 profiles at $\theta = 5\pi/12$ from first-principles calculations. (d) Maximum absolute value of the polarization components induced by the flexoelectric effect in the wall as a function of the rotation angle θ, calculated from the phase-field method. P_1 remains identical while P_2 flips with θ. Both P_1 and P_2 are independent of P_3. θ indicates the angle between the domain wall and the crystallographic direction $[1\,0\,0]_C$. The subscript C denotes the original crystallographic coordinate of the pseudocubic lattice. The domain wall lies in the x_2-x_3 plane and perpendicular to the x_1 direction. Reprinted with permission from [45] Copyright © 2014, American Physical Society.

theorized the direct and indirect mechanism of uncharged domain wall conductivity where flexoelectric and rotostrictive couplings are involved. Morozovska et al. demonstrated that the flexoelectric coupling and angle-dependent electrostriction lead to the local band bending and thus anisotropic domain wall conductivity [91].

4.3.2. Morphotropic phase boundaries

Morphotropic phase boundaries (MPB) are phase boundaries associated with structural phase transitions without composition changes. The most famous MPB exists in PZT near 52/48 composition and is believed to account for the high piezoelectric performance in this perovskite solution system. A strain-stabilized MPB has been reported in $BiFeO_3$ by Zeches et al. [286] where the coexistence of rhombohedral-like and tetragonal-like polymorphs leads to huge structural variation across the MPB, indicating a high likelihood for flexoelectric-related effects to occur. Chu et al. [200] firstly observed an enhanced anisotropic interfacial photocurrent at the MPB of highly strained $BiFeO_3$ thin films. They used phase-field simulations to show that the strong flexoelectric effect at the domain wall gives rise to the charged domain walls. The charges across a wall generate a strong built-in electric field, which separates the electron-hole pairs and consequently enhances the photocurrent. In similar mixed-phase $BiFeO_3$ thin films, Cheng et al. [287] established a correlation between the elastic stiffness modulation and piezoresponse across the phase boundary. They believe that the flexoelectric effect gives rise to the enhancement of piezoelectric responses at the boundaries and rhombohedral-like phase which accounts for the giant electromechanical properties of mixed-phase $BiFeO_3$ thin films. Additionally, modulated phases and their evolution at the ferroelectric-antiferroelectric MPB in Sm-doped $BiFeO_3$ have been spatially resolved by high-resolution scanning transition electron microscopy [288]. Theoretical analysis has attributed this instability to the negative effective domain wall energy which arises from flexoelectric coupling between local structural and polarization orderings in ferroics. The intrinsic flexoelectric coupling is also believed as the driving force for incommensurate phase transitions in antiferroelectricity in $PbZrO_3$ [289] and other incommensurate crystals [290].

4.3.3. Heterogeneous interfaces

The heterogeneous interfaces separating different crystalline materials usually possess distinctive properties and lead to emergent phenomena. The structural, physical, and chemical gradients across the heterogeneous interfaces suggest that strong flexoelectric effects may spontaneously occur in the proximity. Majdoub et al. [291] demonstrated that the dead layers at the metal-dielectric interfaces are associated with the flexoelectric effect using a continuum theory. Similarly, Liu and Wang [292,293] showed that the flexoelectric effect gives rise to enhanced piezoelectric responses in layered super-lattice structures.

4.3.4. Surfaces

Surface polarization has been widely observed in nonpolar dielectric materials. Its emergence may have several different origins, such as surface piezoelectricity [294,295], band gap modifications [296], and surface reconstructions [297]. Even if the surface polarization originates purely from the strain, it still at least has two possible origins, i.e., surface piezoelectricity and surface flexoelectricity [28]. Due to the complexity of surfaces, only a few works have been dedicated to the surface flexoelectric effect. Theoretically, Morozovska et al. investigated the flexoelectric effect at the surfaces using LGD theory [88]. It was found that the flexoelectricity-induced polarization could reach as high as 1–5 $\mu C/cm^2$ at the surfaces of incipient ferroelectric $SrTiO_3$. Experimentally, Tararam et al. characterized the nanoscale electromechanical properties of noncentrosymmetric $CaCu_3Ti_4O_{12}$ ceramics using PFM [298]. They believe that the surface flexoelectricity gives rise to the observed polarization which shows direction and amplitude dependence on grain orientation. Recently, Yang et al. used *in situ* grazing incidence X-ray diffraction and X-ray reflectivity to explore the surface structure of a single domain epitaxial $BiFeO_3$ film with the (1 1 1) orientation [299]. They found large strain gradients ($\sim 10^7$ m^{-1}) at the surface region of the film, giving rise to an irreversible surface structure transition at 500 K via the surface flexoelectric effect. It should be noted that extreme care is needed to separate the surface flexoelectric effect from other interfering effects.

4.3.5. Other defects

Apart from the interfaces, which can be regarded as 2D defects of a crystal structure, there are other types of defects where the ideal periodicity of crystal breaks down. In the proximity of these defects in dielectric materials, large structural variation occurs, and consequently, flexoelectricity can manifest itself. Theoretical predictions of polarization appearance in the vicinity of dislocations, voids, and cracks due to the flexoelectric coupling have been documented [112,300]. A very recent STEM observation on the polarization appearance around the dislocations in $SrTiO_3$ thin films [301] has provided evidence at the atomic level.

4.4. Manifestations by other gradients

The flexoelectric coupling, by definition, connects structural gradients and polarization orderings or vice versa. However, in many classes of materials, especially in ferroics, there are other direct couplings between the structural and polarization orderings that may indirectly mediate flexoelectric effects. In this sense, flexoelectric effects can be indirectly mediated by other graded fields. For example, Kim et al. [302] reported a graded electrical field generated by a thermal gradient across a BST sample with symmetric geometry, which further causes measurable strain due to the converse flexoelectricity. Li et al. [240] demonstrated a giant transient enhancement of strain gradients in $BiFeO_3$ initiated by an optical approach, which can serve as a new dynamical control of flexoelectricity.

The dynamic flexoelectric effect, as phenomenologically defined in Section 2.2, describes the induced polarization due to the acceleration of the medium. In this sense, by measuring the inherent vibration modes of crystals, such as the phonon spectrum, one can identify the role of flexoelectric effect by fitting the spectrum using lattice dynamics theories with flexoelectric coupling considered. For example, Astafiev et al. have shown significant flexoelectric coupling between ferroelectric soft-mode and acoustic phonon branch leads to a sharp maximum in the field dependence of dielectric loss in $SrTiO_3$ [303].

Additionally, the converse flexoelectric effect, e.g., applying a uniform electric field gives rise to a nonuniform strain, or, applying a nonuniform field generates a uniform strain, can be realized as for the direct flexoelectric effect. In this sense, a graded field is not necessary to induce flexoelectric phenomena. Several pieces of experimental evidence on the flexoelectric bending enabled by the converse flexoelectric effect have been documented [304–306]. Very recently, other manifestations of converse flexoelectric effects have been reported, such as the mimicry of piezoelectric responses in non-piezoelectric materials [307], electronic hybridization and lattice vibration enabled by artificial inhomogeneous fields [308], and enhanced actuation in ceramics with graded permittivity by geometric design [309].

The above discussions on a variety of ways to manifest flexoelectric effects at micro and nanoscale are summarized in Table 4.1. The essential philosophy is that *flexoelectricity, by coupling with graded fields, enables a viable way to break the symmetry of materials, thereby giving access to emergent phenomena that are otherwise forbidden in the pristine state*. Finally, as a closing remark for this section, we would like to add a caveat to using this philosophy in the opposite way. After all, it is not always justified to attribute every emergent phenomenon to flexoelectricity in systems subjected to an intrinsic or extrinsic gradient.

5. Challenges: Ambiguities and controversies

Although significant progress has been made in the past two decades in understanding solid-state flexoelectricity, there are remaining ambiguities and controversies even at the conceptual level. There are three major outstanding issues: (1) the arbitrariness and ambiguities in some fundamental concepts due to the lack of convention, (2) the order-of-magnitude discrepancies between

Table 4.1
Summary of various manifestations of flexoelectric effects.

Type of gradients	Source of gradients	Property/Phenomena	Reference
Strain gradient	Strain relaxation	Self-poling	[226–228,310]
		PE loop change (imprint, double loop)	[226,228]
		Dielectric degradation	[84,85]
	Dislocations	Emergence of piezoelectric response	[112]
	Crack	Fracture toughening	[155,112]
Stress gradient	AFM pressing	Mechanical switching	[241,256,257,259]
		DW motion (correlated switching)	[244]
		Charged defect migration	[262–264]
		Phase transition at MPB	[266–269]
		Bulk photovoltaic effect (flexo-photovoltaic effect)	[311]
	Nanoindentation	Indentation size effect	[189,191,192]
		Indentation asymmetry	[270]
Inherent interfaces and defects	Surface	Ferroelectricity and critical thickness	[312–314]
		Shear surface acoustic wave	[43]
		Surface polarity	[298,299]
	Domain walls	Bichiral, mixed Ising-Neél-Bloch components	[45,168,275,315]
		Polarity in incipient ferroelectrics	[170,316]
		DW conduction	[90,273,317]
	Heterogeneous interface	Dead layer	[291]
		Emergence of polarity, piezoelectric response	[88,89,318]
		Enhanced piezoelectric response	[292,293]
	Morphotropic phase boundary	Enhanced piezoelectric response	[287]
		Enhanced anisotropic photocurrent	[200]
Intrinsic vibration	Phonon	Antiferroelectric phase transition	[289]
		Incommensurate phases transition	[288]
Electric fields	Graded field	Bending	[157,319]
	Uniform gradients	Surface bending	[31,304,305]
Chemical inhomogeneity	Composition gradient	Built-in field	[87]

theoretically computed and experimentally measured flexoelectric coefficients, and (3) the disagreements among theoretical evaluations of the flexoelectric coefficient. In this section, we attempt to clarify the ambiguities in the basic concepts, discuss possible origins for the discrepancies in evaluating flexoelectricity, and reveal the subtleties among theoretical calculations of flexoelectric tensors. Some open questions are briefly mentioned as well.

5.1. Ambiguities in some basic concepts

5.1.1. Flexoelectric phenomena

The flexoelectricity is a multidisciplinary topic involving researchers from materials science, chemistry, physics, mechanical engineering, electrical engineering, etc. As a result, there is a lack of consistency in the convention of terminology and symbols, causing confusions even at the fundamental level. On the one hand, the same or similar terminology may refer to disparate phenomena. For example, *flexoelectricity* also refers to the coupling between electric polarization and inhomogeneous magnetization in the magnetism community (a.k.a. *spin flexoelectricity*) [320–322]. On the other hand, different types of terminology have been used to denote the same phenomenon. For instance, nonlocal piezoelectric effect [31,32,323] or flexure-electric effect [324] has been used in some early works to refer to the phenomenon known as the flexoelectric effect in nowadays' context. Therefore, it is of primary importance to unify the terminology.

Another ambiguity is related to the diverse contributions of a flexoelectric response. According to Tagantsev's [28], unlike piezoelectricity which is purely a static bulk property, the flexoelectric response in a finite sample consists of bulk and surface contributions that are comparable in amplitude. The bulk flexoelectricity is characterized by different tensor coefficients under static and dynamic stimuli while the surface contribution inevitably combines a flexoelectricity-originated and a surface piezoelectricity response. For most experimental measurement of flexoelectricity, the static bulk and surface contributions can be comparable, whereas corresponding theoretical models generally assume a bulk static flexoelectric contribution only. Therefore, it may be inappropriate to interpret the experimental values as the bulk flexoelectric property of the material. Instead, it is encouraged to explicitly elucidate which types (bulk or surface, static or dynamic) of flexoelectric coefficients one refers to before making a comparison.

The direct flexoelectric effect has its converse counterpart known as the converse or inverse flexoelectric effect. However, it is unclear how to define this converse flexoelectric effect in a thermodynamically consistent way. Specifically, the converse flexoelectric effect can refer to the homogeneous strain/stress response induced by a graded electric/polarization field, as defined in some works (e.g., Ref. [12]); it has also been used to denote the inhomogeneous strain/stress response caused by a homogeneous electric/polarization field [31,304,305,325]. This ambiguity is closely related to the paradox that "a flexoelectric sensor is not an actuator at the same time" which has been addressed by considering the finite-size effect [11,95]. However, an unambiguous treatment of the

converse flexoelectric effect is still absent.

Finally, arising interests in the flexoelectric effects in 2D materials, polymers, and soft bio-membranes (c.f. Section 6.2) may generate other new concepts. For example, as the soft and low-dimensional materials can sustain large bending curvature, it is very likely the relationship between a strain gradient and the induced electric displacement is no longer linear, which may have a distinct origin from the linear flexoelectricity that is being intensively investigated so far. In this sense, it is necessary to differentiate between the linear and nonlinear flexoelectricity [60,74,200].

5.1.2. Flexoelectric tensors

The flexoelectric tensor μ_{ijkl} is often defined as a fourth-rank tensor linking the strain gradient to the induced electric polarization. At first glance, it resembles other fourth-rank tensors, e.g., elastic stiffness c_{ijkl} compliance s_{ijkl} and electrostrictive tensor Q_{ijkl}, but scrutiny of μ_{ijkl} reveals complications due to its reduced symmetry. Here, we first briefly describe three possible ambiguities in the definition of a flexoelectric tensor, including the definitions, the symbols, and the subscript orderings. Next, we focus on the flexoelectric tensor defined by the symmetrized strain tensor and discuss the feasibility of using the reduced notation for flexoelectric tensors in cubic and isotropic materials.

5.1.2.1. Definition of flexoelectric tensors. The ambiguity in the definition of the flexoelectric tensor is threefold. First, various forms of the constitutive equation for the flexoelectric effect have been adopted. Consequently, different versions of flexoelectric tensors are defined. Taking the electric field $\boldsymbol{E}$ and the mechanical strain $\boldsymbol{\varepsilon}$ as the two independent thermodynamic state variables, one can readily derive the constitutive equation for an isothermal process as

$$P_i = \epsilon_0 \chi_{ij}^{\varepsilon} E_j + e_{ijk}^{E} \varepsilon_{jk} + \mu_{ijkl}^{E} \varepsilon_{kl,j} \tag{5.1a}$$

$$\sigma_{ij} = c_{ijkl}^{E} \varepsilon_{kl} + e_{kij}^{\varepsilon} E_k + \mu_{klij}^{\varepsilon} E_{k,l} \tag{5.1b}$$

where c_{ijkl}^{E}, $\epsilon_0 \chi_{ij}^{\varepsilon}$,$e_{ijk}^{E}$ and e_{kij}^{ε}, and μ_{klij}^{E} and μ_{klij}^{ε} are the corresponding elastic, dielectric, piezoelectric, and flexoelectric coefficients, respectively. The superscript indicates the tensor quantities are determined under fixed-electric field or fixed-strain conditions. Following Maxwell relationship, one can easily prove that $e_{ijk}^{E} = e_{kij}^{\varepsilon}$ and $\mu_{ijkl}^{E} = \mu_{klij}^{\varepsilon}$. Similarly, by choosing other pairs of state variables, the other versions of constitutive equations combining dielectric, piezoelectric, and flexoelectric properties can be obtained as

$$\varepsilon_{ij} = s_{ijkl}\sigma_{kl} + g_{kij} P_k + F_{klij} P_{k,l} \tag{5.1c}$$

$$E_i = (\epsilon_0)^{-1}\eta_{ij} P_j + g_{ijk}\sigma_{jk} + F_{ijkl}\sigma_{kl,j} \tag{5.1d}$$

$$P_i = \epsilon_0 \chi_{ij} E_j + d_{ijk}\sigma_{jk} + \mathcal{M}_{ijkl}\sigma_{kl,j} \tag{5.1e}$$

$$\varepsilon_{ij} = s_{ijkl}\sigma_{kl} + d_{kij} E_k + \mathcal{M}_{klij} E_{k,l} \tag{5.1f}$$

$$E_i = (\epsilon_0)^{-1}\eta_{ij} P_j + h_{ijk}\varepsilon_{jk} + f_{ijkl}\varepsilon_{kl,j} \tag{5.1g}$$

$$\sigma_{ij} = c_{ijkl}\varepsilon_{kl} + h_{kij} P_k + f_{klij} P_{k,l} \tag{5.1h}$$

The superscripts of relevant materials property tensors are omitted for simplicity. In Eqs. (5.1a–h), e_{ijk}, g_{ijk}, d_{ijk}, and h_{ijk} represent the components of the four types of piezoelectric tensors while μ_{ijkl}, F_{ijkl}, f_{ijkl} and $\mathscr{M}_{ijkl}$ are for flexoelectric tensors. The latter four are mutually related by

$$\mu_{ijkl} = \epsilon_0 \chi_{im} f_{mjkl} \tag{5.2a}$$

$$F_{ijkl} = s_{ijmn} f_{mnkl} \tag{5.2b}$$

$$\mathcal{M}_{ijkl} = s_{ijmn}\mu_{mnkl} \tag{5.2c}$$

$$\mathcal{M}_{ijkl} = \epsilon_0 \chi_{im} F_{mjkl} \tag{5.2d}$$

Generally, the flexoelectric coefficient is recognized as the linear relationship between a strain gradient and polarization, e.g., μ_{ijkl} in Eqs. (5.1a, b) with an SI unit as C/m. Another commonly used flexoelectric tensor is the f_{ijkl} in Eqs. (5.2 g,h), which is also termed *the flexoelectric coupling* (*flexocoupling*) *coefficient*, or the *flexovoltage coefficient* [97], with an SI unit of V. It is believed the flexocoupling coefficient serves as a ground-state property, which is nearly independent of temperature and dielectric permittivity.

The second ambiguity originates from the different metrics of the deformation, i.e., the definition of the strain tensor. For flexoelectric effect in solids, the deformation is usually infinitesimal, and the linearized strain tensor is often adopted. The symmetrized is defined as $\varepsilon_{ij} = \frac{1}{2}(u_{i,j} + u_{j,i})$ while the unsymmetrized as $\nu_{ij} = u_{i,j}$. In the couple stress theory of flexoelectricity [56,57,326], the rotation gradient is used as the metric for the higher order elasticity, i.e., the gradient of the anti-symmetry part of the displacement gradients, $\omega_{ij} = \frac{1}{2}(u_{i,j} - u_{j,i})$. For systems with large deformation, the nonlinearized strain tensor becomes a convenient choice [60,123]. For simplicity, here we focus on the infinitesimal strain definition and discuss the difference in deriving flexoelectric tensors by using the symmetrized or the unsymmetrized strain tensor. This ambiguity was underlined by Hong [15] in

developing the microscopic theory of flexoelectricity. Following Hong et al. [15], we write the *type-I flexoelectric tensor* as

$$\mu^{\mathrm{I}}_{ijkl} = \frac{\partial P_i}{\partial \eta_{j,kl}} \tag{5.3}$$

where $\eta_{j,kl}$ is the gradient of the unsymmetrized strain. This definition is straightforward for complex mathematical derivations in the microscopic theory of flexoelectricity (e.g., Ref. [15]). Sometimes it is more convenient to use the *type-II flexoelectric tensor* defined as

$$\mu^{\mathrm{II}}_{ijkl} = \frac{\partial P_i}{\partial \varepsilon_{kl,j}} \tag{5.4}$$

where $\varepsilon_{kl,j}$ is the gradient of symmetric strain ε_{kl}. This type-II flexoelectric tensor is more suitable for formulating the thermodynamic LGD models and for drawing comparisons with experimental measurements. Besides, type-I and type-II flexoelectric tensors can be mutually converted using the relations

$$\mu^{\mathrm{II}}_{ijkl} = \mu^{\mathrm{I}}_{iklj} + \mu^{\mathrm{I}}_{iljk} - \mu^{\mathrm{I}}_{ijkl} \tag{5.5a}$$

$$\mu^{\mathrm{I}}_{ijkl} = \frac{1}{2}(\mu^{\mathrm{II}}_{ikjl} + \mu^{\mathrm{II}}_{iljk}) \tag{5.5b}$$

In the present review, we use μ_{ijkl} to denote the type-II flexoelectric tensor unless otherwise stated.

Lastly, the subscript ordering for a flexoelectric tensor matters. For the type-II flexoelectric tensor defined in Eq. (5.4), only two of the four subscripts representing the symmetrized strain are interchangeable. However, the position of this pair of interchangeable indices varies in different works. The inconsistent use of the subscript ordering may lead to misinterpretation. For instance, μ_{1122} may refer to the transverse (the last two subscripts are interchangeable, $\mu_{\mathbf{1122}}$ (bold here for emphasis)) or the shear (the middle two subscripts are interchangeable, $\mu_{\mathbf{1122}}$ (bold here for emphasis)) components of a flexoelectric tensor. Here in this review, unless otherwise stated, we keep using the last two subscripts as interchangeable indexes for the strain tensor, which has been most often used in literature.

Based on the discussion above, we suggested a convention of the terminology, definitions, symbols and subscript orderings as listed in Table 5.1.

5.1.2.2. The symmetry of flexoelectric tensors. Flexoelectricity exists in all crystals because it is described by the fourth-rank flexoelectric tensor. However, unlike other fourth-rank tensors such as the electrostrictive tensor (Q_{ijkl}) and the elastic stiffness/compliance tensor (c_{ijkl}/s_{ijkl}), the flexoelectric tensor is invariant only by interchanging the two indexes of the symmetrized strain tensor, i.e., $\mu_{ijkl} = \mu_{ijlk}$, whereas other possible symmetries, e.g., $Q_{ijkl} = Q_{jikl} = Q_{ijlk}$ and $c_{ijkl} = c_{jikl} = c_{klij}$, are not applicable to μ_{ijkl}. Using the three-dimensional rotation group theory, Quang and He [330] calculated the number and types of all possible rotational symmetries for flexoelectric tensors and the number of independent tensor components for each symmetry class. Later, Shu et al. [331,332] used the fundamental tensor relationship, obtained the same results, and further extended the symmetry analysis to converse flexoelectric tensors. Table 5.2 summarizes the number of nonzero components of c_{ijkl}/s_{ijkl}, Q_{ijkl}, and μ_{ijkl} for different point groups and Curie groups. Compared with the other common fourth-rank tensors, the flexoelectric tensors (both direct and inverse) generally have more independent nonzero components. For example, for the point group with the lowest symmetry, there are 54 independent components for μ_{ijkl} whereas 36 for Q_{ijkl} and 21 for c_{ijkl}/s_{ijkl}.

Notably, the number of independent components is identical for all these fourth-rank tensors in the cubic and the isotropic point groups. As a result, Voigt notation commonly used for c_{ijkl}/s_{ijkl} has been extensively adopted to reduce the fourth-rank flexoelectric tensor into a 6-by-6 matrix, e.g., in Ref. [12]. However, the conventional Voigt notation, as pointed out by Shu et al. [333], does not

Table 5.1
The unified definitions of flexoelectric tensors.

Naming and SI units	Definition	Symbols appear in the literature
Flexoelectric coefficients		
Type-I flexoelectric coefficients μ^{I}_{ijkl}, (C/m)	$\mu^{\mathrm{I}}_{ijkl} = \left(\frac{\partial P_i}{\partial \nu_{kl,j}}\right)_E$ where $\nu_{kl} = \frac{\partial u_k}{\partial x_l}$	μ in Refs. [15,69,77] f in Ref. [30]
Type-II flexoelectric coefficients μ^{II}_{ijkl} [b], (C/m)	$\mu^{\mathrm{II}}_{ijkl} = \left(\frac{\partial P_i}{\partial \varepsilon_{kl,j}}\right)_E$ where $\varepsilon_{kl} = \frac{1}{2}\left(\frac{\partial u_k}{\partial x_l} + \frac{\partial u_l}{\partial x_k}\right)$	μ in Refs. [12,34–39,75,178,179,291,327–329] f in Refs. [166,189,198,218,226,241] F in Ref. [330]
Flexoelectric coupling coefficients (type-II)		
a.k.a. flexocoupling, flexovoltage coefficients f_{ijkl}, in V	$f_{ijkl} = (\epsilon_0)^{-1}\eta_{lm}\mu^{\mathrm{II}}_{mjkl}$ where $\chi_{im}\eta_{mj} = \delta_{ij}$	$2(\gamma + \eta)$ in Ref. [84,85,313] h in Ref. [69] f in Ref. [5,11,178] φ in Ref. [79] g in Ref. [15]

Table 5.2
The number of nonzero components of three fourth-rank tensors for different point groups and Curie groups. Reprinted with permission from [331] Copyright © 2011, AIP Publishing LLC.

Point groups and Curie groups	Elastic stiffness/compliance tensor (c/s)	Electrostrictive tensor (Q)	Direct/inverse flexoelectric tensor (μ/μ^*)
1, $\bar{1}$	21	36	54
2, m, 2/m	13	20	28
222, mm2, mmm	9	12	15
3, $\bar{3}$	7	12	18
32, 3m, $\bar{3}$m	6	8	10
4, $\bar{4}$, 4/m	7	10	14
4mm, $\bar{4}$2m, 422, 4/mmm	6	7	8
6, $\bar{6}$, 6/m, ∞, ∞/m	5	8	12
622, 6mm, $\bar{6}$m2, 6/mmm, ∞2, ∞m, ∞/mm	5	6	7
23, m3	3	4	5
432, $\bar{4}$3m, m3m	3	3	3
∞∞, ∞∞m	2	2	2

generally apply for the low-symmetry flexoelectric tensor. Instead, a 6-by-9 matrix should be used to adequately represent the 54 independent components of a direct flexoelectric tensor while a 3-by-18 matrix for the converse flexoelectric tensor. The full matrix notations of the flexoelectric tensors for all point groups are given in Refs. [331,333]. Nevertheless, for crystals with the cubic symmetry, it is still safe to use three components to denote the longitudinal, transverse, and shear components of a flexoelectric tensor, i.e., $\mu_{1111} = \mu_{11}$, $\mu_{1122} = \mu_{12}$, $\mu_{1212} = \mu_{44}$. Very recent, it has been suggested by Eliseev et al. that there exists a hidden symmetry in the flexoelectric tensor, which may lead to a further reduction in the number of independent components [334].

5.1.2.3. The upper limit of flexoelectric coupling tensors. There is a constraint on the strength of flexocoupling coefficient f_{ijkl}, known as the upper limit of bulk static flexoelectricity [217], which can be derived from the thermodynamic stability criteria of the parent phase. Beyond this limit, incommensurate polarization states will emerge, as confirmed by phase-field simulations [46,163]. For cubic perovskites, the upper limit of the flexoelectric tensor can be written as

$$f_{1212}^2 < c_{1212}g_{1212} \tag{5.6a}$$

$$(f_{1111} - f_{1122})^2 < (c_{1111} - c_{1122})(g_{1111} - g_{1122}) \tag{5.6b}$$

where c_{ijkl} and g_{ijkl} are the tensor components of the elastic stiffness and the gradient energy coefficient. This upper bound estimation has been extensively adopted to examine the rationality of the measured or calculated flexocoupling constants [15,79]. However, this relation depends on whether higher-order coupling terms are included in the total thermodynamic potential (c.f. Eqs. (2.1) and (2.15)). With the strain-gradient contribution, i.e., $\frac{1}{2}v\left(\frac{\partial\varepsilon}{\partial x}\right)^2$, added into the free energy, Morozovska et al. [92] demonstrated the upper limit in Eq. (5.6) reduces to a more general form

$$f^2 < cg + \alpha_S v \tag{5.7}$$

where α_S is a function of Landau-Devonshire parameters (the α's in Eq. (2.1)), and thus, the upper bound limit becomes temperature-dependent. Essentially, the higher-order coupling terms serve as a modification of the smooth criteria of the thermodynamic potential which has been changed by the Lifshitz form of the flexoelectric contribution. In this sense, for thermodynamic consistency, the coupling term of strain gradient elasticity should always be incorporated within the phenomenological free energy of bulk flexoelectricity, i.e., Eq. (2.1), as advocated by many authors as well [51,164,335]. Otherwise, the upper limit given by Eq. (5.6) needs to be satisfied.

5.1.3. Flexoelectric fields

The concept, *flexoelectric field* (*flexo-field*), is coined to represent an *effective electric field* in the materials subjected to a mechanical strain gradient. The flexoelectric field is commonly utilized to evaluate the strength of flexoelectricity in many emergent phenomena, e.g., in Ref. [241]. However, the same terminology has been used to refer to logically distinct physical quantities by different authors, which may cause confusion and even misinterpretation of the observed phenomena.

The key point to differentiate is whether the *flexoelectric field* refers to the *cause* of polarization or the *outcome* of the polarization induced by a strain gradient.

From a macroscopic perspective, a strain gradient acts as a driving force to produce electric polarization via the flexoelectric effect (c.f. Section 2.2.1). Since the driving force of polarization has the same SI unit (V/m) as an electric field, it is convenient to equate the strain gradient to a local electric field defined as

$$E_i = f_{ijkl}\varepsilon_{kl,j} \tag{5.8}$$

which is thus termed the *flexoelectric field*. Notably, the flexoelectric field defined in this sense is by no means a macroscopic electric field [11]. It is not curl-free in general and cannot be associated with an electrostatic potential. As a result, one should not expect the

Table 5.3
Possible reasons for the discrepancy between the measured and calculated flexoelectric coefficients.

Possible reasons	Typical materials	References
From experiments		
Reorientation of existing polar nanoregions above T_C	PMN-PT single crystal	[181]
Order-disorder phase transition character	$BaTiO_3$ single crystal	[97]
Local chemical inhomogeneity	BST ceramics	[337]
Flexoelectric poling	BST ceramics	[337]
Surface contribution above T*	$BaTiO_3$ single crystal	[97]
Surface polarity	$BaTiO_3$ ceramics	[339]
Inhomogeneity induced by synthesis and processing	BST ceramics	[336]
From theories and calculations		
Pseudo Jahn-Teller effect needs to be considered in theoretical estimations	$BaTiO_3$	[340]
Subtleties in *ab initio* calculations	$BaTiO_3$, $SrTiO_3$	[15,77,218]
Oversimplification of the models in experiments	General	[154]
Surface contribution need to be included in *ab initio* calculations	$SrTiO_3$	[79]
Other relevant effects need to be included in *ab intio* calculations	$SrTiO_3$	[50,80]
Surface contribution need to be included in the phenomenological theory	General	[95]

flexoelectric field can act on charged species as a real macroscopic electric field.

On the other hand, a strain gradient corresponds to the inhomogeneous deformation of the ionic lattice as well as causes change in the electronic structure. Consequently, the local charge redistribution gives rise to a variation of *local* electric fields. The flexoelectric field defined as such plays a role in situations where the flexoelectric effect is associated with the transport of charged entities, e.g., oxygen vacancy, electrons and holes, and doping elements. In this context, rigorously speaking, the *flexoelectric field* should be regarded as a *depolarization field*.

5.2. The discrepancy between experiments and calculations

There is a well-known order-of-magnitude discrepancy between the theoretically estimated and the experimentally measured flexoelectric coefficients. Specifically, experimental measurement of the flexoelectric coefficient in the paraelectric phase of many perovskite oxides reaches up to several tens of μC/m, whereas theoretical estimations suggest the intrinsic flexoelectricity should not exceed several nC/m. Even by comparing the flexoelectric coupling coefficient *f*, which is insensitive to temperature and dielectric permittivity, there are still one-to-two orders of magnitude discrepancies: the theoretical range is 1–20 V whereas the experimental results generally exceed ~100 V.

Part of the disparity may originate from the unawareness of different types of flexoelectric coefficients, as discussed in Section 5.1, but the real cause is still under debate. It is suspected either some extrinsic contributions are unintentionally mixed up with the intrinsic flexoelectricity in experimental measurement or some key features of flexoelectricity have not been appropriately captured by theoretical computations. Therefore, many recent studies have attempted to reconcile this issue through experimental efforts [97,181,207,336–339] and theoretical investigations [15,79,96,154,340]. Here, we summarized a few factors in Table 5.3 that we believe are responsible for the disparity of flexoelectric coefficients. The details of some factors are briefly discussed below.

5.2.1. The breaking of the microscopic centrosymmetry

In many ferroelectric ceramics and single crystals, anomaly high flexoelectric coefficients have been measured above the ferroelectric phase transition temperature T_C. Nominally, there is no macroscopic ferroelectric polarization above T_C, but practically, several mechanisms allow for local ferroelectric polarization to persist in the paraelectric phase, which may play a role in the overall flexoelectric response. We call these mechanisms as the breaking of microscopic (local) symmetry.

For example, the polar nanoregion is a characteristic short-range ordering in ferroelectric relaxors and has been regarded as the reason for the enhanced flexoelectricity in the early work of Ma and Cross [34]. For relaxor-ferroelectric solutions, such as $Pb(Mg_{1/3}Nb_{2/3})O_3$-$PbTiO_3$ (PMN-PT) single crystals, Narvaez et al. [181] observed large differences in the measured flexoelectric response upon heating and cooling across the transition temperature (Fig. 5.1a), suggesting the "parasitic" ferroelectricity within the high-temperature phase. This thermal hysteresis disappears when the temperature elevates beyond T* ($T^* \gg T_C$) accompanied by the onset of anelastic softening. Above T*, the flexocoupling coefficient reduces to a theoretical magnitude (~10 V) and becomes constant, indicating the intrinsic strength of the flexoelectricity. It is believed that, at least in the relaxor-based crystals, the polar nanoregions remain ferroelastically active within $T_C \sim T^*$, which can be reoriented by the applied graded strain and thus imitate the flexoelectric response. Therefore, the measurement of intrinsic flexoelectric properties should be performed higher than T* to eliminate the intervention from the polar nanoregions.

Detecting residual ferroelectricity in the high-temperature non-polar phase has also been reported in $(Ba_{1-x}Sr_x)TiO_3$ (BST) ceramics where the record-high flexoelectric coefficients were documented [337]. There are several explanations for the residual ferroelectricity in BST ceramics, aside from invoking the polar nanoregion mechanism. For example, chemical nonuniformity in BST ceramics gives rise to inhomogeneous local transition temperatures [341]. Therefore, some regions may stay in the ferroelectric phase

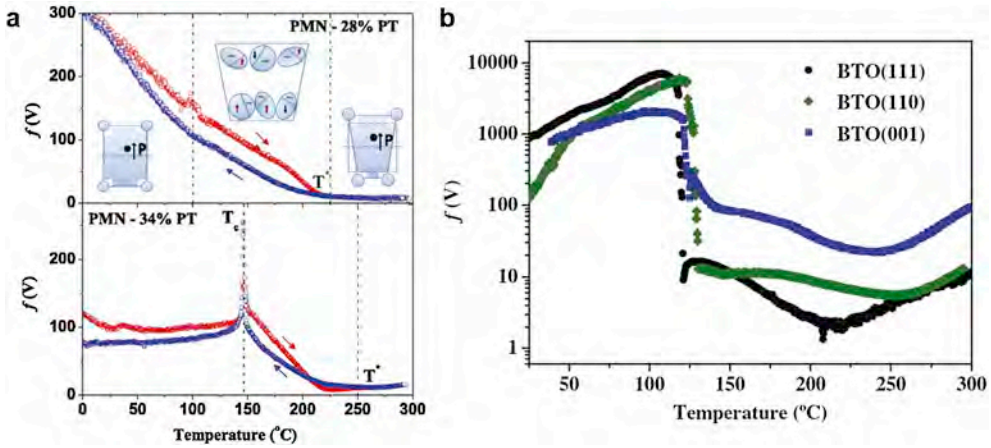

Fig. 5.1. Temperature dependence of the flexoelectric coupling coefficients of (a) PMN-28%PT and PMN-34%PT single crystals and (b) $BaTiO_3$ single crystals with different crystallographic orientations. (a) Reprinted with permission from [181] Copyright © 2014, AIP Publishing LLC (b) Reprinted with permission from [97] Copyright © 2015, American Physical Society.

even the temperature exceeds the nominal T_C. Interestingly, huge above-T_C flexoelectricity has also been reported in high quality $BaTiO_3$ single crystals (Fig. 5.1b) [97]. In this chemically homogeneous system, the residual ferroelectricity may come from the mixed order-disorder/displacive phase transition of $BaTiO_3$-based materials [341–344], which have been rationalized by the pseudo Jahn-Teller effect [340]. A recent report shows a fatigue behavior in the flexoelectric responses in lead-free ceramics, which may also be attributed to the residual ferroelectricity subjected to the domain pinning effect [345].

5.2.2. The breaking of the macroscopic centrosymmetry

The previous mechanism deals with the local symmetry breaking. In some situations, however, macroscopic symmetry breaking occurs and can also significantly contribute to the overall flexoelectric response. Biancoli et al. performed a series of careful measurement of the pyroelectric, thermal, and structural properties of BST ceramics and single crystals [336]. They found "flexoelectric" charges are obtained even if there is no graded strain applied to the unpoled samples. The detected pyroelectric charges and thermal stimulated current suggest the breaking of macroscopic centric symmetry and preexisting polarity in the sample, which is responsible for the assumed strong flexoelectric response. This symmetry-breaking may be due to the inhomogeneous redistribution of charges or polar entities introduced during the high-temperature processing, but the exact mechanism is still unclear. Likewise, breaking the macroscopic centrosymmetry of the sample can also be realized through the so-called flexoelectric poling, as demonstrated by Garten et al. [337]. By bending an unpoled BST ceramic [337], an internal bias as high as 9 kV/m can be built into the sample, even after the strain gradient was removed. Further evidence in the macroscopic symmetry breaking due to long-range structural [346] and local chemical inhomogeneities [347] has been recently documented. These findings remind us of the importance to examine the non-centrosymmetric state of the sample before conducting a flexoelectric measurement. For example, a very recent experimental work by Shu et al. [207] has not seen the macroscopic centrosymmetry breaking in their BST ceramic samples.

5.2.3. The pseudo Jahn-Teller effect

The pseudo Jahn-Teller effect [348] is an extension of the Jahn-Teller effect [349], which describes two or more pseudo-degenerate states. According to the pseudo Jahn-Teller effect, the perturbation of vibronic coupling can induce spontaneous symmetry breaking. Bersuker [340] employed the pseudo Jahn-Teller effect to explain the order-of-magnitude difference in the flexoelectric effects in paraelectric $BaTiO_3$ and $SrTiO_3$. The author found that the criterion of the pseudo Jahn-Teller effect is satisfied in $BaTiO_3$ but not in $SrTiO_3$. Therefore, the application of a strain gradient to $BaTiO_3$ creates static local dipolar distortion, which accounts for the enhanced flexoelectricity. The author also predicted enhanced flexoelectricity in NbO_6-octahedral-containing perovskites such as PMN-PT and $KNbO_3$. This conclusion is aligned with Narvaez et al.'s observation of PMN-PT single crystals [181]. In this sense, $KNbO_3$ would also be an interesting flexoelectric material to explore.

5.2.4. Surface effects

Yurkov and Tagantsev [96] have theoretically shown that the surface contribution (both surface piezoelectricity and surface flexoelectricity) to a flexoelectric response is comparable to that of the bulk, even when the surface/bulk ratio is small. Therefore, the measured flexoelectric coefficient may inevitably contain the contribution from both surface effects. The experimental evidence of a surface contribution to the enhanced flexoelectricity was presented by Narvaez et al. [97] in the flexocoupling coefficients of $BaTiO_3$ single crystal slab with different crystallographic orientations. It is shown an anomaly strong flexoelectricity, particularly in the

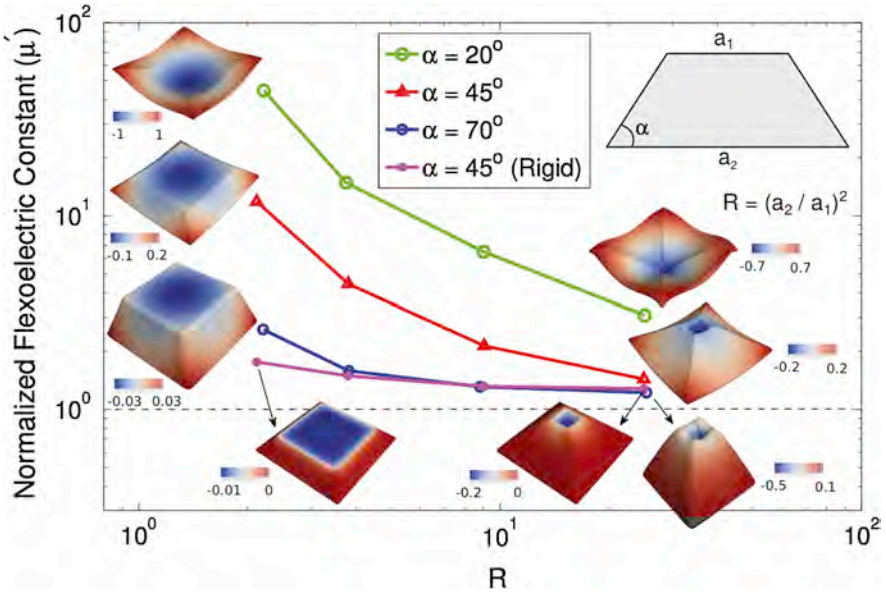

Fig. 5.2. Normalized flexoelectric constant μ′ as a function of the pyramid area ratio R. The results are obtained considering different inclination angles α. The inset shows the distribution of the through-thickness displacement (u_2) in the deformed configuration of the pyramid for the lowest and highest area ratios. The deformation is exaggerated by a factor of 10 for clarity. The color bar indicates the displacement scale in each case, normalized by a factor of 10^{-5} m. Reprinted with permission from [154] Copyright © 2015, American Physical Society.

(0 0 1)-oriented crystal, persists into high-temperature regime ($T > T^*$) where the regular and residual ferroelectricity both disappear (Fig. 5.1b). The large anisotropy in the flexocoupling tensor is believed as a sign for a substantial surface effect. Recent first-principles studies of the flexoelectric coefficient with surface effects considered [79,80] have supported this conjecture. However, it remains unclear whether the nature of this surface effect is related to the surface piezoelectricity or the surface flexoelectricity or both. Very recently, another mechanism related to spontaneously polarized surface layers is proposed for ferroelectric ceramics [339,350].

5.2.5. Oversimplification of strain gradient distribution in experiments

In most experimental measurements for flexoelectricity, a simplified analytical model is generally assumed to obtain the expression between the measured flexoelectric response to the applied gradient (e.g., Ref. [12]). However, this treatment is questioned by Abdollahi et al. [61,154]. The authors conducted 2D and 3D finite element modeling on two typical experimental schemes used for flexoelectric coefficient measurement, i.e., cantilever beam bending and truncated pyramid compression. They found the flexoelectric effect is sensitive to sample geometry, and the simplification of strain gradients made in experiments may lead to overestimation of flexoelectric coefficients. As shown in Fig. 5.2, the deviation can be as high as an order of magnitude and becomes more severe for small-sized samples. This finding adds a caveat to the experimental measurement of flexoelectric properties: using simplified analytical approximations can lead to significant overestimation of flexoelectric constants.

5.2.6. Other plausible reasons

There have been a few recent proposals to account for the “giant” flexoelectricity observed in previous experiments. For example, Abdollahi et al. [351] suggested that, in a beam bending model, the asymmetric distribution of piezoelectric coefficient can lead to an apparent flexoelectric response, which is insensitive to space inversion and thus cannot be easily distinguished from intrinsic flexoelectricity. Moreover, their computation shows that even a 1% change in the piezoelectricity across 1 mm may cause an effective flexoelectric coefficient of 1 μC/m. In another theoretical contribution, Morozovska et al. [352] discussed the possibility that the dynamic flexoelectricity can contribute to the giant static flexoelectric effect in spatially inhomogeneous samples, such as soft electrets [353,354] and bended piezoelectric bimorphs [351] under high-frequency loading.

5.3. Disagreements among theoretical results

In the previous section, we described a few possible explanations for the discrepancies between theoretically calculated and experimentally measured flexoelectric coefficients. However, disagreement in the order-of-magnitude and even the sign of flexoelectric tensors also exist among different theoretical calculations. In this subsection, we shall discuss the subtleties and ambiguities associated with the theoretically calculated flexoelectric coefficients that can help rationalize the disagreements.

For the time being, the most studied flexoelectric single crystals are $SrTiO_3$ and $BaTiO_3$. Therefore, we collected the calculated flexoelectric/flexocoupling constants of $SrTiO_3$ and $BaTiO_3$ from literature and listed them in Table 5.4. For a better comparison, we labelled the conditions and assumptions under which the flexoelectric tensors are computed to unravel the origin of discrepancies among these works. Some key factors are discussed in detail below.

5.3.1. Different macroscopic contributions of flexoelectricity

As mentioned in Section 2.2, a flexoelectric response of a finite sample contains four different contributions from either the bulk or the surface, and, in either a static or a dynamic regime. The inclusion of surface effects by Stengel [79] demonstrates that the value of a flexocoupling tensor can change substantially for different surface terminations and even the sign may reverse. Moreover, the recent work by Kvasov and Tagantsev [83] indicates the significance of dynamic effects which can also be comparable to the static bulk counterparts [83] and also determine the sign. Notably, however, it remains controversial whether the static and dynamic flexoelectric tensors are two separate quantities or identical in nature. For a detailed discussion on this issue, readers are referred to Ref. [78], Ref. [29], and Ref. [19].

5.3.2. Different microscopic contributions to flexoelectricity

From a microscopic perspective, a flexoelectric response involves purely electronic and lattice-mediated contributions. These two sources may even compete and cancel out. As shown by Hong and Vanderbilt [15,77], while the electronic part always has a negative sign for all the studied cubic symmetry materials, the lattice dipole part may be either positive or negative, depending on the force-pattern. Therefore, when comparing calculated flexoelectric coefficients, it is necessary to ensure the two contains the same microscopic contributions and the force patterns adopted are identical.

5.3.3. Dependence on electric boundary conditions

Similar to piezoelectric coefficients, the strength of the flexoelectric coefficients defined under different electric/mechanical boundary conditions may vary considerably (c.f. Section 5.1). As shown by Hong and Vanderbilt [15], the flexoelectric coefficient evaluated under the fixed-D boundary condition, unlike its counterpart defined under the fixed-E boundary condition, does not scale with the dielectric permittivity. With the high permittivity of perovskite ferroelectrics, one can expect order-of-magnitude differences between the room-temperature flexoelectric coefficients calculated under different electric boundary condition. It should also be noted that a few existing calculations do not explicitly specify the electric boundary conditions, e.g., [69,178,220], or adopt a mixed boundary condition, e.g., Ref. [77]. Therefore, a direct comparison of the results from these work with others would be meaningless.

5.3.4. Subtleties associated with the induced macroscopic electric field

The fixed-E boundary condition also brings other non-trivial issues in calculations. First, for the longwave method using a periodical supercell, the incommensurate atomic displacements lead to a macroscopic electric field along the wave propagation direction. As a result, the Taylor expansion of atomic displacements with respect to the wave vector at zone center suffers from a severe non-analyticity. In order to obtain well-defined flexoelectric property, the induced macroscopic electric field needs to be eliminated, either by suppressing the self-consistent electrostatic potential or by assuming a certain screening mechanism [355]. Second, there is an inherent arbitrariness in specifying the short-circuit boundary condition because the concept of macroscopic field is ill-defined in a non-uniformly deformed body [50,80,355]. This arbitrariness is associated with the reference energy dependence, which has been regarded [50,80] as a significant cause of the discrepancy among different theoretical calculations of flexoelectricity. To rationalize these ambiguities, Stengel [80] proposed to consistently treat the absolute deformation potential effect together with the flexoelectricity. Besides, the mixed-space approach developed recently to resolve the macroscopic electric field issue in lattice dynamics of polar materials may also shed some lights on quantifying the flexoelectric coefficient [356].

5.3.5. Force-pattern dependence

The lattice-mediated flexoelectric constants depend on the mass distribution of the crystal, an issue known as the force-pattern dependence [15]. In the direct method of calculating flexoelectric tensors, e.g., [218,220], the periodic strain gradient is applied by fixing one set of sublattice atoms while relaxing the others, which implicitly assumes a specific force-pattern. In the indirect methods, e.g., Ref. [15], the authors compared the lattice-mediated flexoelectric coefficients obtained by assuming either even-force or mass-weighted force distributions and found the latter is generally more negative than the former. As also pointed out in Ref. [15], a combination of longitudinal and shear flexoelectric components can give a positive overall flexoelectric constant for the bending mode of a slab even though the sign of each component is negative. Additionally, this force-pattern dependence of flexoelectric tensors also suggests the dynamic nature of the flexoelectricity in the sense that this material property depends on the atomic mass distribution.

Table 5.4
Ab initio calculated flexoelectric constants of $SrTiO_3$ and $BaTiO_3$.

		Hong 2010 [218]	Xu 2013 [220]	Hong 2011 [77]	Hong 2013 [15]	Hong 2013 [15]	Stengel 2014 [79]	Cyrus 2018 [81]	Hong 2013 [15]				Stengel 2014 [79]				
Tensor and units		Flexoelectric coefficients (nC/m)											Flexocoupling coefficients (V)				
Type		II	II	I	II	II	II	II	I			II					
$SrTiO_3$	Longitudinal	−1.38	−0.89	−0.145	−0.144	−0.9	−0.88	−0.87	−0.156	−48.4	−48.4	−36.9	−17.7	−13.5	−16.15	−1.8	0.8
	Transverse	N/A	2.3		N/A		−0.83	−0.84	−0.172-*	−5.0	−43.5	−40.2	−19.5*	−15.7	−18.07-*	0.6	−2.63
	Shear		−6.6				−0.08	−0.08	N/A	−24.2	−5.0	−1.4		N/A		−3.88	−2.01
$BaTiO_3$	Longitudinal	−0.37	−0.36	−0.142	−0.156	−1.1	N/A		−0.161	−370.8	−370.8	−334.4	−18.2	−16.4		N/A	
	Transverse	N/A	1.6		N/A				−0.209-*	−2.5	−475.9	−464.3	−23.6*	−21.5			
	Shear		−1.5						N/A	−239.2	−2.5	13.8			N/A		
Macroscopic contributions									bulk						bulk + surface (SrO-term)		bulk + surface (TiO_2-term)
Microscopic contributions		mixed			electronic				lattice + electronic			lattice + electronic	lattice + electronic	lattice + electronic	electronic		
Force pattern		A-site fixed			N/A				mass-weighted			even-force	mass-weighted	even-force	N/A		
Electric boundary conditions		fixed-D				fixed-E			fixed-D		fixed-E				N/A		
Temperature		0									298 K						

* Represent a combination of longitudinal and transverse components, e.g., $f_{1122} + 2f_{1221}$.

5.3.6. Pseudopotential dependence

Hong and Vanderbilt [15,77] found that the longitudinal electronic flexoelectric coefficient depends on the choice of pseudopotentials. This is understandable because the formulation of the electronic flexoelectric tensor involves the charge-density response function. This response function significantly differs when calculated using an all-electron description or using a pseudopotential approximation. To correct the difference, the authors suggested a method known as the rigid-core correction [77]. This pseudopotential dependence can also be mitigated by a strategy where the surface contribution to flexoelectricity is considered using a consistent pseudopotential [19,79].

5.4. Closing remarks of this section

The past two decades have witnessed significant advances in both the theoretical prediction and the experimental measurement of flexoelectric tensors. We summarize a few critical comments:

1. Consistent convention in the terminology, definitions, and symbols are of primary importance before making a rational comparison.
2. The order-of-magnitude discrepancy between experimental and theoretical results of flexoelectric coefficients can be rationalized, considering the extrinsic contribution by the residual ferroelectricity, the macroscopic breaking of centrosymmetry, and the surface effects, the subtleties and ambiguities in theoretical calculations, as well as the oversimplification of experimental models.
3. There are still several open questions in the fundamentals of solid-state flexoelectricity. First, an unambiguous definition of the reverse flexoelectric effect is absent. Second, the relation between the surface flexoelectricity and the surface piezoelectricity remain underexplored. Likewise, it remains unclear whether the static and dynamic bulk flexoelectricity are identical.
4. Many flexoelectric-induced phenomena can also be interpreted by other mechanisms. For example, doubt has been cast on whether bending induced polarity in $SrTiO_3$ single crystals is induced by flexoelectricity or other mechanisms associated with deformation and defects [338].

6. Perspectives: Promising applications and emerging trends

The application of flexoelectric effects relies on two basic features: the scaling effect and the symmetry-breaking effect. Due to the presence of a gradient term in its definition, the flexoelectric effect becomes more and more pronounced as the system dimension goes down from the macroscopic to the nanoscopic. This unique scalability can be illustrated by the hierarchy of the flexoelectricity from a few centimeters down to sub-nanometers, as shown in Fig. 6.1. At each level, flexoelectric-related phenomena can be found, and, correspondingly, potential applications can be envisaged. On the other hand, the symmetry-breaking nature of the flexoelectricity has brought much more opportunities beyond electromechanical applications. Many phenomena or physical properties that are absent in centrosymmetric materials, e.g., pyroelectricity [357] and bulk photovoltaic effect [311], can be triggered by introducing a controlled graded field into the system.

In the first part of this section, we shall follow the hierarchy of flexoelectric effects and discuss the promising applications at each length scale. Notably, some topics in Fig. 6.1 such as the strain gradient engineering and the tip-induced effects have been elaborately discussed in Section 4. In addition, the flexoelectric effect in low-dimensional systems is beyond the scope of the present review. We shall briefly touch upon this topic in the second part of this section, which is devoted to highlight some emerging trends and to offer a prospect of flexoelectricity-related research.

6.1. Promising applications of flexoelectricity

6.1.1. Flexible electronics (~cm)

At the macroscopic length scale, it is usually difficult to create large strain gradients within a rigid solid. However, substantial mechanical deformation can be generated through the flexible material such as rubber. The flexible electronic devices integrate the flexoelectric active material with a flexible matrix to realize large electromechanical responses for energy harvesting and converting. One representative example is the stretchable energy harvester fabricated by Qi et al. [358,359], who has “printed” wavy piezoelectric nanoribbons onto a bendable rubber substrate. The buckled PZT nanoribbons sustain large strain gradients and give rise to up to 70% enhancement in the apparent piezoelectric performance, which is attributed to the flexoelectric effect [359]. Similar ideas have also been applied to other flexible electronic devices which take PZT nanoribbons [360], $BaTiO_3$ thin film [361], PZT nanofibers [362], PMN-PT nanowires [363], and PZT-decorated multi-walled carbon nanotubes [364] as the electromechanically active component. It is also worth mentioning that many elastomers have demonstrated appreciable flexoelectric properties which can work as the active material themselves. Therefore, it would be interesting to see polymer-based flexoelectric energy harvesters in the near future.

6.1.2. Flexoelectric structures (mm ~ cm)

Another strategy for exploiting flexoelectric effects at the microscale is to design new flexoelectric structures. Flexoelectric structures are often made from one single material but with specially designed shape from which substantial gradients can be generated. In fact, the setups of the direct method for measuring the flexoelectric coefficients (c.f. Section 3.1 and Fig. 3.1) can be

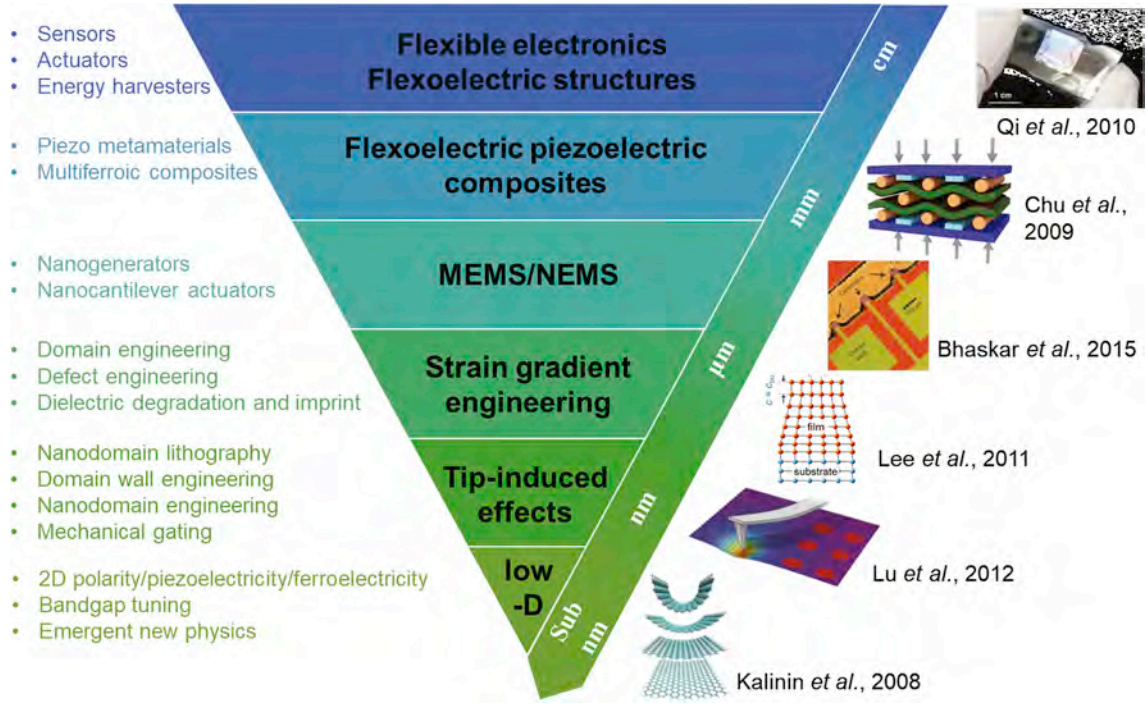

Fig. 6.1. The hierarchy of flexoelectric effects and potential applications at different length scales. Images (from upper to lower) are adapted or replotted from [358] with permission Copyright © 2010, American Chemical Society, [328] with permission Copyright © 2009 AIP Publishing, [319] with permission Copyright © 2015, Nature Publishing Group, [226] with permission Copyright © 2011 American Physical Society, [241] with permission Copyright © 2012 The American Association for the Advancement of Science, [143] with permission Copyright © 2008 American Physical Society. Abbreviations: micro-electronmechanical/nano-electromechanical (MEMS/NEMS), low-dimensional (low-D).

regarded as some typical flexoelectric structures. Fig. 6.2 shows three basic structure for the design of a flexoelectric accelerometer [365]. Similar to the design for a piezoelectric accelerometer, there are three modes, namely, the axial, shear, and bending modes utilizing primarily the longitudinal, shear, and transverse components of a flexoelectric tensor, respectively. These three designs can serve as the "building blocks" for more complex flexoelectric structures. Other interesting designs of flexoelectric structures include the multilayered cantilevers [366,367], truncated pyramid cantilever [365], bended wafers [368,369], half-hollow cylinders [370], micromachined diaphragms [371,372], circular rings [128–130], conic shells [134], etc.

These unique flexoelectric structures made of appropriate flexoelectric materials can be used for sensing, actuating, energy generating and harvesting applications. Jiang's group has conducted a series of systematic studies in these directions (see the Review articles [17,18]). For example, Huang et al. [373] fabricated a $Ba_{0.64}Sr_{0.36}TiO_3$ micro-bar to detect strain gradient change using the flexoelectric effect for monitoring crack propagation, reaching a high sensitivity of 88 pC·m. Later, Huang et al. designed and fabricated a flexoelectric unimorph accelerometer using $Ba_{0.65}Sr_{0.35}TiO_3$ [365]. The accelerator provides a sensitivity of 0.84 pC/g in

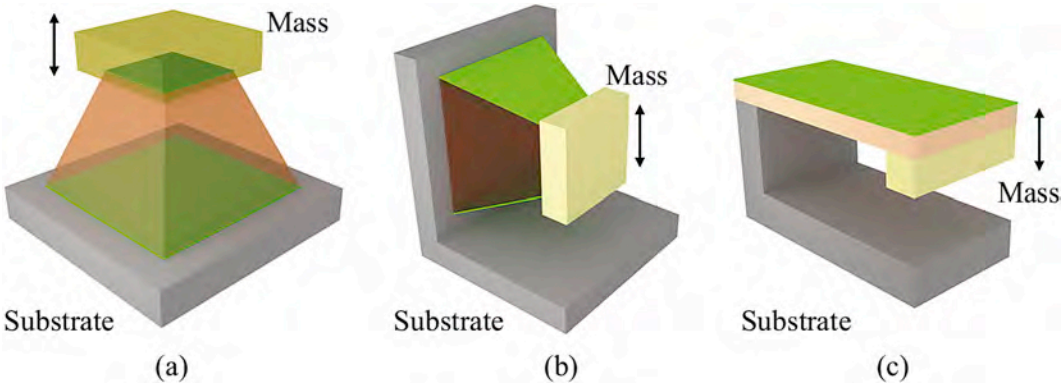

Fig. 6.2. Basic structures of flexoelectric accelerometers (yellow layers represent the electrodes on the flexoelectric components): (a) axial, (b) shear, and (c) bending modes. Reprinted with permission from [365] Copyright © 2013, SAGE Publishing.

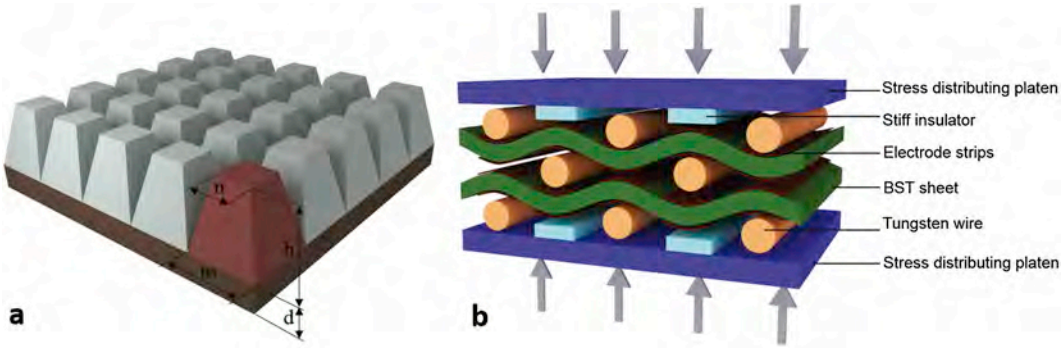

Fig. 6.3. Flexoelectric composites: (a) diagrammatic drawing of a flexoelectric piezoelectric composite [329], *m*, *n*, and *h* are the dimensions of the BST building unit, and d is the thickness of the BST substrate; (b) cross-section of a flexure mode composite using fine tungsten wires to induce strong transverse strain gradient [328]. (a) Replotted from [329] with permission Copyright © 2006 AIP Publishing. (b) Replotted from [328] with permission Copyright © 2009 AIP Publishing.

the working frequency from 10 Hz to 1.6 kHz. Kwon et al. fabricated a multilayer cantilever, which displayed amplified charge output [366]. With the scaling effect, the micro-scaled multilayer flexoelectric cantilevers are expected to perform with higher sensitivity than the piezoelectric cantilevers. The direct measurement of curvature [374] and torque [375] have been realized utilizing the flexoelectric-based sensors, which have profound implications for *in situ* structural health monitoring. Recently, Kwon et al. reported that a new type of microphone with both high sensitivity and strong resonance was fabricated using the flexoelectric $Ba_{0.67}Sr_{0.33}TiO_3$ [376]. This device has the potential to exhibit even higher sensitivity when further miniaturized, which is promising for acoustic sensing applications.

It is worth mentioning that the topology optimization tends to become a powerful tool for the design of fined and complicated flexoelectric structures [64,66,67]. For example, Nanthakumar et al. [64] have presented a mixed finite element formulation combined with topological optimization to maximize the energy converting efficiency of flexoelectric nanostructures. Their simulation results demonstrated the superiority of flexoelectricity, compared with piezoelectricity and surface piezoelectricity, in achieving the comparable efficiency with thinner structure. More technical improvements in the topology optimization methods have been made [66,67] allowing for more accurate and efficient design of complex flexoelectric structures.

6.1.3. Flexoelectric composites (μm ~ mm)

At this level, the research interests of the flexoelectricity concentrate on making piezoelectric composites from non-piezoelectric materials. Originally proposed by Fousek, Cross, and Litvin [377], this idea has been the primary motivation for the research of flexoelectric materials for a long time. Conventional piezoelectric composites contain at least one piezoelectric component, which is often lead-containing PZT for higher permittivity. With purely flexoelectric materials, it is expected that the composites can achieve comparably high piezoelectric responses as common single-phase piezoelectrics. Sharma et al. provided a theoretical ground for the feasibility from the continuum mechanics-based analysis [327]. On the other hand, some problems suffered from single-phase piezoelectric material, such as fatigue and harmonic signal problems [378], can also be avoided with certain design strategies.

Two representative examples of such a piezoelectric metamaterial were illustrated in Fig. 6.3. The truncated pyramid array (Fig. 6.3a) convert a uniform mechanical load to a local longitudinal strain gradient across each pyramid unit. Utilizing this structure and taking BST as the active material, Zhu et al. [329] obtained an effective piezoelectric $d_{33} \sim 6$ pC/N. This moderate performance has later been improved by miniaturizing the structure from millimeters to microns [379], reaching up to $d_{33} \sim 51$ pC/N for 50 μm pyramid unit. The considerable increase of the apparent piezoelectric response proves the excellent scalability of the flexoelectric composites. A record-breaking design was achieved by Chu et al. [328] with the flexural model sandwiched structure shown in Fig. 6.3b. In this composite, BST ceramic sheet and tungsten wires were alternately stacked to induce a shear strain gradient between neighboring layers. The effective non-resonance d_{33} was measured to be ~4350 pC/N near the Curie temperature in a six-unit/three-layer composite, which surpasses most piezoelectric single crystals. The following work has realized the tunability of the resonance frequency of this flexoelectric composites [212]. Besides, possible flexoelectric structures based on the flexural mode design have been examined by finite element simulations; a 50 times enhancement of the effective d_{33} is predicted [380].

Recently, Zhou et al. proposed a new design pathway for the piezoelectric metamaterial [368,381]. They have shown that by applying an asymmetric chemical reduction of the $(1-x)Na_{1/2}Bi_{1/2}TiO_3$–$xBaTiO_3$ ceramics, two gradient-generating mechanisms, namely, the spontaneous curvature and chemical inhomogeneity, can be induced. Consequently, the effective piezoelectric coefficient $d_{33} > 3500$ pC/N has been achieved with a good stability at high temperature (> 400 °C).

Finally, it is worth mentioning that some design ideas to enhance the magnetoelectric coupling in multiferroic composites mediated by flexoelectricity have been proposed [136,382–384], and the experimental verification of which would be encouraging [385].

6.1.4. Flexoelectric N/MEMS (nm ~ μm)

The flexoelectric effect has long been regarded as a desirable property for advanced nano-/micro-electromechanical systems (N/MEMS) due to its universality and excellent scaling effect [12], yet the experimental realization only emerges very recently. Bhaskar

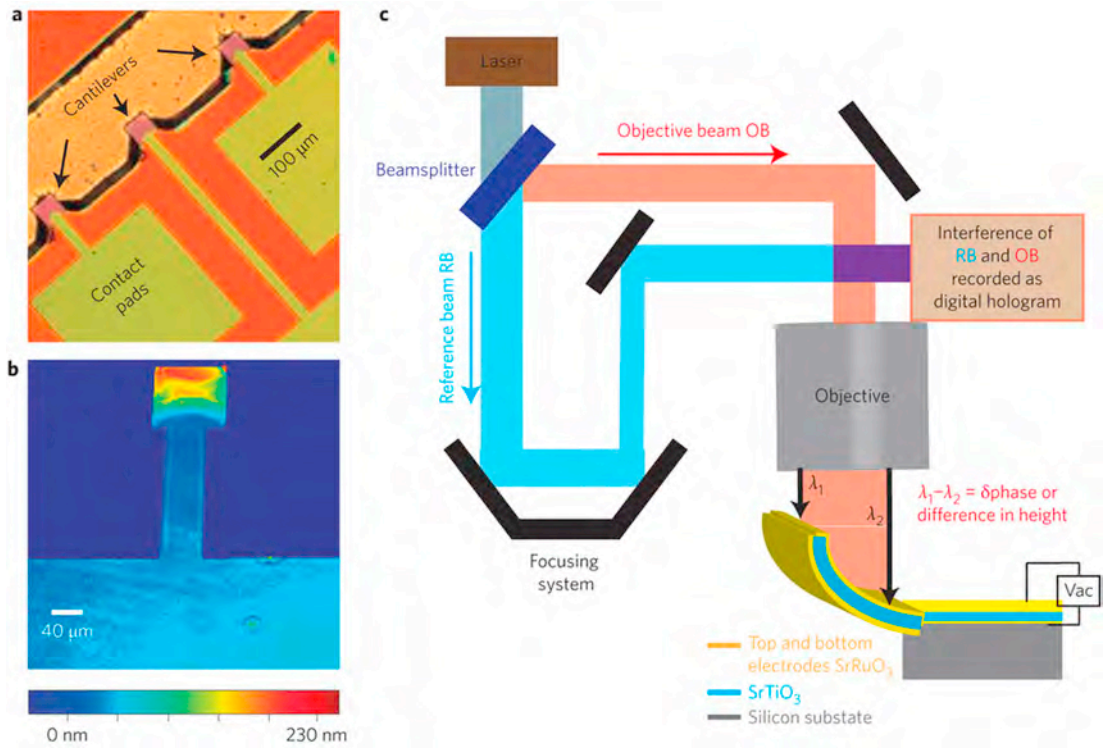

Fig. 6.4. (a) Optical image of an array of $SrTiO_3$ nanocantilevers. (b) A three-dimensional image of one $SrTiO_3$ nanocantilever with a colour scale corresponding to the out-of-plane displacement. (c) The digital holographic microscope splits a coherent laser beam into an objective beam and a reference beam. The objective beam is focused onto the sample and the light reflected is collected to form an interference pattern with the reference beam. Any difference in height along the sample surface results in a corresponding difference in the phase of the light reflected back from it. Reprint with permission from [319] Copyright © 2015, Nature Publishing Group.

et al. fabricated a silicon-compatible thin-film cantilever actuator with a single flexoelectrically active layer of $SrTiO_3$ [319]. The experimental design is shown in Fig. 6.4. The figure of merit (curvature divided by the electric field) of this flexoelectric MEMS reaches as high as 3.33 MV^{-1}, comparable to that of state-of-the-art piezoelectric bimorph cantilevers. This breakthrough is impressive, demonstrating that flexoelectricity can undoubtedly be explored to fabricate electromechanical actuators and compatibly integrated into N/MEMS. In the following work, Bhaskar et al. studied the piezoelectric and flexoelectric response exhibited by nanoscale ferroelectrics [157]. It was demonstrated that the piezoelectricity and flexoelectricity can either collaborate or compete with each other, which leads to a diode-like asymmetric electromechanical response. This effect needs to be considered when designing micro- or nano-scale electromechanical devices.

The superiority of utilizing flexoelectricity for the N/MEMS design is multifold. First, Flexoelectricity exists in materials of all symmetry groups. In principle, flexoelectric devices can be fabricated from silicon or any of its gate dielectrics. Second, because they can be made from ordinary dielectrics, flexoelectric devices can have a linear performance other than hysteretic. Also, using ordinary dielectrics allows flexoelectric devices to function at extreme temperatures, which is not possible for piezoelectric devices that can only work below the Curie temperature. Besides, flexoelectricity also simplifies device design. For flexoelectric actuators, a single dielectric layer is sufficient to achieve field-induced bending whereas the piezoelectric actuator needs to be bimorphs, which also suffers from a potential risk of delamination. Therefore, we would expect an increasing growth in the research interests and applications of flexoelectric-based N/MEMS in the future.

6.2. Emerging trends in flexoelectric research

6.2.1. Flexoelectric-mediated effects

Recent research efforts on flexoelectric effect have been focused on its coupling with other material properties and functionalities. The flexoelectric effect created by giant local strain gradients modifies the internal field, interacts with charge carriers, and consequently introduces anomalous conduction [259], transport [230], bulk photovoltaic [311], and photocurrent [200] phenomena. Since the flexoelectric effect is not limited by the symmetry of crystal structures, some recent research efforts have also been devoted to creating piezoelectricity [52,327], pyroelectricity [357,386,387], caloric effects [388–393], using central symmetric materials. For example, Starkov and Starkov generalized the thermodynamic theory of multicaloric effect in single-phase solids and formalized the caloric effect of deformation gradient [392,393]. Petal et al. studied the flexocaloric effect in $Ba_{0.67}Sr_{0.33}TiO_3$ [388] and

$Ba_{0.5}Sr_{0.5}TiO_3$ [386], and predicted that the pyroelectric coefficient of a paraelectric state can be as high as $11 \times 10^4 C \cdot m^{-2} \cdot K^{-1}$. Further experiments are needed to validate these predictions. Another emerging trend in the study of flexoelectric effect is finding an alternative way to generate giant strain gradients other than using domain engineering or physical deformation. For instance, Li et al. demonstrated that strain gradients can be dramatically enhanced by optical means in $BiFeO_3$ thin films [240]. It offers an approach to manipulate the direct flexoelectric effect without physical deformation.

6.2.2. General flexo-type couplings

There have been attempts to extend the flexoelectric coupling to generic flexo-type couplings in pursuit of new material functionalities. For example, Eliseev et al. studied the spontaneous flexomagnetic effect in nanoferroics [49], linear magnetoelectric coupling, and ferroelectricity induced by the flexomagnetic effect in ferroics [40]. They also studied the emergence of spatially modulated structures induced by flexoantiferrodistortive coupling [41]. Tanygin derived the thermodynamic potential of flexomagnetoelectric interactions [98] and found that the thermodynamic potential requires four phenomenological constants other than just one Lifshitz coefficient unless the fixed electric polarization induces the inhomogeneity of magnetization. Zvezdin and Pyatakov investigated the flexomagnetoelectric effect in multiferroic $BiFeO_3$ [99,100,322]. They explained how the inhomogeneous magnetoelectric interaction results in the modulated magnetic structure and the increase of electric polarization. The microscopic origin of the spin flexoelectricity responsible for the spin cycloid ordering was also analyzed. Lukashev and Sbirianov studied the flexomagnetic effect in frustrated triangular magnetic structures [394]. Using first-principles calculations and Monte Carlo simulations, they demonstrated the linear dependence of magnetization on strain gradient in Mn-based antiperovskite compounds. Hertel discussed curvature-induced magnetochirality [395]. It was shown that the inversion asymmetry connected with curved magnetic surfaces leads to magnetochiral effects. It should be noted that most of the above-mentioned theoretical studies still need further experimental validation.

6.2.3. Complex systems sustaining large strain gradients

In addition to oxide dielectric materials, the research focus of flexoelectric effect has also been extended to low-dimensional materials [142–144,396–408], semiconductors [409], biomembranes [3,4], antiferroelectric materials [410], biological tissues [411–414], and polymers [59,71,182,415–420]. Since flexoelectric effects are strongly dependent on the spatial scale, 2D membranes of atomistic scale thickness are likely to display strong electromechanical coupling. The exploration of flexoelectricity in low dimensional materials has been mostly based on theoretical calculations, though a few experimental attempts have been made very recently [421,422]. It was demonstrated that carbon nanostructures have the linear dependence of flexoelectric atomic dipole moments on local curvature [143,396], while BN sheet exhibits an unusual nonlinear electromechanical dependence [144]. Using first-principles calculations, Yu et al. showed that mechanical bending shifts the Fermi level and changes the conductivity of 2D material MoS_2, which implicitly indicates the role of flexoelectric effect [400]. For a more thorough discussion of flexoelectricity in 2D materials and membranes, the reader can refer to recent reviews [7,8].

7. Summary

The flexoelectric effect, as a higher-order linear electromechanical coupling, connects electric polarization to strain gradient. It applies to all crystal symmetry groups and exhibits strong scaling effects. This article summarizes recent progress in both theoretical and experimental research on flexoelectric effects. These include the advances in developing the first-principles theory of flexoelectric effects at the electronic structure as well as mesoscale phase-field method and continuum mechanics models based on phenomenological thermodynamics. The recent implementation of first-principles theories made it possible to generate all the flexoelectric coefficients. The phase-field method and continuum mechanics are powerful in modeling, understanding, and predicting the stabilities and evolution of domain structures and studying the influence of flexoelectric and generic flexo-type effects under various boundary conditions.

Experimentally, we conducted a thorough survey on the flexoelectric coefficients of several ferroelectric oxides and compared the strength and weakness of different measurement approaches. Furthermore, it has been demonstrated that flexoelectric effects can be employed to control the internal electric field, manipulate transport properties, as well as switch ferroelectric domains. The ability to mechanically switch ferroelectric domains at the nanoscale via the flexoelectric effect has potential high storage density memory applications. New prototypes of sensors and actuators taking advantage of flexoelectric effects have been proposed with potential applications in N/MEMS. The flexoelectric effects will become even more prominent due to the miniaturization of devices and the scaling effect of flexoelectricity. It has also been shown that the flexoelectric effects can also be utilized in composites to produce and enhance robust piezoelectric performances.

Although significant advances have been made over the last few years, this review calls for the need for the unification of the terminology and flexoelectric tensor notations. Significant efforts are still required to reconcile the orders of magnitude differences between the measured flexoelectric coefficients theoretical predictions as well as among those calculated flexoelectric coefficients. There is a strong need for advances in characterization techniques to accurately measure the local strain state of a solid in order to reliably determine the flexoelectric coefficients due to the sensitivity of flexoelectric effects to the local environment. There are still many potential new material systems and applications of flexoelectricity that remain to be explored. A good example is the very recent demonstration of utilizing flexoelectricity to generate the bulk photovoltaic effects [311].

Acknowledgment

This work was supported by National Science Foundation (NSF) through Grant No. DMR 1410714 and DMR-1744213. Long-Qing Chen also gratefully acknowledges the support by the Hamer Professorship. Shujun Zhang thanks to the support of ARC (FT140100698). Authors would like to thank Mr. Xiaoxing Cheng for the help on schematic figures and Professor Baixiang Xu at Technical University of Darmstadt for comments and suggestions on the manuscript.

References

[1] Meyer Robert B. Piezoelectric effects in liquid crystals. Phys Rev Lett 1969;22:918–21.
[2] Buka A, Éber N. Flexoelectricity in liquid crystals: theory, experiments and applications. World Scientific; 2012.
[3] Petrov AG. Flexoelectricity of model and living membranes. Biochim Biophys Acta - Biomembr 2002;1561:1–25. https://doi.org/10.1016/S0304-4157(01)00007-7.
[4] Petrov AG. Flexoelectricity and mechanotransduction. Curr Top Membr 2007;58:121–50. https://doi.org/10.1016/S1063-5823(06)58005-6.
[5] Zubko P, Catalan G, Tagantsev AK. Flexoelectric effect in solids. Annu Rev Mater Res 2013;43:387–421. https://doi.org/10.1146/annurev-matsci-071312-121634.
[6] Ma W. Flexoelectricity: strain gradient effects in ferroelectrics. Phys Scr T 2007;T129:180–3. https://doi.org/10.1088/0031-8949/2007/T129/041.
[7] Krichen S, Sharma P. Flexoelectricity: a perspective on an unusual electromechanical coupling. J Appl Mech 2016;83:030801https://doi.org/10.1115/1.4032378.
[8] Ahmadpoor F, Sharma P. Flexoelectricity in two-dimensional crystalline and biological membranes. Nanoscale 2015;7:16555–70. https://doi.org/10.1039/C5NR04722F.
[9] Ma LL, Chen WJ, Zheng Y. Flexoelectric effect at the nanoscale; 2018 https://doi.org/10.1007/978-981-10-6855-3_18-1.
[10] Glinchuk MD, Eliseev EA, Morozovska AN. Spontaneous flexoelectric effect in nanosystems (topical review). Ferroelectrics 2016;500:90–8. https://doi.org/10.1080/00150193.2016.1214994.
[11] Yudin PV, Tagantsev AK. Fundamentals of flexoelectricity in solids. Nanotechnology 2013;24:432001https://doi.org/10.1088/0957-4484/24/43/432001.
[12] Cross LE. Flexoelectric effects: charge separation in insulating solids subjected to elastic strain gradients. J Mater Sci 2006;41(1):53–63.
[13] Lee D, Noh TW. Giant flexoelectric effect through interfacial strain relaxation. Philos Trans R Soc A Math Phys Eng Sci 2012;370:4944–57. https://doi.org/10.1098/rsta.2012.0200.
[14] Nguyen TD, Mao S, Yeh YW, Purohit PK, McAlpine MC. Nanoscale flexoelectricity. Adv Mater 2013;25:946–74. https://doi.org/10.1002/adma.201203852.
[15] Hong J, Vanderbilt D. First-principles theory and calculation of flexoelectricity. Phys Rev B - Condens Matter Mater Phys 2013;88:174107https://doi.org/10.1103/PhysRevB.88.174107.
[16] Fu JY, Cross LE. On the flexoelectric effects in solid dielectrics: theories and applications. Ferroelectrics 2007;354:238–45. https://doi.org/10.1080/00150190701455005.
[17] Jiang X, Huang W, Zhang S. Flexoelectric nano-generator: materials, structures and devices. Nano Energy 2013;2:1079–92. https://doi.org/10.1016/j.nanoen.2013.09.001.
[18] Huang S, Qi L, Huang W, Shu L, Zhou S, Jiang X. Flexoelectricity in dielectrics: materials, structures and characterizations. J Adv Dielectr 2018;08:1830002. https://doi.org/10.1142/S2010135X18300025.
[19] Tagantsev AK. Flexoelectricity in solids: from theory to applications; 2016.
[20] Mashkevich VS, Tolpygo KB, Electrical. Optical and elastic properties of diamond type crystals. I. J Exp Theor Phys (Russian Orig - ZhETF) 1957;5:435–9.
[21] Tolpygo KB. Long wavelength oscillations of diamond-type crystals including long range forces. Sov Physics-Solid State 1963;4:1297–305.
[22] Mindlin RD. Polarization gradient in elastic dielectrics. Int J Solids Struct 1968;4:637–42. https://doi.org/10.1016/0020-7683(68)90079-6.
[23] Scott JF. Lattice perturbations in $CaWO_4$ and $CaMoO_4$. J Chem Phys 1968;48:874–6. https://doi.org/10.1063/1.1668727.
[24] Kogan SM. Piezoelectric effect under an inhomogeneous strain and acoustic scattering of carriers in crystal. FizTverdTela (Leningrad) 1963;5:2069–70.
[25] Harris P. Mechanism for the shock polarization of dielectrics. J Appl Phys 1965;36:739–41. https://doi.org/10.1063/1.1714210.
[26] Indenbom VL, Loginov EB, Osipov MA. Flexoelectric effect and crystal-structure. Kristallografiya 1981;26:1157–62.
[27] Indenbom VL, Loginov EB, Osipov MA. The flexoelectric effect and the structure of crystals. Sov Phys - Crystallogr 1981;26:656–8.
[28] Tagantsev AK. Theory of flexoelectric effect in crystals. SovPhys JETP 1985;61:1246.
[29] Tagantsev AK. Piezoelectricity and flexoelectrisity in crystalline dielectrics. Phys Rev B 1986;34:5883–9.
[30] Tagantsev AK. Electric polarization in crystals and its response to thermal and elastic perturbations. Phase Transitions 1991;35:119–203. https://doi.org/10.1080/01411599108213201.
[31] Bursian EV. OI Z. Changes in curvature of a ferroelectric film due to polarization. Sov Phys SOLID STATE, USSR 1968;10:1121.
[32] Bursian EV, OI Z, Makarov KV. Ferroelectric plate polarization by bending. Izv Akad Nauk SSSR Seriya Fiz 1969;33:1098.
[33] Bursian EV, Trunov NN. Nonlocal piezo-effect. Fiz Tverd Tela 1974;16:1187–90.
[34] Ma W, Cross LE. Large flexoelectric polarization in ceramic lead magnesium niobate. Appl Phys Lett 2001;79:4420–2. https://doi.org/10.1063/1.1426690.
[35] Ma W, Cross LE. Flexoelectricity of barium titanate. Appl Phys Lett 2006;88:2004–7. https://doi.org/10.1063/1.2211309.
[36] Ma W, Cross LE. Flexoelectric effect in ceramic lead zirconate titanate. Appl Phys Lett 2005;86:1–3. https://doi.org/10.1063/1.1868078.
[37] Ma W, Cross LE. Strain-gradient-induced electric polarization in lead zirconate titanate ceramics. Appl Phys Lett 2003;82:3293–5. https://doi.org/10.1063/1.1570517.
[38] Ma W, Cross LE. Observation of the flexoelectric effect in relaxor Pb(Mg1/3Nb2/3)O3ceramics. Appl Phys Lett 2001;78:2920–1. https://doi.org/10.1063/1.1356444.
[39] Ma W, Cross LE. Flexoelectric polarization of barium strontium titanate in the paraelectric state. Appl Phys Lett 2002;81:3440–2. https://doi.org/10.1063/1.1518559.
[40] Eliseev EA, Glinchuk MD, Khist V, Skorokhod VV, Blinc R, Morozovska AN. Linear magnetoelectric coupling and ferroelectricity induced by the flexomagnetic effect in ferroics. Phys Rev B - Condens Matter Mater Phys 2011;84:1–16. https://doi.org/10.1103/PhysRevB.84.174112.
[41] Eliseev EA, Kalinin SV, Gu Y, Glinchuk MD, Khist V, Borisevich A, et al. Universal emergence of spatially modulated structures induced by flexo-antiferrodistortive coupling in multiferroics. Phys Rev B - Condens Matter Mater Phys 2013;88:224105https://doi.org/10.1103/PhysRevB.88.224105.
[42] Morozovska AN, Vysochanskii YM, Varenyk OV, Silibin MV, Kalinin SV, Eliseev EA. Flexocoupling impact on the generalized susceptibility and soft phonon modes in the ordered phase of ferroics. Phys Rev B - Condens Matter Mater Phys 2015;92:1–10. https://doi.org/10.1103/PhysRevB.92.094308.
[43] Eliseev EA, Morozovska AN, Glinchuk MD, Kalinin SV. Lost surface waves in nonpiezoelectric solids. Phys Rev B 2017;96:1–11. https://doi.org/10.1103/PhysRevB.96.045411.
[44] Morozovska AN, Eliseev EA, Tagantsev AK, Bravina SL, Chen LQ, Kalinin SV. Thermodynamics of electromechanically coupled mixed ionic-electronic conductors: deformation potential, Vegard strains, and flexoelectric effect. Phys Rev B - Condens Matter Mater Phys 2011;83:1–10. https://doi.org/10.1103/PhysRevB.83.195313.
[45] Gu Y, Li M, Morozovska AN, Wang Y, Eliseev EA, Gopalan V, et al. Flexoelectricity and ferroelectric domain wall structures: phase-field modeling and DFT calculations. Phys Rev B - Condens Matter Mater Phys 2014;89:174111https://doi.org/10.1103/PhysRevB.89.174111.
[46] Ahluwalia R, Tagantsev AK, Yudin P, Setter N, Ng N, Srolovitz DJ. Influence of flexoelectric coupling on domain patterns in ferroelectrics. Phys Rev B - Condens

Matter Mater Phys 2014;89:174105https://doi.org/10.1103/PhysRevB.89.174105.
[47] Chen HT, Soh AK, Ni Y. Phase field modeling of flexoelectric effects in ferroelectric epitaxial thin films. Acta Mech 2014;225:1323–33. https://doi.org/10.1007/s00707-013-1045-5.
[48] Sahin E, Dost S. A strain-gradients theory of elastic dielectrics with spatial dispersion. Int J Eng Sci 1988;26:1231–45. https://doi.org/10.1016/0020-7225(88)90043-2.
[49] Eliseev EA, Morozovska AN, Glinchuk MD, Blinc R. Spontaneous flexoelectric/flexomagnetic effect in nanoferroics. Phys Rev B - Condens Matter Mater Phys 2009;79:1–10. https://doi.org/10.1103/PhysRevB.79.165433.
[50] Stengel M. Unified ab initio formulation of flexoelectricity and strain-gradient elasticity. Phys Rev B 2016;93:1–23. https://doi.org/10.1103/PhysRevB.93.245107.
[51] Mao S, Purohit PK. Insights Into flexoelectric solids from strain-gradient elasticity. J Appl Mech 2014;81:081004https://doi.org/10.1115/1.4027451.
[52] Maranganti R, Sharma ND, Sharma P. Electromechanical coupling in nonpiezoelectric materials due to nanoscale nonlocal size effects: Green's function solutions and embedded inclusions. Phys Rev B - Condens Matter Mater Phys 2006;74:014110https://doi.org/10.1103/PhysRevB.74.014110.
[53] Askes H, Aifantis EC. Gradient elasticity in statics and dynamics: An overview of formulations, length scale identification procedures, finite element implementations and new results. Int J Solids Struct 2011;48:1962–90. https://doi.org/10.1016/j.ijsolstr.2011.03.006.
[54] Mindlin RD, Eshel NN. On first strain-gradient theories in linear elasticity. Int J Solids Struct 1968;4:109–24. https://doi.org/10.1016/0020-7683(68)90036-X.
[55] Mindlin RD, Tiersten HF. Effects of couple-stresses in linear elasticity. Arch Ration Mech Anal 1962;11:415–48. https://doi.org/10.1007/BF00253946.
[56] Hadjesfandiari AR. Size-dependent piezoelectricity. Int J Solids Struct 2013;50:2781–91. https://doi.org/10.1016/j.ijsolstr.2013.04.020.
[57] Li A, Zhou S, Qi L, Chen X, Anqing L, Shenjie Z, et al. A flexoelectric theory with rotation gradient effects for elastic dielectrics. Model Simul Mater Sci Eng 2015;24:015009https://doi.org/10.1088/0965-0393/24/1/015009.
[58] Li A, Zhou S, Qi L, Chen X. A reformulated flexoelectric theory for isotropic dielectrics. J Phys D Appl Phys 2015;48:465502https://doi.org/10.1088/0022-3727/48/46/465502.
[59] Deng Q, Liu L, Sharma P. Flexoelectricity in soft materials and biological membranes. J Mech Phys Solids 2014;62:209–27. https://doi.org/10.1016/j.jmps.2013.09.021.
[60] Wang KF, Wang BL. Non-linear flexoelectricity in energy harvesting. Int J Eng Sci 2017;116:88–103. https://doi.org/10.1016/j.ijengsci.2017.02.010.
[61] Abdollahi A, Peco C, Millán D, Arroyo M, Arias I. Computational evaluation of the flexoelectric effect in dielectric solids. J Appl Phys 2014;116. https://doi.org/10.1063/1.4893974.
[62] Mao S, Purohit PK, Aravas N. Mixed finite-element formulations in piezoelectricity and flexoelectricity. Proc R Soc A Math Phys Eng Sci 2016;472:(20150879). https://doi.org/10.1098/rspa.2015.0879.
[63] Mao Y, Ai S, Xiang X, Chen C. Theory for dielectrics considering the direct and converse flexoelectric effects and its finite element implementation. Appl Math Model 2016;40:7115–37. https://doi.org/10.1016/j.apm.2015.12.042.
[64] Nanthakumar SS, Zhuang X, Park HS, Rabczuk T. Topology optimization of flexoelectric structures. J Mech Phys Solids 2017;105:217–34. https://doi.org/10.1016/j.jmps.2017.05.010.
[65] He B, Javvaji B, Zhuang X. Size dependent flexoelectric and mechanical properties of barium titanate nanobelt: a molecular dynamics study. Phys B Condens Matter 2018;545:527–35. https://doi.org/10.1016/j.physb.2018.01.031.
[66] Ghasemi H, Park HS, Rabczuk T. A multi-material level set-based topology optimization of flexoelectric composites. Comput Methods Appl Mech Eng 2018;332:47–62. https://doi.org/10.1016/j.cma.2017.12.005.
[67] Ghasemi H, Park HS, Rabczuk T. A level-set based IGA formulation for topology optimization of flexoelectric materials. Comput Methods Appl Mech Eng 2017;313:239–58. https://doi.org/10.1016/j.cma.2016.09.029.
[68] Askar A, Lee PCY, Cakmak AS. Lattice-dynamics approach to the theory of elastic dielectrics with polarization gradient. Phys Rev B 1970;1:3525–37. https://doi.org/10.1103/PhysRevB.1.3525.
[69] Maranganti R, Sharma P. Atomistic determination of flexoelectric properties of crystalline dielectrics. Phys Rev B - Condens Matter Mater Phys 2009;80:054109https://doi.org/10.1103/PhysRevB.80.054109.
[70] Schulz M, Marvan M. The theory of flexoelectric effect of polymer glasses. Colloid Polym Sci 1991;269:553–5. https://doi.org/10.1007/BF00659908.
[71] Marvan M, Havránek A. Flexoelectric effect in elastomers. Prog Colloid Polym Sci 2007;78:33–6. https://doi.org/10.1007/bfb0114342.
[72] Marvan M, Havránek A. Static volume flexoelectric effect in a model of linear chains. Solid State Commun 1997;101:493–6. https://doi.org/10.1016/S0038-1098(96)00623-0.
[73] Klíč A, Marvan M. Theoretical study of the flexoelectric effect based on a simple model of ferroelectric material. Integr Ferroelectr 2004;63:155–9. https://doi.org/10.1080/10584580490459341.
[74] Chu K, Yang CH. Nonlinear flexoelectricity in noncentrosymmetric crystals. Phys Rev B 2017;96:1–5. https://doi.org/10.1103/PhysRevB.96.104102.
[75] Resta R. Towards a bulk theory of flexoelectricity. Phys Rev Lett 2010;105:127601https://doi.org/10.1103/PhysRevLett. 105.127601.
[76] Martin RM. Piezoelectricity. Phys Rev B 1972;5:1607–13. https://doi.org/10.1103/PhysRevB.5.1607.
[77] Hong J, Vanderbilt D. First-principles theory of frozen-ion flexoelectricity. Phys Rev B - Condens Matter Mater Phys 2011;84:1–5. https://doi.org/10.1103/PhysRevB.84.180101.
[78] Stengel M. Flexoelectricity from density-functional perturbation theory. Phys Rev B - Condens Matter Mater Phys 2013;88:174106https://doi.org/10.1103/PhysRevB.88.174106.
[79] Stengel M. Surface control of flexoelectricity. Phys Rev B - Condens Matter Mater Phys 2014;90:1–5. https://doi.org/10.1103/PhysRevB.90.201112.
[80] Stengel M. From flexoelectricity to absolute deformation potentials: the case of $SrTiO_3$. Phys Rev B - Condens Matter Mater Phys 2015;92:1–7. https://doi.org/10.1103/PhysRevB.92.205115.
[81] Dreyer CE, Stengel M, Vanderbilt D, Stengel M. Current-density implementation for calculating flexoelectric coefficients. Phys Rev B 2018;98:1–20. https://doi.org/10.1103/PhysRevB.98.075153.
[82] Tolédano JC, Tolédano P. The Landau theory of phase transitions: aplication to structural, incommensurate, magnetic, and liquid crystal systems. Singapore: World Scientific, Singapore; 1987.
[83] Kvasov A, Tagantsev AK. Dynamic flexoelectric effect in perovskites from first-principles calculations. Phys Rev B - Condens Matter Mater Phys 2015;92:054104https://doi.org/10.1103/PhysRevB.92.054104.
[84] Catalan G, Sinnamon LJ, Gregg JM. The effect of flexoelectricity on the dielectric properties of inhomogeneously strained ferroelectric thin films. J Phys Condens Matter 2004;16:2253–64. https://doi.org/10.1088/0953-8984/16/13/006.
[85] Catalan G, Noheda B, McAneney J, Sinnamon LJ, Gregg JM. Strain gradients in epitaxial ferroelectrics. Phys Rev B - Condens Matter Mater Phys 2005;72:020102https://doi.org/10.1103/PhysRevB.72.020102.
[86] Zhang J, Xu R, Damodaran AR, Chen ZH, Martin LW. Understanding order in compositionally graded ferroelectrics: flexoelectricity, gradient, and depolarization field effects. Phys Rev B - Condens Matter Mater Phys 2014;89:1–11. https://doi.org/10.1103/PhysRevB.89.224101.
[87] Karthik J, Mangalam RVK, Agar JC, Martin LW. Large built-in electric fields due to flexoelectricity in compositionally graded ferroelectric thin films. Phys Rev B - Condens Matter Mater Phys 2013;87:1–6. https://doi.org/10.1103/PhysRevB.87.024111.
[88] Morozovska AN, Eliseev EA, Kalinin SV, Chen LQ, Gopalan V. Surface polar states and pyroelectricity in ferroelastics induced by flexo-roto field. Appl Phys Lett 2012;100:1–6. https://doi.org/10.1063/1.3701152.
[89] Morozovska AN, Eliseev EA, Glinchuk MD, Chen LQ, Gopalan V. Interfacial polarization and pyroelectricity in antiferrodistortive structures induced by a flexoelectric effect and rotostriction. Phys Rev B - Condens Matter Mater Phys 2012;85:094107https://doi.org/10.1103/PhysRevB.85.094107.
[90] Eliseev EA, Morozovska AN, Gu Y, Borisevich AY, Chen LQ, Gopalan V, et al. Conductivity of twin-domain-wall/surface junctions in ferroelastics: Interplay of deformation potential, octahedral rotations, improper ferroelectricity, and flexoelectric coupling. Phys Rev B - Condens Matter Mater Phys 2012;86:1–10. https://doi.org/10.1103/PhysRevB.86.085416.

[91] Morozovska AN, Vasudevan RK, Maksymovych P, Kalinin SV, Eliseev EA. Anisotropic conductivity of uncharged domain walls in $BiFeO_3$. Phys Rev B - Condens Matter Mater Phys 2012;86:1–9. https://doi.org/10.1103/PhysRevB.86.085315.
[92] Morozovska AN, Eliseev EA, Scherbakov CM, Vysochanskii YM. Influence of elastic strain gradient on the upper limit of flexocoupling strength, spatially modulated phases, and soft phonon dispersion in ferroics. Phys Rev B 2016;94:1–14. https://doi.org/10.1103/PhysRevB.94.174112.
[93] Morozovska AN, Glinchuk MD, Eliseev EA, Vysochanskii YM. Flexocoupling-induced soft acoustic modes and the spatially modulated phases in ferroelectrics. Phys Rev B 2017;96:1–11. https://doi.org/10.1103/PhysRevB.96.094111.
[94] Deng Q, Shen S. The flexodynamic effect on nanoscale flexoelectric energy harvesting: a computational approach. Smart Mater Struct 2018;27:105001https://doi.org/10.1088/1361-665X/aadab3.
[95] Tagantsev AK, Yurkov AS. Flexoelectric effect in finite samples. J Appl Phys 2012;112:044103https://doi.org/10.1063/1.4745037.
[96] Yurkov AS, Tagantsev AK. Strong surface effect on direct bulk flexoelectric response in solids. Appl Phys Lett 2016;108:022904https://doi.org/10.1063/1.4939975.
[97] Narvaez J, Saremi S, Hong J, Stengel M, Catalan G. Large flexoelectric anisotropy in paraelectric barium titanate. Phys Rev Lett 2015;115:1–5. https://doi.org/10.1103/PhysRevLett. 115.037601.
[98] Tanygin BM. On the free energy of the flexomagnetoelectric interactions. J Magn Magn Mater 2011;323:1899–902. https://doi.org/10.1016/j.jmmm.2011.02.035.
[99] Pyatakov AP, Zvezdin AK. Flexomagnetoelectric interaction in multiferroics. Eur Phys J B 2009;71:419–27. https://doi.org/10.1140/epjb/e2009-00281-5.
[100] Zvezdin AK, Pyatakov AP. Flexomagnetoelectric effect in bismuth ferrite. Phys Status Solidi Basic Res 2009;246:1956–60. https://doi.org/10.1002/pssb.200945214.
[101] Toupin RA. Elastic materials with couple-stresses. Arch Ration Mech Anal 1962;11:385–414. https://doi.org/10.1007/BF00253945.
[102] Shen S, Hu S. A theory of flexoelectricity with surface effect for elastic dielectrics. J Mech Phys Solids 2010;58:665–77. https://doi.org/10.1016/j.jmps.2010.03.001.
[103] Majdoub MS, Sharma P, Cagin T. Enhanced size-dependent piezoelectricity and elasticity in nanostructures due to the flexoelectric effect. Phys Rev B - Condens Matter Mater Phys 2008;77:1–9. https://doi.org/10.1103/PhysRevB.77.125424.
[104] Poya R, Gil AJ, Ortigosa R, Palma R. On a family of numerical models for couple stress based flexoelectricity for continua and beams. J Mech Phys Solids 2019;125:613–52. https://doi.org/10.1016/j.jmps.2019.01.013.
[105] Liu L. An energy formulation of continuum magneto-electro-elasticity with applications. J Mech Phys Solids 2014;63:451–80. https://doi.org/10.1016/j.jmps.2013.08.001.
[106] Ebrahimi-nejad S, Boreiry M. Comprehensive nonlocal analysis of piezoelectric nanobeams with surface effects in bending, buckling and vibrations under magneto-electro-thermo-mechanical loading. Mater Res Express 2018;5:035028. https://doi.org/10.1088/2053-1591/aab46d.
[107] Lecoutre G, Daher N, Devel M, Hirsinger L. Principle of virtual power applied to deformable semiconductors with strain, polarization, and magnetization gradients. Acta Mech 2017;228:1681–710. https://doi.org/10.1007/s00707-016-1787-y.
[108] Mohammadi P, Liu LP, Sharma P. A theory of flexoelectric membranes and effective properties of heterogeneous membranes. J Appl Mech 2013;81:011007. https://doi.org/10.1115/1.4023978.
[109] Thai TQ, Rabczuk T, Zhuang X. A large deformation isogeometric approach for flexoelectricity and soft materials. Comput Methods Appl Mech Eng 2018.
[110] Jiao F, Wei P, Li Y. Wave propagation through a flexoelectric piezoelectric slab sandwiched by two piezoelectric half-spaces. Ultrasonics 2018;82:217–32. https://doi.org/10.1016/j.ultras.2017.08.008.
[111] Yang W, Hu T, Liang X, Shen S. On band structures of layered phononic crystals with flexoelectricity. Arch Appl Mech 2017. https://doi.org/10.1007/s00419-017-1332-z.
[112] Mao S, Purohit PK. Defects in flexoelectric solids. J Mech Phys Solids 2015;84:95–115. https://doi.org/10.1016/j.jmps.2015.07.013.
[113] Ray MC. Exact solutions for flexoelectric response in nanostructures. J Appl Mech 2014;81:091002. https://doi.org/10.1115/1.4027806.
[114] Barati MR. Closed-form nonlinear frequency of flexoelectric nanobeams with surface and nonlocal effects under closed circuit electric field. Mater Res Express 2018;5. https://doi.org/10.1088/2053-1591/aaa9a6.
[115] Barati MR. Investigating nonlinear vibration of closed circuit flexoelectric nanobeams with surface effects via Hamiltonian method. Microsyst Technol 2017:1–11. https://doi.org/10.1007/s00542-017-3549-8.
[116] Baroudi S, Najar F, Jemai A. Static and dynamic analytical coupled field analysis of piezoelectric flexoelectric nanobeams: a strain gradient theory approach. Int J Solids Struct 2017:1–15. https://doi.org/10.1016/j.ijsolstr.2017.11.014.
[117] Ebrahimi F, Barati MR. Magnetic field effects on nonlocal wave dispersion characteristics of size-dependent nanobeams. Appl Phys A Mater Sci Process 2017;123. https://doi.org/10.1007/s00339-016-0646-y.
[118] Hadjesfandiari AR, Hajesfandiari A, Zhang H, Dargush GF. Size-dependent couple stress Timoshenko beam theory; 2017. p. 1–48.
[119] Liang X, Hu S, Shen S. Nanoscale mechanical energy harvesting using piezoelectricity and flexoelectricity. Smart Mater Struct 2017;26:035050. https://doi.org/10.1088/1361-665X/26/3/035050.
[120] Yan Z. Modeling of a nanoscale flexoelectric energy harvester with surface effects. Phys E Low-Dimens Syst Nanostruct 2017;88:125–32. https://doi.org/10.1016/j.physe.2017.01.001.
[121] Shen Z, Chen W. Converse flexoelectric effect in comb electrode piezoelectric microbeam. Phys Lett Sect A Gen At Solid State Phys 2012;376:1661–3. https://doi.org/10.1016/j.physleta.2012.03.049.
[122] Majdoub MS, Sharma P, Çağin T, Çağin T. Dramatic enhancement in energy harvesting for a narrow range of dimensions in piezoelectric nanostructures. Phys Rev B - Condens Matter Mater Phys 2008;78:2008–9. https://doi.org/10.1103/PhysRevB.78.121407.
[123] Deng Q, Kammoun M, Erturk A, Sharma P. Nanoscale flexoelectric energy harvesting. Int J Solids Struct 2014;51:3218–25. https://doi.org/10.1016/j.ijsolstr.2014.05.018.
[124] Zhang DP, Lei YJ, Adhikari S. Flexoelectric effect on vibration responses of piezoelectric nanobeams embedded in viscoelastic medium based on nonlocal elasticity theory. Acta Mech 2018. https://doi.org/10.1007/s00707-018-2116-4.
[125] Ebrahimi F, Barati MR. Static stability analysis of embedded flexoelectric nanoplates considering surface effects. Appl Phys A Mater Sci Process 2017;123:1–15. https://doi.org/10.1007/s00339-017-1265-y.
[126] Baskaran S, Thiruvannamalai S, Heo H, Lee HJ, Francis SM, Ramachandran N, et al. Converse piezoelectric responses in nonpiezoelectric materials implemented via asymmetric configurations of electrodes. J Appl Phys 2010;108. https://doi.org/10.1063/1.3486459.
[127] Zhang Z, Yan Z, Jiang L. Flexoelectric effect on the electroelastic responses and vibrational behaviors of a piezoelectric nanoplate. J Appl Phys 2014;116. https://doi.org/10.1063/1.4886315.
[128] Wang KF, Wang BL. Energy gathering performance of micro/nanoscale circular energy harvesters based on flexoelectric effect. Energy 2018;149:597–606. https://doi.org/10.1016/j.energy.2018.02.069.
[129] Tzou H, Deng B, Li H. Flexoelectric actuation and vibration control of ring shells. J Vib Acoust 2017;139:031014. https://doi.org/10.1115/1.4036097.
[130] Hu S, Li H, Tzou H. Flexoelectric responses of circular rings. J Vib Acoust 2013;135:021003. https://doi.org/10.1115/1.4023044.
[131] Yan Z. Exact solutions for the electromechanical responses of a dielectric nano-ring. J Intell Mater Syst Struct 2017;28:1140–9. https://doi.org/10.1177/1045389X16666183.
[132] Kwon SR. Structural analysis of truncated pyramids for flexoelectric sensing. J Mech Sci Technol 2017;31:5971–5. https://doi.org/10.1007/s12206-017-1141-x.
[133] Zeng S, Wang BL, Wang KF. Static stability analysis of nanoscale piezoelectric shells with flexoelectric effect based on couple stress theory. Microsyst Technol 2018;4:1–11. https://doi.org/10.1007/s00542-018-3734-4.
[134] Li H, Hu S, Tzou H. Modal signal analysis of conical shells with flexoelectric sensors. J Intell Mater Syst Struct 2015;26:1551–63. https://doi.org/10.1177/1045389X14544150.

[135] Tzou HSS, Zhang XFF. A flexoelectric double-curvature nonlinear shell energy harvester. J Vib Acoust 2016;138:031006. https://doi.org/10.1115/1.4032719.
[136] Ray MC. Enhanced magnetoelectric effect in multiferroic composite beams due to flexoelectricity and transverse deformations. Int J Mech Mater Des 2017. https://doi.org/10.1007/s10999-017-9380-7.
[137] Shi S, Li P, Jin F. The mechanical analysis of thermo-magneto-electric laminated composites in nanoscale with the consideration of surface and flexoelectric effects. Smart Mater Struct 2018;27. https://doi.org/10.1088/1361-665X/aa995c.
[138] Abdollahi A, Arias I. Constructive and destructive interplay between piezoelectricity and flexoelectricity in flexural sensors and actuators. J Appl Mech 2015;82:121003. https://doi.org/10.1115/1.4031333.
[139] Yan Z, Jiang L. Modified continuum mechanics modeling on size-dependent properties of piezoelectric nanomaterials: a review. Nanomaterials 2017;7:27. https://doi.org/10.3390/nano7020027.
[140] Nguyen BH, Nanthakumar SS, Zhuang X, Wriggers P, Rabczuk T, Jiang X, et al. Dynamic flexoelectric effect on piezoelectric nanostructures. Eur J Mech 2018:1–10.
[141] Born M, Huang K, Lax M. Dynamical theory of crystal lattices vol. 23. Clarendon Press; 2005https://doi.org/10.1119/1.1934059.
[142] Dumitrică T, Landis CM, Yakobson BI. Curvature-induced polarization in carbon nanoshells. Chem Phys Lett 2002;360:182–8. https://doi.org/10.1016/S0009-2614(02)00820-5.
[143] Kalinin SV, Meunier V. Electronic flexoelectricity in low-dimensional systems. Phys Rev B - Condens Matter Mater Phys 2008;77:1–4. https://doi.org/10.1103/PhysRevB.77.033403.
[144] Naumov I, Bratkovsky AM, Ranjan V. Unusual flexoelectric effect in two-dimensional noncentrosymmetric sp2-bonded crystals. Phys Rev Lett 2009;102:2–5. https://doi.org/10.1103/PhysRevLett. 102.217601.
[145] Stengel M. Microscopic response to inhomogeneous deformations in curvilinear coordinates. Nat Commun 2013;4:1–8. https://doi.org/10.1038/ncomms3693.
[146] Banerjee AS, Suryanarayana P. Cyclic density functional theory: a route to the first principles simulation of bending in nanostructures. J Mech Phys Solids 2016;96:605–31. https://doi.org/10.1016/j.jmps.2016.08.007.
[147] Dong L, Niu Q. Geometrodynamics of electrons in a crystal under position and time-dependent deformation. Phys Rev B 2018;98(11):115162. https://doi.org/10.1103/PhysRevB.98.115162.
[148] Deng F, Deng Q, Shen S. A three-dimensional mixed finite element for flexoelectricity. J Appl Mech 2018;85:31009–10. https://doi.org/10.1115/1.4038919.
[149] Hughes TJRR, Cottrell JA, Bazilevs Y. Isogeometric analysis: CAD, finite elements, NURBS, exact geometry and mesh refinement. Comput Methods Appl Mech Eng 2005;194:4135–95. https://doi.org/10.1016/j.cma.2004.10.008.
[150] Liu C, Wang J, Xu G, Kamlah M, Zhang TY. An isogeometric approach to flexoelectric effect in ferroelectric materials. Int J Solids Struct 2019;162:198–210. https://doi.org/10.1016/j.ijsolstr.2018.12.008.
[151] Do HV, Lahmer T, Zhuang X, Alajlan N, Nguyen-xuan H, Rabczuk T. An isogeometric analysis to identify the full flexoelectric complex material properties based on electrical impedance curve. Comput Struct 2019;214:1–14. https://doi.org/10.1016/j.compstruc.2018.10.019.
[152] Nguyen BH, Zhuang X, Rabczuk T. NURBS-based formulation for nonlinear electro-gradient elasticity in semiconductors. Comput Methods Appl Mech Eng 2019;346:1074–95. https://doi.org/10.1016/j.cma.2018.08.026.
[153] Zhang Z, Geng D, Wang X. Calculation of the piezoelectric and flexoelectric effects in nanowires using a decoupled finite element analysis method. J Appl Phys 2016;119:154104. https://doi.org/10.1063/1.4946843.
[154] Abdollahi A, Millán D, Peco C, Arroyo M, Arias I. Revisiting pyramid compression to quantify flexoelectricity: a three-dimensional simulation study. Phys Rev B - Condens Matter Mater Phys 2015;91:1–8. https://doi.org/10.1103/PhysRevB.91.104103.
[155] Abdollahi A, Peco C, Millán D, Arroyo M, Catalan G, Arias I. Fracture toughening and toughness asymmetry induced by flexoelectricity. Phys Rev B - Condens Matter Mater Phys 2015;92:094101. https://doi.org/10.1103/PhysRevB.92.094101.
[156] Cordero-Edwards K, Kianirad H, Canalias C, Sort J, Catalan G. Flexoelectric fracture-ratchet effect in ferroelectrics. Phys Rev Lett 2019;122:135502. https://doi.org/10.1103/PhysRevLett. 122.135502.
[157] Bhaskar UK, Banerjee N, Abdollahi A, Solanas E, Rijnders G, Catalan G, et al. Flexoelectric MEMS: towards an electromechanical strain diode. Nanoscale 2016;8:1293–8. https://doi.org/10.1039/c5nr06514c.
[158] Chen L-Q. Phase-field method of phase transitions/domain structures in ferroelectric thin films: a review. J Am Ceram Soc 2008;91:1835–44. https://doi.org/10.1111/j.1551-2916.2008.02413.x.
[159] Wang J-J, Wang B, Chen L-Q. Understanding, predicting, and designing ferroelectric domain structures and switching guided by the phase-field method. Annu Rev Mater Res 2019;49.
[160] Chen WJ, Zheng Y, Xiong WM, Feng X, Wang B, Wang Y. Effect of mechanical loads on stability of nanodomains in ferroelectric ultrathin films: towards flexible erasing of the non-volatile memories. Sci Rep 2014;4:5339. https://doi.org/10.1038/srep05339.
[161] Gu Y. Phase-field modeling of flexoelectric effect in perovskite ferroelectrics. PhD Thesis; Chen, LQ 2014.
[162] Chen HT, Zhang SD, Soh AK, Yin WY. Phase field modeling of flexoelectricity in solid dielectrics. J Appl Phys 2015;118:034106. https://doi.org/10.1063/1.4926795.
[163] Jiang L, Zhou Y, Zhang Y, Yang Q, Gu Y, Chen LQ. Polarization switching of the incommensurate phases induced by flexoelectric coupling in ferroelectric thin films. Acta Mater 2015;90:344–54. https://doi.org/10.1016/j.actamat.2015.02.039.
[164] Jiang L, Xu X, Zhou Y. Interrelationship between flexoelectricity and strain gradient elasticity in ferroelectric nanofilms: a phase field study. J Appl Phys 2016;120:234102. https://doi.org/10.1063/1.4972222.
[165] Cao Y, Chen L-QQ, Kalinin SV. Role of flexoelectric coupling in polarization rotations at the a-c domain walls in ferroelectric perovskites. Appl Phys Lett 2017;110:202903. https://doi.org/10.1063/1.4983560.
[166] Catalan G, Lubk A, Vlooswijk AHGG, Snoeck E, Magen C, Janssens A, et al. Flexoelectric rotation of polarization in ferroelectric thin films. Nat Mater 2011;10:963–7. https://doi.org/10.1038/nmat3141.
[167] Li M, Wang B, Liu H-J, Huang Y-L, Zhang J, Ma X, et al. Direct observation of weakened interface clamping effect enabled ferroelastic domain switching. Acta Mater 2019;171:184–9. https://doi.org/10.1016/j.actamat.2019.04.003.
[168] Li M, Gu Y, Wang Y, Chen L-Q, Duan W. First-principles study of 180◦ domain walls in BaTiO3: mixed Bloch-Néel-Ising character. Phys Rev B 2014;90:054106. https://doi.org/10.1103/PhysRevB.90.054106.
[169] Wang YJ, Li J, Zhu YL, Ma XL. Phase-field modeling and electronic structural analysis of flexoelectric effect at 180° domain walls in ferroelectric $PbTiO_3$. J Appl Phys 2017;122. https://doi.org/10.1063/1.5017219.
[170] Gu Y, Wang N, Xue F, Chen LQ. Origin of interfacial polar order in incipient ferroelectrics. Phys Rev B - Condens Matter Mater Phys 2015;91:174103. https://doi.org/10.1103/PhysRevB.91.174103.
[171] Gu Y, Hong Z, Britson J, Chen LQ. Nanoscale mechanical switching of ferroelectric polarization via flexoelectricity. Appl Phys Lett 2015;106:022904. https://doi.org/10.1063/1.4905837.
[172] Cao Y, Li Q, Chen LQ, Kalinin SV. Coupling of electrical and mechanical switching in nanoscale ferroelectrics. Appl Phys Lett 2015;107:202905. https://doi.org/10.1063/1.4935977.
[173] Chen W, Zheng Y, Feng X, Wang B. Utilizing mechanical loads and flexoelectricity to induce and control complicated evolution of domain patterns in ferroelectric nanofilms. J Mech Phys Solids 2015;79:108–33. https://doi.org/10.1016/j.jmps.2015.04.003.
[174] Chen W, Liu J, Ma L, Liu L, Jiang GL, Zheng Y. Mechanical switching of ferroelectric domains beyond flexoelectricity. J Mech Phys Solids 2018;111:43–66. https://doi.org/10.1016/j.jmps.2017.10.011.
[175] Xu X, Jiang L, Zhou Y. Reduction of leakage currents in ferroelectric thin films by flexoelectricity: a phase field study. Smart Mater Struct 2017;26. https://doi.org/10.1088/1361-665X/aa8dc8.
[176] Mbarki R, Haskins JB, Kinaci A, Cagin T. Temperature dependence of flexoelectricity in $BaTiO_3$ and $SrTiO_3$ perovskite nanostructures. Phys Lett Sect A Gen At Solid State Phys 2014;378:2181–3. https://doi.org/10.1016/j.physleta.2014.05.011.

[177] Chatzopoulos A, Beck P, Roth J, Trebin HR. Atomistic modeling of flexoelectricity in periclase. Phys Rev B 2016;93:024105. https://doi.org/10.1103/PhysRevB.93.024105.
[178] Ponomareva I, Tagantsev AK, Bellaiche L. Finite-temperature flexoelectricity in ferroelectric thin films from first principles. Phys Rev B - Condens Matter Mater Phys 2012;85:104101. https://doi.org/10.1103/PhysRevB.85.104101.
[179] Fu JY, Zhu W, Li N, Cross LE. Experimental studies of the converse flexoelectric effect induced by inhomogeneous electric field in a barium strontium titanate composition. J Appl Phys 2006;100:024112. https://doi.org/10.1063/1.2219990.
[180] Kityk AV, Schranz W, Sondergeld P, Havlik D, Salje EKH, Scott JF. Low-frequency superelasticity and nonlinear elastic behavior of $SrTiO_3$ crystals. Phys Rev B 2000;61:946–56. https://doi.org/10.1103/PhysRevB.61.946.
[181] Narvaez J, Catalan G. Origin of the enhanced flexoelectricity of relaxor ferroelectrics. Appl Phys Lett 2014;104:162903. https://doi.org/10.1063/1.4871686.
[182] Zhang S, Xu M, Ma G, Liang X, Shen S. Experimental method research on transverse flexoelectric response of poly(vinylidene fluoride). Jpn J Appl Phys 2016;55:071601. https://doi.org/10.7567/JJAP.55.071601.
[183] Shu L, Huang W, Ryung Kwon S, Wang Z, Li F, Wei X, et al. Converse flexoelectric coefficient f 1212 in bulk $Ba_{0.67}Sr_{0.33}TiO_3$. Appl Phys Lett 2014;104. https://doi.org/10.1063/1.4882060.
[184] Axe JD, Harada J, Shirane G. Anomalous acoustic dispersion in centrosymmetric crystals with soft optic phonons. Phys Rev B 1970;1:1227–34. https://doi.org/10.1103/PhysRevB.1.1227.
[185] Shirane G, Axe JD, Harada J, Remeika JP. Soft ferroelectric modes in lead titanate. Phys Rev B 1970;2:155–9. https://doi.org/10.1103/PhysRevB.2.155.
[186] Harada J, Axe JD, Shirane G. Neutron-scattering study of soft modes in cubic $BaTiO_3$. Phys Rev B 1971;4:155–62. https://doi.org/10.1103/PhysRevB.4.155.
[187] Freire JD, Katiyar RS. Lattice dynamics of crystals with tetragonal $BaTiO_3$ structure. Phys Rev B 1988;37:2074–85. https://doi.org/10.1103/PhysRevB.37.2074.
[188] Shandarov SM, Burimov NI, Shmakov SS, Zuev PV, Urban AE, Gorbachev VS, et al. Contribution from the inverse flexoelectic effect to the photorefractive response in a bismuth titanium oxide. Bull Russ Acad Sci Phys 2012;76:1297–300. https://doi.org/10.3103/S1062873812120283.
[189] Gharbi M, Sun ZH, Sharma P, White K. The origins of electromechanical indentation size effect in ferroelectrics. Appl Phys Lett 2009;95. https://doi.org/10.1063/1.3231442.
[190] Zhou H, Pei Y, Hong J, Fang D. Analytical method to determine flexoelectric coupling coefficient at nanoscale. Appl Phys Lett 2016;108. https://doi.org/10.1063/1.4943660.
[191] Robinson CR, White KW, Sharma P. Elucidating the mechanism for indentation size-effect in dielectrics. Appl Phys Lett 2012;101:10–2. https://doi.org/10.1063/1.4753799.
[192] Gharbi M, Sun ZH, Sharma P, White K, El-Borgi S. Flexoelectric properties of ferroelectrics and the nanoindentation size-effect. Int J Solids Struct 2011;48:249–56. https://doi.org/10.1016/j.ijsolstr.2010.09.021.
[193] Das S, Wang B, Paudel TR, Park SM, Tsymbal EY, Chen L-QQ, et al. Enhanced flexoelectricity at reduced dimensions revealed by mechanically tunable quantum tunnelling. Nat Commun 2019;10:1–7. https://doi.org/10.1038/s41467-019-08462-0.
[194] Shu L, Wei X, Jin L, Li Y, Wang H, Yao X. Enhanced direct flexoelectricity in paraelectric phase of $Ba(Ti_{0.87}Sn_{0.13})O_3$ ceramics. Appl Phys Lett 2013;102. https://doi.org/10.1063/1.4802450.
[195] Shu L, Wan M, Wang Z, Wang L, Lei S, Wang T, et al. Large flexoelectricity in Al_2O_3-doped $Ba(Ti_{0.85}Sn_{0.15})O_3$ ceramics. Appl Phys Lett 2017;110:192903. https://doi.org/10.1063/1.4983195.
[196] Li Y, Shu L, Zhou Y, Guo J, Xiang F, He L, et al. Enhanced flexoelectric effect in a non-ferroelectric composite. Appl Phys Lett 2013;103. https://doi.org/10.1063/1.4824168.
[197] Li Y, Shu L, Huang W, Jiang X, Wang H. Giant flexoelectricity in $Ba_{0.6}Sr_{0.4}TiO_3/Ni_{0.8}Zn_{0.2}Fe_2O_4$ composite. Appl Phys Lett 2014;105. https://doi.org/10.1063/1.4899060.
[198] Zubko P, Catalan G, Buckley A, Welche PRL, Scott JF. Strain-gradient-induced polarization in $SrTiO_3$ single Crystals. Phys Rev Lett 2007;99:99–102. https://doi.org/10.1103/PhysRevLett. 99.167601.
[199] Shu L, Huang W, Ryung Kwon S, Wang Z, Li F, Wei X, et al. flexoelectric coefficient f 1212 in bulk $Ba_{0.67}Sr_{0.33}TiO_3$. Appl Phys Lett 2014;104:232902. https://doi.org/10.1063/1.4882060.
[200] Chu K, Jang B-KK, Sung JH, Shin YA, Lee E-SS, Song K, et al. Enhancement of the anisotropic photocurrent in ferroelectric oxides by strain gradients. Nat Nanotechnol 2015;10:972–9. https://doi.org/10.1038/nnano.2015.191.
[201] Scott JF, Salje EKH, Carpenter MA. Domain wall damping and elastic softening in $SrTiO_3$: evidence for polar twin walls. Phys Rev Lett 2012;109:187601. https://doi.org/10.1103/PhysRevLett. 109.187601.
[202] Shu L, Wan M, Jiang X, Li F, Zhou N, Huang W, et al. Frequency dispersion of flexoelectricity in PMN-PT single crystal. AIP Adv 2017;7:2–8. https://doi.org/10.1063/1.4973684.
[203] Shu L, Li T, Wang Z, Li F, Fei L, Rao Z, et al. Flexoelectric behavior in PIN-PMN-PT single crystals over a wide temperature range. Appl Phys Lett 2017;111. https://doi.org/10.1063/1.5001265.
[204] Huang S, Kim T, Hou D, Cann D, Jones JL, Jiang X. Flexoelectric characterization of $BaTiO_3$-0.08Bi(Zn1/2Ti1/2)O_3. Appl Phys Lett 2017;110. https://doi.org/10.1063/1.4984212.
[205] Huang W, Kim K, Zhang S, Yuan F-GG, Jiang X. Scaling effect of flexoelectric (Ba, Sr)TiO_3 microcantilevers. Phys Status Solidi - Rapid Res Lett 2011;5:350–2. https://doi.org/10.1002/pssr.201105326.
[206] Shu L, Wei X, Jin L, Li Y, Wang H, Yao X. Enhanced direct flexoelectricity in paraelectric phase of $Ba(Ti_{0.87}Sn_{0.13})O_3$ ceramics. Appl Phys Lett 2013;102. https://doi.org/10.1063/1.4802450.
[207] Shu L, Wang T, Jiang X, Huang W. Verification of the flexoelectricity in barium strontium titanate through d33 meter. AIP Adv 2016;6. https://doi.org/10.1063/1.4968524.
[208] Kwon SR, Huang W, Shu L, Yuan FG, Maria JP, Jiang X. Flexoelectricity in barium strontium titanate thin film. Appl Phys Lett 2014;105. https://doi.org/10.1063/1.4898139.
[209] Hana P. Study of flexoelectric phenomenon from direct and from inverse flexoelectric behavior of PMNT ceramic. Ferroelectrics 2007;351:196–203. https://doi.org/10.1080/00150190701354281.
[210] Zhang S, Liu K, Xu M, Shen H, Chen K, Feng B, et al. Investigation of the 2312 flexoelectric coefficient component of polyvinylidene fluoride: deduction, simulation, and mensuration. Sci Rep 2017;7:1–9. https://doi.org/10.1038/s41598-017-03403-7.
[211] Hana P, Marvan M, Burianova L, Zhang SJ, Furman E, Shrout TR. Study of the inverse flexoelectric phenomena in ceramic lead magnesium niobate-lead titanate. Ferroelectrics 2006;336:137–44. https://doi.org/10.1080/00150190600696006.
[212] Hu T, Deng Q, Shen S. Probing flexoelectricity via a split Hopkinson pressure bar experiment. Appl Phys Lett 2018;112:242902. https://doi.org/10.1063/1.5029421.
[213] Hehlen B, Arzel L, Tagantsev AK, Courtens E, Inaba Y, Yamanaka A, et al. Brillouin-scattering observation of the TA-TO coupling in $SrTiO_3$. Phys Rev B 1998;57:989–92.
[214] Vaks VG. Introdution to microscopic theory of ferroelectrics. Moscow: Nauka; 1973.
[215] Cowley RA. Lattice dynamics and phase transitions of strontium titanate. Phys Rev 1964;134:134.A981. https://doi.org/10.1103/PhysRev.
[216] Farhi E, Tagantsev AKA, Currat R, Hehlen B, Courtens E, Boatner LAA. Low energy phonon spectrum and its parameterization in pure $KTaO_3$ below 80 K. Eur Phys J B 2000;15:615–23. https://doi.org/10.1007/PL00011049.
[217] Yudin PV, Ahluwalia R, Tagantsev AK. Upper bounds for flexoelectric coefficients in ferroelectrics. Appl Phys Lett 2014;104:2–5. https://doi.org/10.1063/1.4865208.
[218] Hong J, Catalan G, Scott JF, Artacho E. The flexoelectricity of barium and strontium titanates from first principles. 112201 J Phys Condens Matter 2010;22. https://doi.org/10.1088/0953-8984/22/11/112201.

[219] Hong J, Catalan G, Fang DN, Artacho E, Scott JF. Topology of the polarization field in ferroelectric nanowires from first principles. Phys Rev B - Condens Matter Mater Phys 2010;81:1–4. https://doi.org/10.1103/PhysRevB.81.172101.
[220] Xu T, Wang J, Shimada T, Kitamura T. Direct approach for flexoelectricity from first-principles calculations: cases for $SrTiO_3$ and BaTiO3. J Phys Condens Matter 2013;25:415901. https://doi.org/10.1088/0953-8984/25/41/415901.
[221] Li G, Huang X, Hu J, Zhang W. Shear-strain gradient induced polarization reversal in ferroelectric $BaTiO_3$ thin films: a first-principles total-energy study. Phys Rev B 2017;95:1–8. https://doi.org/10.1103/PhysRevB.95.144111.
[222] Zhuang X, He B, Javvaji B, Park HS. Intrinsic bending flexoelectric constants in two-dimensional materials. Phys Rev B 2019;99. https://doi.org/10.1103/PhysRevB.99.054105.
[223] Li Q, Nelson CT, Hsu S-L, Damodaran AR, Li L-L, Yadav AK, et al. Quantification of flexoelectricity in $PbTiO_3/SrTiO_3$ superlattice polar vortices using machine learning and phase-field modeling. Nat Commun 2017;8:1468. https://doi.org/10.1038/s41467-017-01733-8.
[224] Yadav AK, Nelson CT, Hsu SL, Hong Z, Clarkson JD, Schlepuëtz CM, et al. Observation of polar vortices in oxide superlattices. Nature 2016;530:198–201. https://doi.org/10.1038/nature16463.
[225] García-Fernández P, Wojdeł JC, Íñiguez J, Junquera J. Second-principles method for materials simulations including electron and lattice degrees of freedom. Phys Rev B 2016;93:195137. https://doi.org/10.1103/PhysRevB.93.195137.
[226] Lee D, Yoon A, Jang SY, Yoon JG, Chung JS, Kim M, et al. Giant flexoelectric effect in ferroelectric epitaxial thin films. Phys Rev Lett 2011;107:1–4. https://doi.org/10.1103/PhysRevLett. 107.057602.
[227] Jeon BC, Lee D, Lee MH, Yang SM, Chae SC, Song TK, et al. Flexoelectric effect in the reversal of self-polarization and associated changes in the electronic functional properties of bifeo 3 thin films. Adv Mater 2013;25:5643–9. https://doi.org/10.1002/adma.201301601.
[228] Lee D, Jeon BC, Yoon A, Shin YJ, Lee MH, Song TK, et al. Flexoelectric control of defect formation in ferroelectric epitaxial thin films. Adv Mater 2014;26:5005–11. https://doi.org/10.1002/adma.201400654.
[229] Quackenbush NF, Paik H, Wahila MJ, Sallis S, Holtz ME, Huang X, et al. Stability of the M2 phase of vanadium dioxide induced by coherent epitaxial strain. Phys Rev B 2016;94:085105. https://doi.org/10.1103/PhysRevB.94.085105.
[230] Lee D, Yang SM, Yoon JG, Noh TW. Flexoelectric rectification of charge transport in strain-graded dielectrics. Nano Lett 2012;12:6436–40. https://doi.org/10.1021/nl3038129.
[231] Schlom DG, Chen L-Q, Eom C-B, Rabe KM, Streiffer SK, Triscone J-M. Strain tuning of ferroelectric thin films. Annu Rev Mater Res 2007;37:589–626. https://doi.org/10.1146/annurev.matsci.37.061206.113016.
[232] Agar JC, Damodaran AR, Velarde GA, Pandya S, Mangalam RVK, Martin LW. Complex evolution of built-in potential in compositionally-graded $PbZr_{1-x}Ti_xO_3$ thin films. ACS Nano 2015;9:7332–42. https://doi.org/10.1021/acsnano.5b02289.
[233] Wu P-C, Huang R, Hsieh Y-H, Wang B, Yen M, Ho S-Z, et al. Electrical polarization induced by atomically engineered compositional gradient in complex oxide solid solution. NPG Asia Mater 2019;11:17. https://doi.org/10.1038/s41427-019-0117-y.
[234] Molina-Luna L, Wang S, Pivak Y, Zintler A, Pérez-Garza HH, Spruit RG, et al. Enabling nanoscale flexoelectricity at extreme temperature by tuning cation diffusion. Nat Commun 2018;9:4445. https://doi.org/10.1038/s41467-018-06959-8.
[235] Tang YL, Zhu YL, Liu Y, Wang YJ, Ma XL. Giant linear strain gradient with extremely low elastic energy in a perovskite nanostructure array. Nat Commun 2017;8:15994. https://doi.org/10.1038/ncomms15994.
[236] Tan P, Tian H, Huang F, Meng X, Wang Y, Hu C, et al. Strain-gradient-controlled disorder dynamics in chemically substituted ferroelectrics. Phys Rev Appl 2019;11:24037. https://doi.org/10.1103/PhysRevApplied. 11.024037.
[237] Guo H, Dong S, Rack P, Budai J, Beekman C, Gai Z, et al. Strain doping: reversible single-axis control of a complex oxide lattice via helium implantation. Phys Rev Lett 2015;114:1–6. https://doi.org/10.1103/PhysRevLett. 114.256801.
[238] Herklotz A, Rus SF, Ward TZ. Continuously controlled optical band gap in oxide semiconductor thin films. Nano Lett 2016;16:1782–6. https://doi.org/10.1021/acs.nanolett.5b04815.
[239] Herklotz A, Wong AT, Meyer T, Biegalski MD, Lee HN, Ward TZ. Controlling octahedral rotations in a perovskite via strain doping. Sci Rep 2016;6:1–7. https://doi.org/10.1038/srep26491.
[240] Li Y, Adamo C, Chen P, Evans PG, Nakhmanson SM, Parker W, et al. Giant optical enhancement of strain gradient in ferroelectric $BiFeO_3$ thin films and its physical origin. Sci Rep 2015;5:1–7. https://doi.org/10.1038/srep16650.
[241] Lu H, Bark C-W, Esque de los Ojos D, Alcala J, Eom CB, Catalan G, et al. Mechanical writing of ferroelectric polarization. Science (80-) 2012;335:59–61. https://doi.org/10.1126/science:1218693.
[242] Wen Z, Qiu X, Li C, Zheng C, Ge X, Li A, et al. Mechanical switching of ferroelectric polarization in ultrathin $BaTiO_3$ films: the effects of epitaxial strain. 042907:1–6 Appl Phys Lett2014. https://doi.org/10.1063/1.4863855.
[243] Gómez A, Vila-Fungueiriño JM, Moalla R, Saint-Girons G, Gázquez J, Varela M, et al. Electric and mechanical switching of ferroelectric and resistive states in semiconducting $BaTiO_{3-\delta}$ films on silicon. Small 2017;13:1–10. https://doi.org/10.1002/smll.201701614.
[244] Lu H, Liu S, Ye Z, Yasui S, Funakubo H, Rappe AM, et al. Asymmetry in mechanical polarization switching. Appl Phys Lett 2017;110. https://doi.org/10.1063/1.4983381.
[245] Guo EJ, Roth R, Das S, Dörr K. Strain induced low mechanical switching force in ultrathin $PbZr_{0.2}Ti_{0.8}O_3$ films. Appl Phys Lett 2014;105. https://doi.org/10.1063/1.4889892.
[246] Lu H, Lee D, Klyukin K, Tao L, Wang B, Lee H, et al. Tunneling hot spots in ferroelectric $SrTiO_3$. Nano Lett 2018;18:491–7. https://doi.org/10.1021/acs.nanolett.7b04444.
[247] Celano U, Popovici M, Florent K, Lavizzari S, Favia P, Paulussen K, et al. Flexoelectric effect in Al-doped hafnium oxide. Nanoscale 2018;10:8471–6. https://doi.org/10.1039/C8NR00618K.
[248] Zhao HY, Cai K, Cheng ZX, Ma Z, Kimura H, Jia T. Mechanical and electrical switching of local ferroelectric domains of $K_{0.5}Bi_{4.5}Ti_4O_{15}$ film. J Mater Sci Mater Electron 2016;27:5613–7. https://doi.org/10.1007/s10854-016-4467-8.
[249] Chen X, Tang X, Chen XZ, Chen YL, Guo X, Ge HX, et al. Nonvolatile data storage using mechanical force-induced polarization switching in ferroelectric polymer. Appl Phys Lett 2015;106:042903. https://doi.org/10.1063/1.4906859.
[250] Chen L, Cheng Z, Xu W, Meng X, Yuan G, Liu J, et al. Electrical and mechanical switching of ferroelectric polarization in the 70 nm $BiFeO_3$ film. Sci Rep 2016;6:19092. https://doi.org/10.1038/srep19092.
[251] Park SM, Wang B, Das S, Chae SC, Chung J-SS, Yoon J-GG, et al. Selective control of multiple ferroelectric switching pathways using a trailing flexoelectric field. Nat Nanotechnol 2018;13:366–70. https://doi.org/10.1038/s41565-018-0083-5.
[252] Kim DJ, Paudel TR, Lu H, Burton JD, Connell JG, Tsymbal EY, et al. Room-temperature ferroelectricity in hexagonal $TbMnO_3$ thin films. Adv Mater 2014;26:7660–5. https://doi.org/10.1002/adma.201403301.
[253] Jia T, Kimura H, Cheng Z, Zhao H, Kim Y-HH, Osada M, et al. Mechanical force involved multiple fields switching of both local ferroelectric and magnetic domain in a $Bi_5Ti_3FeO_{15}$ thin film. NPG Asia Mater 2017;9:e349–59. https://doi.org/10.1038/am.2017.3.
[254] Cao Y, Morozovska A, Kalinin SV. Pressure-induced switching in ferroelectrics: phase-field modeling, electrochemistry, flexoelectric effect, and bulk vacancy dynamics. Phys Rev B 2017;96:184109. https://doi.org/10.1103/PhysRevB.96.184109.
[255] Sharma P, Ryu S, Viskadourakis Z, Paudel TR, Lee H, Panagopoulos C, et al. Electromechanics of ferroelectric-like behavior of $LaAlO_3$ thin films. Adv Funct Mater 2015;25:6538–44. https://doi.org/10.1002/adfm.201502483.
[256] Lu H, Wang B, Li T, Lipatov A, Lee H, Rajapitamahuni A, et al. Nanodomain engineering in ferroelectric capacitors with graphene electrodes. Nano Lett 2016;16:6460–6. https://doi.org/10.1021/acs.nanolett.6b02963.
[257] Yusuf MH, Gura A, Du X, Dawber M. Local control of the resistivity of graphene through mechanically induced switching of a ferroelectric superlattice. 2D Mater 2017;4. https://doi.org/10.1088/2053-1583/aa636f.
[258] McQuaid RGP, Campbell MP, Whatmore RW, Kumar A, Marty Gregg J. Injection and controlled motion of conducting domain walls in improper ferroelectric

Cu-Cl boracite. Nat Commun 2017;8:15105. https://doi.org/10.1038/ncomms15105.
[259] Lu H, Kim DJ, Bark CW, Ryu S, Eom CB, Tsymbal EY, et al. Mechanically-induced resistive switching in ferroelectric tunnel junctions. Nano Lett 2012;12:6289–92. https://doi.org/10.1021/nl303396n.
[260] Chen WJ, Yuan S, Ma LL, Ji Y, Wang B, Zheng Y. Mechanical switching in ferroelectrics by shear stress and its implications on charged domain wall generation and vortex memory devices. RSC Adv 2018;8:4434–44. https://doi.org/10.1039/c7ra12233k.
[261] Alsubaie A, Sharma P, Liu G, Nagarajan V, Seidel J. Mechanical stress-induced switching kinetics of ferroelectric thin films at the nanoscale. Nanotechnology 2017;28:075709. https://doi.org/10.1088/1361-6528/aa536d.
[262] Sharma P, Ryu S, Burton JD, Paudel TR, Bark CW, Huang Z, et al. Mechanical tuning of $LaAlO_3/SrTiO_3$ interface conductivity. Nano Lett 2015;15:3547–51. https://doi.org/10.1021/acs.nanolett.5b01021.
[263] Das S, Wang B, Cao Y, Rae Cho M, Jae Shin Y, Yang SM, et al. Controlled manipulation of oxygen vacancies using nanoscale flexoelectricity. Nat Commun 2017;8:1–8. https://doi.org/10.1038/s41467-017-00710-5.
[264] Kim Y, Kelly SJ, Morozovska A, Rahani EK, Strelcov E, Eliseev E, et al. Mechanical control of electroresistive switching. Nano Lett 2013;13:4068–74. https://doi.org/10.1021/nl401411r.
[265] Seol D, Yang SM, Jesse S, Choi M. Dynamic mechanical control of local vacancies in Dynamic mechanical control of local vacancies in NiO thin films; 2018.
[266] Heo Y, Jang BK, Kim SJ, Yang CH, Seidel J. Nanoscale mechanical softening of morphotropic $BiFeO_3$. Adv Mater 2014;26:7568–72. https://doi.org/10.1002/adma.201401958.
[267] Li YJ, Wang JJ, Ye JC, Ke XX, Gou GY, Wei Y, et al. Mechanical switching of nanoscale multiferroic phase boundaries. Adv Funct Mater 2015;25:3405–13. https://doi.org/10.1002/adfm.201500600.
[268] Sharma P, Heo Y, Jang BK, Liu Y, Nagarajan V, Li J, et al. Morphotropic phase elasticity of strained $BiFeO_3$. Adv Mater Interfaces 2016;3:1–8. https://doi.org/10.1002/admi.201600033.
[269] Cao Y, Yang S, Jesse S, Kravchenko I, Yu P, Chen L-QQ, et al. Exploring polarization rotation instabilities in super-tetragonal $BiFeO_3$ epitaxial thin films and their technological implications. Adv Electron Mater 2016;2:1600307. https://doi.org/10.1002/aelm.201600307.
[270] Cordero-Edwards K, Domingo N, Abdollahi A, Sort J, Catalan G. Ferroelectrics as smart mechanical materials. Adv Mater 2017;29:1–6. https://doi.org/10.1002/adma.201702210.
[271] Meier D, Seidel J, Cano A, Delaney K, Kumagai Y, Mostovoy M, et al. Anisotropic conductance at improper ferroelectric domain walls. Nat Mater 2012;11:284–8. https://doi.org/10.1038/nmat3249.
[272] Seidel J, Martin LW, He Q, Zhan Q, Chu YH, Rother A, et al. Conduction at domain walls in oxide multiferroics. Nat Mater 2009;8:229–34. https://doi.org/10.1038/nmat2373.
[273] Eliseev EA, Morozovska AN, Svechnikov GS, Maksymovych P, Kalinin SV. Domain wall conduction in multiaxial ferroelectrics. Phys Rev B - Condens Matter Mater Phys 2012;85:1–11. https://doi.org/10.1103/PhysRevB.85.045312.
[274] Houchmandzadeh B, Lajzerowicz J, Salje EKH. Order parameter coupling and chirality of domain walls. J Phys Condens Matter 1991;3:5163–9. https://doi.org/10.1088/0953-8984/3/27/009.
[275] Yudin PV, Tagantsev AK, Eliseev EA, Morozovska AN, Setter N. Bichiral structure of ferroelectric domain walls driven by flexoelectricity. Phys Rev B - Condens Matter Mater Phys 2012;86:1–9. https://doi.org/10.1103/PhysRevB.86.134102.
[276] Calleja M, Dove MT, Salje EK. Trapping of oxygen vacancies on twin walls of $CaTiO_3$: a computer simulation study related content anisotropic ionic transport in quartz: the effect of twinboundaries. J Phys Condens Matter 2003;15:2301–7.
[277] Goncalves-Ferreira L, Redfern SAT, Artacho E, Salje E, Lee WT. Trapping of oxygen vacancies in the twin walls of perovskite. Phys Rev B - Condens Matter Mater Phys 2010;81:1–7. https://doi.org/10.1103/PhysRevB.81.024109.
[278] Salje EKHH, Aktas O, Carpenter MA, Laguta VV, Scott JF. Domains within domains and walls within walls: evidence for polar domains in cryogenic $SrTiO_3$. Phys Rev Lett 2013;111:1–5. https://doi.org/10.1103/PhysRevLett. 111.247603.
[279] Van Aert S, Turner S, Delville R, Schryvers D, Van Tendeloo G, Salje EKH. Direct observation of ferrielectricity at ferroelastic domain boundaries in $CaTiO_3$ by electron microscopy. Adv Mater 2012;24:523–7. https://doi.org/10.1002/adma.201103717.
[280] Barone P, Di Sante D, Picozzi S. Improper origin of polar displacements at $CaTiO_3$ and $CaMnO_3$ twin walls. Phys Rev B 2014;89:144104. https://doi.org/10.1103/PhysRevB.89.144104.
[281] Yokota H, Usami H, Haumont R, Hicher P, Kaneshiro J, Salje EKH, et al. Direct evidence of polar nature of ferroelastic twin boundaries in $CaTiO_3$ obtained by second harmonic generation microscope. Phys Rev B - Condens Matter Mater Phys 2014;89:144109. https://doi.org/10.1103/PhysRevB.89.144109.
[282] Goncalves-Ferreira L, Redfern SAT, Artacho E, Salje EKH. Ferrielectric twin walls in $CaTiO_3$. Phys Rev Lett 2008;101:1–4. https://doi.org/10.1103/PhysRevLett. 101.097602.
[283] Catalan G, Seidel J, Ramesh R, Scott JF. Domain wall nanoelectronics. Rev Mod Phys 2012;84:119–56. https://doi.org/10.1103/RevModPhys. 84.119.
[284] Tagantsev AK, Courtens E, Arzel L. Prediction of a low-temperature ferroelectric instability in antiphase domain boundaries of strontium titanate. Phys Rev B 2001;64:224107. https://doi.org/10.1103/physrevb.64.224107.
[285] Maksymovych P, Morozovska AN, Yu P, Eliseev EA, Chu YH, Ramesh R, et al. Tunable metallic conductance in ferroelectric nanodomains. Nano Lett 2012;12:209–13. https://doi.org/10.1021/nl203349b.
[286] Zeches RJ, Rossell MD, Zhang JX, Hatt AJ, He Q, Yang C-HH, et al. A strain-driven morphotropic phase boundary in $BiFeO_3$. Science (80-) 2009;326:977–80. https://doi.org/10.1126/science.1177046.
[287] Cheng CE, Liu HJ, Dinelli F, Chen YC, Chang C, Chien Forest Shih-Sen, et al. Revealing the flexoelectricity in the mixed-phase regions of epitaxial $BiFeO_3$ thin films. Sci Rep 2015;5:8091. https://doi.org/10.1038/srep08091.
[288] Borisevich AY, Eliseev EA, Morozovska AN, Cheng CJ, Lin JY, Chu YH, et al. Atomic-scale evolution of modulated phases at the ferroelectric- antiferroelectric morphotropic phase boundary controlled by flexoelectric interaction. Nat Commun 2012;3:775–8. https://doi.org/10.1038/ncomms1778.
[289] Tagantsev AK, Vaideeswaran K, Vakhrushev SB, Filimonov AV, Burkovsky RG, Shaganov A, et al. The origin of antiferroelectricity in $PbZrO_3$. Nat Commun 2013;4:2229. https://doi.org/10.1038/ncomms3229.
[290] Scott JF. Flexoelectric spectroscopy. J Phys Condens Matter 2013;25. https://doi.org/10.1088/0953-8984/25/33/331001.
[291] Majdoub MS, Maranganti R, Sharma P. Understanding the origins of the intrinsic dead layer effect in nanocapacitors. Phys Rev B - Condens Matter Mater Phys 2009;79:1–8. https://doi.org/10.1103/PhysRevB.79.115412.
[292] Liu C, Wu H, Wang J. Giant piezoelectric response in piezoelectric/dielectric superlattices due to flexoelectric effect. Appl Phys Lett 2016;109:1–6. https://doi.org/10.1063/1.4967003.
[293] Liu C, Wang J. Size-dependent electromechanical properties in piezoelectric superlattices due to flexoelectric effect. Theor Appl Mech Lett 2017;7:88–92. https://doi.org/10.1016/j.taml.2017.02.007.
[294] Kholkin A, Bdikin I, Ostapchuk T, Petzelt J. Room temperature surface piezoelectricity in $SrTiO_3$ ceramics via piezoresponse force microscopy. Appl Phys Lett 2008;93:2006–9. https://doi.org/10.1063/1.3037220.
[295] Dai S, Gharbi M, Sharma P, Park HS. Surface piezoelectricity: Size effects in nanostructures and the emergence of piezoelectricity in non-piezoelectric materials. J Appl Phys 2011;110. https://doi.org/10.1063/1.3660431.
[296] Heifets E, Eglitis RI, Kotomin EA, Maier J, Borstel G. First-principles calculations for $SrTiO_3$(1 0 0) surface structure. Surf Sci 2002;513:211–20. https://doi.org/10.1016/S0039-6028(02)01730-2.
[297] Herger R, Willmott PR, Bunk O, Schlepütz CM, Patterson BD, Delley B. Surface of strontium titanate. Phys Rev Lett 2007;98:76102. https://doi.org/10.1103/PhysRevLett. 98.076102.
[298] Tararam R, Bdikin IK, Panwar N, Varela JA, Bueno PR, Kholkin AL. Nanoscale electromechanical properties of $CaCu_3Ti_4O_{12}$ ceramics. J Appl Phys 2011;110:052019. https://doi.org/10.1063/1.3623767.
[299] Yang T, Zhang X, Chen B, Guo H, Jin K, Wu X, et al. The evidence of giant surface flexoelectric field in (111) oriented $BiFeO_3$ thin film. ACS Appl Mater

Interfaces 2017;9:5600–6. https://doi.org/10.1021/acsami.6b15162.
[300] Zhao X, Soh AKK. The effect of flexoelectricity on domain switching in the vicinity of a crack in ferroelectrics. J Eur Ceram Soc 2018;38:1341–8. https://doi.org/10.1016/j.jeurceramsoc.2017.10.009.
[301] Gao P, Yang S, Ishikawa R, Li N, Feng B, Kumamoto A, et al. Atomic-scale measurement of flexoelectric polarization at $SrTiO_3$ dislocations. Phys Rev Lett 2018;120:267601. https://doi.org/10.1103/PhysRevLett. 120.267601.
[302] Kim T, Huang W, Huang S, Jiang X. Thermal gradient induced flexoelectric effects in bulk $Ba_{0.67}Sr_{0.33}TiO_3$. Appl Phys Lett 2016;108. https://doi.org/10.1063/1.4949358.
[303] Astafiev KF, Tagantsev AK, Setter N. Quasi-Debye microwave loss as an intrinsic limitation of microwave performance of tunable components based on $SrTiO_3$ and $Ba_xSr_{1-x}TiO_3$ ferroelectrics. J Appl Phys 2005;97. https://doi.org/10.1063/1.1829149.
[304] Rumyantseva ED, Zalesskii VG. Strain of a $BaTiO_3$ single crystal caused by the converse flexoelectric effect. Phys Solid State 2016;58:689–94. https://doi.org/10.1134/s1063783416040211.
[305] Zalesskii VG, Rumyantseva ED. Converse flexoelectric effect in the $SrTiO_3$ single crystal. Phys Solid State 2014;56:1352–4. https://doi.org/10.1134/s106378341407035x.
[306] Koirala P, Mizzi CA, Marks LD. Direct observation of large flexoelectric bending at the nanoscale in lanthanide scandates. Nano Lett 2018;18:3850–6. https://doi.org/10.1021/acs.nanolett.8b01126.
[307] Abdollahi A, Domingo N, Arias I, Catalan G. Converse flexoelectricity yields large piezoresponse force microscopy signals in non-piezoelectric materials. Nat Commun 2019;10:1266. https://doi.org/10.1038/s41467-019-09266-y.
[308] Wang K, Wang C, Huang S, Xie W, Cai HL, Zhang FM, et al. Anisotropic lattice strain induced by the enhanced electronic hybridization in $SrTiO_3$. Appl Phys Lett 2018;113:242903. https://doi.org/10.1063/1.5053927.
[309] Zhang S, Liu K, Wen X, Wu T, Xu M, Shen S. Converse flexoelectricity with relative permittivity gradient. Appl Phys Lett 2019;114:52903. https://doi.org/10.1063/1.5053413.
[310] Guo R, Shen L, Wang H, Lim Z, Lu W, Yang P, et al. Tailoring self-polarization of $BaTiO_3$ thin films by interface engineering and flexoelectric effect. Adv Mater Interfaces 2016;3:1600737. https://doi.org/10.1002/admi.201600737.
[311] Yang M-MM, Kim DJ, Alexe M. Flexo-photovoltaic effect. Science (80-) 2018;360:904–7. https://doi.org/10.1126/science.aan3256.
[312] Morozovska AN, Glinchuk MD. Flexo-chemo effect in nanoferroics as a source of critical size disappearance at size-induced phase transitions. J Appl Phys 2016;119:094109. https://doi.org/10.1063/1.4942859.
[313] Zhou H, Hong J, Zhang Y, Li F, Pei Y, Fang D. Flexoelectricity induced increase of critical thickness in epitaxial ferroelectric thin films. Phys B Condens Matter 2012;407:3377–81. https://doi.org/10.1016/j.physb.2012.04.041.
[314] Eliseev EA, Vorotiahin IS, Fomichov YM, Glinchuk MD, Kalinin SV, Genenko YA, et al. Defect-driven flexochemical coupling in thin ferroelectric films. Phys Rev B 2018;97:1–17. https://doi.org/10.1103/PhysRevB.97.024102.
[315] Mbarki R, Borvayeh L, Sabati M. Investigation of the flexoelectric coupling effect on the 180° domain wall structure and interaction with defects. J Mater Sci Eng 2016;5:4–9. https://doi.org/10.4172/2169-0022.1000264.
[316] Salje EKH, Li S, Stengel M, Gumbsch P, Ding X. Flexoelectricity and the polarity of complex ferroelastic twin patterns. Phys Rev B 2016;94:1–11. https://doi.org/10.1103/PhysRevB.94.024114.
[317] Eliseev EA, Yudin PV, Kalinin SV, Setter N, Tagantsev AK, Morozovska AN. Structural phase transitions and electronic phenomena at 180-degree domain walls in rhombohedral $BaTiO_3$. Phys Rev B - Condens Matter Mater Phys 2013;87:1–9. https://doi.org/10.1103/PhysRevB.87.054111.
[318] Sharma ND, Landis CM, Sharma P. Piezoelectric thin-film superlattices without using piezoelectric materials. J Appl Phys 2010;108. https://doi.org/10.1063/1.3443404.
[319] Bhaskar UK, Banerjee N, Abdollahi A, Wang Z, Schlom DG, Rijnders G, et al. A flexoelectric microelectromechanical system on silicon. Nat Nanotechnol 2016;11:263–6. https://doi.org/10.1038/nnano.2015.260.
[320] Pyatakov AP, Sergeev AS, Mikailzade FA, Zvezdin AK. Spin flexoelectricity and chiral spin structures in magnetic films. J Magn Magn Mater 2015;383:255–8. https://doi.org/10.1016/j.jmmm.2014.11.035.
[321] Mills DL, Dzyaloshinskii IE. Influence of electric fields on spin waves in simple ferromagnets: role of the flexoelectric interaction. Phys Rev B - Condens Matter Mater Phys 2008;78:184422. https://doi.org/10.1103/PhysRevB.78.184422.
[322] Zvezdin AK, Pyatakov AP. On the problem of coexistence of the weak ferromagnetism and the spin flexoelectricity in multiferroic bismuth ferrite. EPL 2012;99:57003. https://doi.org/10.1209/0295-5075/99/57003.
[323] Bursian EV. The importance of the unlocal piezoeffect in domain structure formation in ferroelectrics. Ferroelectrics 2004;307:177–9. https://doi.org/10.1080/00150190490493014.
[324] Gridnev S. Flexure-electrical effect in ferroelectric and paraelectric ceramics with perovskite structure. Appl. Ferroelectr. In: ISAF'96., Proc. Tenth IEEE Int. Symp., vol. 2, IEEE; 1996. p. 891–3.
[325] Shandarov SM, Shmakov SS, Zuev PV, Burimov NI, Kargin YF, Shepelevich VV, et al. Contribution of the inverse flexoelectric effect to counterpropagating two-wave mixing of light beams in photorefractive crystals. J Opt Technol 2013;80:409–14. https://doi.org/10.1364/jot.80.000409.
[326] Hadjesfandiari AR, Dargush GF. Couple stress theory for solids. Int J Solids Struct 2011;48:2496–510. https://doi.org/10.1016/j.ijsolstr.2011.05.002.
[327] Sharma ND, Maranganti R, Sharma P. On the possibility of piezoelectric nanocomposites without using piezoelectric materials. J Mech Phys Solids 2007;55:2328–50. https://doi.org/10.1016/j.jmps.2007.03.016.
[328] Chu B, Zhu W, Li N, Cross LE. Flexure mode flexoelectric piezoelectric composites. J Appl Phys 2009;106:2012–5. https://doi.org/10.1063/1.3262495.
[329] Zhu W, Fu JY, Li N, Cross L. Piezoelectric composite based on the enhanced flexoelectric effects. Appl Phys Lett 2006;89. https://doi.org/10.1063/1.2382740.
[330] Le Quang H, He Q-C. The number and types of all possible rotational symmetries for flexoelectric tensors. Proc R Soc A Math Phys Eng Sci 2011;467:2369–86. https://doi.org/10.1098/rspa.2010.0521.
[331] Shu L, Wei X, Pang T, Yao X, Wang C. Symmetry of flexoelectric coefficients in crystalline medium. J Appl Phys 2011;110:104106. https://doi.org/10.1063/1.3662196.
[332] Shu L, Wei X, Pang T, Yao X, Wang C. Erratum: "Symmetry of flexoelectric coefficients in crystalline medium" [J. Appl. Phys. 110, 104106 (2011)]. J Appl Phys 2014;116:129901. https://doi.org/10.1063/1.4896397.
[333] Shu L, Li F, Huang W, Wei X, Yao X, Jiang X. Relationship between direct and converse flexoelectric coefficients. J Appl Phys 2014;116:144105. https://doi.org/10.1063/1.4897647.
[334] Eliseev EA, Morozovska AN. Hidden symmetry of flexoelectric coupling. Phys Rev B 2018;98:94108. https://doi.org/10.1103/PhysRevB.98.094108.
[335] Vorotiahin IS, Eliseev EA, Li Q, Kalinin SV, Genenko YA, Morozovska AN. Tuning the polar states of ferroelectric films via surface charges and flexoelectricity. Acta Mater 2017;137:85–92. https://doi.org/10.1016/j.actamat.2017.07.033.
[336] Biancoli A, Fancher CM, Jones JL, Damjanovic D. Breaking of macroscopic centric symmetry in paraelectric phases of ferroelectric materials and implications for flexoelectricity. Nat Mater 2015;14:224–9. https://doi.org/10.1038/nmat4139.
[337] Garten LM, Trolier-Mckinstry S. Enhanced flexoelectricity through residual ferroelectricity in barium strontium titanate. J Appl Phys 2015;117:094102. https://doi.org/10.1063/1.4913858.
[338] Lu C, Nakajima N, Maruyama H. Observation of the flexoelectricity of a $SrTiO_3$ single crystal by x-ray absorption and emission spectroscopies. J Phys Condens Matter 2017;29:045702. https://doi.org/10.1088/1361-648X/29/4/045702.
[339] Zhang X, Pan Q, Tian D, Zhou W, Chen P, Zhang H, et al. Large flexoelectriclike response from the spontaneously polarized surfaces in ferroelectric ceramics. Phys Rev Lett 2018;121:57602. https://doi.org/10.1103/PhysRevLett.121.057602.
[340] Bersuker IB. Pseudo Jahn-Teller effect in the origin of enhanced flexoelectricity. Appl Phys Lett 2015;106:022903. https://doi.org/10.1063/1.4905679.
[341] Tikhomirov O, Jiang H, Levy J. Direct observation of local ferroelectric phase transitions in $Ba_xSr_{1-x}TiO_3$ thin films. Appl Phys Lett 2000;77:2048–50. https://doi.org/10.1063/1.1311950.

[342] Zalar B, Laguta VV, Blinc R. NMR evidence for the coexistence of order-disorder and displacive components in barium titanate. Phys Rev Lett 2003;90:37601. https://doi.org/10.1103/PhysRevLett.90.037601.

[343] Tenne DA, Soukiassian A, Xi XX, Choosuwan H, Guo R, Bhalla AS. Lattice dynamics in $Ba_xSr_{1-x}TiO_3$ thin films studied by Raman spectroscopy. J Appl Phys 2004;96:6597–605. https://doi.org/10.1063/1.1806553.

[344] Senn MS, Keen DA, Lucas TCA, Hriljac JA, Goodwin AL. Emergence of long-range order in $BaTiO_3$ from local symmetry-breaking distortions. Phys Rev Lett 2016;116:1–5. https://doi.org/10.1103/PhysRevLett.116.207602.

[345] Zhu J, Chen T, Shu L, Wang Z, Huang W, Fei L, et al. Flexoelectric fatigue in (K, Na, Li)(Nb, Sb)O_3 ceramics. Appl Phys Lett 2018;113:182901. https://doi.org/10.1063/1.5045716.

[346] Simons H, Haugen AB, Jakobsen AC, Schmidt S, Stöhr F, Majkut M, et al. Long-range symmetry breaking in embedded ferroelectrics. Nat Mater 2018;17:814. https://doi.org/10.1038/s41563-018-0116-3.

[347] Aktas O, Salje EKH. Macroscopic symmetry breaking and piezoelectricity in relaxor ferroelectric lead magnesium niobate. Appl Phys Lett 2018;113:202901. https://doi.org/10.1063/1.5055001.

[348] Bersuker IB. Pseudo-Jahn-teller effect – a two-state paradigm in formation, deformation, and transformation of molecular systems and solids. Chem Rev 2013;113:1351–90. https://doi.org/10.1021/cr300279n.

[349] Bersuker I. The Jahn-Teller Effect. Cambridge, UK: Cambridge University Press; 2006.

[350] Zhou W, Chen P, Hou Y, Chen P, Zhang H, Chu B. The surface mechanism for the flexoelectric response in sodium bismuth titanate-based ferroelectric ceramics. J Am Ceram Soc 2019:1–11. https://doi.org/10.1111/jace.16433.

[351] Abdollahi A, Vásquez-Sancho F, Catalan G. Piezoelectric mimicry of flexoelectricity. Phys Rev Lett 2018;121:205502. https://doi.org/10.1103/PhysRevLett.121.205502.

[352] Morozovska AN, Eliseev EA. Size effect of soft phonon dispersion in nanosized ferroics. Phys Rev B 2019;99:115412. https://doi.org/10.1103/physrevb.99.115412.

[353] Wen X, Li D, Tan K, Deng Q, Shen S. Flexoelectret: an electret with tunable flexoelectric-like response. Phys Rev Lett 2018;122:1–14. https://doi.org/10.1103/PhysRevLett.122.148001.

[354] Rahmati AH, Bauer S, Sharma P, Yang S, Bauer S, Sharma P, et al. Nonlinear bending deformation of soft electrets and prospects for engineering flexoelectricity and transverse d31 piezoelectricity. Soft Matter 2019;15:127–48. https://doi.org/10.1039/c8sm01664j.

[355] Tagantsev AK, Yudin PV. Flexoelectricity in solids: from theory to applications. Comput Mater Contin 2017;45:396.

[356] Wang Y, Shang S-L, Fang H, Liu Z-K, Chen L-Q. First-principles calculations of lattice dynamics and thermal properties of polar solids. Npj Comput Mater 2016;2:16006. https://doi.org/10.1038/npjcompumats.2016.6.

[357] Chen PH, Zhang B. Chu Strain gradient induced thermal-electrical response in paraelectric $Na_{0.5}Bi_{0.5}TiO_3$-based ceramics. Phys Rev Mater 2018;2:034401. https://doi.org/10.1103/PhysRevMaterials.2.034401.

[358] Qi Y, Jafferis NT, Lyons K, Lee CM, Ahmad H, McAlpine MC. Piezoelectric ribbons printed onto rubber for flexible energy conversion. Nano Lett 2010;10:524–5. https://doi.org/10.1021/nl903377u.

[359] Qi Y, Kim J, Nguyen TD, Lisko B, Purohit PK, McAlpine MC. Enhanced piezoelectricity and stretchability in energy harvesting devices fabricated from buckled PZT ribbons. Nano Lett 2011;11:1331–6. https://doi.org/10.1021/nl104412b.

[360] Feng X, Yang BD, Liu Y, Wang Y, Dagdeviren C, Liu Z, et al. Stretchable ferroelectric nanoribbons with wavy configurations on elastomeric substrates. ACS Nano 2011;5:3326–32. https://doi.org/10.1021/nn200477q.

[361] Il Park K, Xu S, Liu Y, Hwang GT, Kang SJL, Wang ZL, et al. $BaTiO_3$ thin film nanogenerator on plastic substrates. Nano Lett 2010;10:4939–43. https://doi.org/10.1021/nl102959k.

[362] Chen X, Xu S, Yao N, Shi Y. 1.6 v nanogenerator for mechanical energy harvesting using PZT nanofibers. Nano Lett 2010;10:2133–7. https://doi.org/10.1021/nl100812k.

[363] Xu S, Yeh Y, Poirier G, Mcalpine M, Register RA, Yao N, et al. Supporting information for flexible piezoelectric PMN-PT nanowire-based nanocomposite and device. Nano Lett 2013;13:1–2.

[364] Han JK, Jeon DH, Cho SY, Kang SW, Yang SA, Bu SD, et al. Nanogenerators consisting of direct-grown piezoelectrics on multi-walled carbon nanotubes using flexoelectric effects. Sci Rep 2016;6:29562. https://doi.org/10.1038/srep29562.

[365] Huang W, Kwon SR, Zhang S, Yuan FG, Jiang X. A trapezoidal flexoelectric accelerometer. J Intell Mater Syst Struct 2014;25:271–7. https://doi.org/10.1177/1045389X13491021.

[366] Kwon SR, Huang WB, Zhang SJ, Yuan FG, Jiang XN. Flexoelectric sensing using a multilayered barium strontium titanate structure. Smart Mater Struct 2013;22:115017. https://doi.org/10.1088/0964-1726/22/11/115017.

[367] Mardana A, Bai M, Baruth A, Ducharme S, Adenwalla S. Magnetoelectric effects in ferromagnetic cobalt/ferroelectric copolymer multilayer films. Appl Phys Lett 2010;97. https://doi.org/10.1063/1.3488814.

[368] Zhou W, Chen P, Pan Q, Zhang X, Chu B. Lead-free metamaterials with enormous apparent piezoelectric response. Adv Mater 2015;27:6349–55. https://doi.org/10.1002/adma.201502562.

[369] Zhang X, Liu J, Chu M, Chu B. Flexoelectric piezoelectric metamaterials based on the bending of ferroelectric ceramic wafers. Appl Phys Lett 2016;109:1–6. https://doi.org/10.1063/1.4961310.

[370] Zhang S, Liu K, Xu M, Shen S. A curved resonant flexoelectric actuator. Appl Phys Lett 2017;111. https://doi.org/10.1063/1.4986370.

[371] Wang Z, Zhang XX, Wang X, Yue W, Li J, Miao J, et al. Giant flexoelectric polarization in a micromachined ferroelectric diaphragm. Adv Funct Mater 2013;23:124–32. https://doi.org/10.1002/adfm.201200839.

[372] Wang Z, Yao Y, Wang X, Yue W, Chen L, Zhang XX. Bending-induced electromechanical coupling and large piezoelectric response in a micromachined diaphragm. Sci Rep 2013;3:1–8. https://doi.org/10.1038/srep03127.

[373] Huang W, Yan X, Kwon SR, Zhang S, Yuan F-G, Jiang X. Flexoelectric strain gradient detection using $Ba_{0.64}Sr_{0.36}TiO_3$ for sensing. Appl Phys Lett 2012;101:252903. https://doi.org/10.1063/1.4772803.

[374] Yan X, Huang W, Ryung Kwon S, Yang S, Jiang X, Yuan FG. A sensor for the direct measurement of curvature based on flexoelectricity. Smart Mater Struct 2013;22:085016. https://doi.org/10.1088/0964-1726/22/8/085016.

[375] Zhang S, Xu M, Liu K, Shen S. A flexoelectricity effect-based sensor for direct torque measurement. J Phys D Appl Phys 2015;48:485502. https://doi.org/10.1088/0022-3727/48/48/485502.

[376] Kwon SR, Huang WB, Zhang SJ, Yuan FG, Jiang XN. Study on a flexoelectric microphone using barium strontium titanate. J Micromechanics Microengineering 2016;26. https://doi.org/10.1088/0960-1317/26/4/045001.

[377] Fousek J, Cross LE, Litvin DB. A4-Possible piezoelectric composites based on the flexoelectric effect. Mater Lett 1999;39:287–91. https://doi.org/10.1016/S0167-577X(99)00020-8.

[378] Fu JY, Cross LE. Separate control of direct and converse piezoelectric effects in flexoelectric piezoelectric composites. Appl Phys Lett 2007;91. https://doi.org/10.1063/1.2790476.

[379] Fu JY, Zhu W, Li N, Smith NB, Eric Cross L. Gradient scaling phenomenon in microsize flexoelectric piezoelectric composites. Appl Phys Lett 2007;91. https://doi.org/10.1063/1.2800794.

[380] Wan M, Yong Z, Huang W, Zhang S, Zhou N, Shu L. Design of a flexure composite with large flexoelectricity. J Mater Sci Mater Electron 2017;28:6505–11. https://doi.org/10.1007/s10854-017-6339-2.

[381] Zhou W, Chu B, Jones JL. Strong electromechanical response in lead zirconate titanate metamaterials. J Am Ceram Soc 2016;99:3317–24. https://doi.org/10.1111/jace.14353.

[382] Chen HT, Soh AK. Influence of flexoelectric effects on multiferroic nanocomposite thin bilayer films. J Appl Phys 2012;112. https://doi.org/10.1063/1.4757013.

[383] Poddar S, de Sa P, Cai R, Delannay L, Nysten B, Piraux L, et al. Room-temperature magnetic switching of the electric polarization in ferroelectric nanopillars. ACS Nano 2018. https://doi.org/10.1021/acsnano.7b07389.
[384] Zhang C, Zhang L, Shen X, Chen W. Enhancing magnetoelectric effect in multiferroic composite bilayers via flexoelectricity. J Appl Phys 2016;119. https://doi.org/10.1063/1.4945107.
[385] Pan Q, Fang C, Luo H, Chu B. Magnetoelectric response from the enhanced ferromagnetism and flexoelectric response in reduced $BiFeO_3$–based ceramics. J Eur Ceram Soc 2019;39:1057–64. https://doi.org/10.1016/j.jeurceramsoc.2018.12.045.
[386] Patel S, Chauhan A, Cuozzo J, Lisenkov S, Ponomareva I, Vaish R. Pyro-paraelectric and flexocaloric effects in barium strontium titanate: a first principles approach. Appl Phys Lett 2016;108:162901. https://doi.org/10.1063/1.4947010.
[387] Bai G, Liu Z, Xie Q, Guo Y, Li W, Yan X. The flexoelectric effect associated size dependent pyroelectricity in solid dielectrics. AIP Adv 2015;5:097117. https://doi.org/10.1063/1.4930595.
[388] Patel S, Chauhan A, Madhar NA, Ilahi B, Vaish R. Flexoelectric induced caloric effect in truncated pyramid shaped $Ba_{0.67}Sr_{0.33}TiO_3$ ferroelectric material. J Electron Mater 2017;46:4166–71. https://doi.org/10.1007/s11664-017-5362-7.
[389] Qiu Y, Wu H, Wang J, Lou J, Zhang Z, Liu A, et al. Giant electrocaloric effect in ferroelectric ultrathin films at room temperature mediated by flexoelectric effect and work function. J Appl Phys 2017;122. https://doi.org/10.1063/1.4992811.
[390] Starkov AS, Starkov IA. Giant piezocaloric effect in PZT ceramic film. Ferroelectrics 2015;483:102–7. https://doi.org/10.1080/00150193.2015.1059147.
[391] Starkov AS, Starkov IA. Impact of the flexocaloric effect on polarization in the flexoelectric layer. Int J Solids Struct 2015;82:65–9. https://doi.org/10.1016/j.ijsolstr.2015.12.013.
[392] Starkov IA, Starkov AS. A generalized thermodynamic theory of the multicaloric effect in single-phase solids. Int J Solids Struct 2016;100–101:187–94. https://doi.org/10.1016/j.ijsolstr.2016.08.015.
[393] Starkov AS, Starkov IA. Multicaloric effect in a solid: new aspects. J Exp Theor Phys 2014;119:258–63. https://doi.org/10.1134/S1063776114070097.
[394] Lukashev P, Sabirianov RF. Flexomagnetic effect in frustrated triangular magnetic structures. Phys Rev B - Condens Matter Mater Phys 2010;82:2–7. https://doi.org/10.1103/PhysRevB.82.094417.
[395] Hertel R. Curvature-induced magnetochirality. Spin 2013;03:1340009. https://doi.org/10.1142/S2010324713400092.
[396] Kvashnin AG, Sorokin PB, Yakobson BI. Flexoelectricity in carbon nanostructures: nanotubes, fullerenes, and nanocones. J Phys Chem Lett 2015;6:2740–4. https://doi.org/10.1021/acs.jpclett.5b01041.
[397] Martin JW, Slavchov RI, Yapp EKY, Akroyd J, Mosbach S, Kraft M. The polarization of polycyclic aromatic hydrocarbons curved by pentagon incorporation: the role of the flexoelectric dipole. J Phys Chem C 2017;121:27154–63. https://doi.org/10.1021/acs.jpcc.7b09044.
[398] Nonnenmann SS, Leaffer OD, Gallo EM, Coster MT, Spanier JE. Finite curvature-mediated ferroelectricity. Nano Lett 2010;10:542–6. https://doi.org/10.1021/nl903384p.
[399] Ortix C, Kiravittaya S, Schmidt OG, Van Den Brink J. Curvature-induced geometric potential in strain-driven nanostructures. Phys Rev B - Condens Matter Mater Phys 2011;84:1–5. https://doi.org/10.1103/PhysRevB.84.045438.
[400] Yu L, Ruzsinszky A, Perdew JP. Bending two-dimensional materials to control charge localization and fermi-level shift. Nano Lett 2016;16:2444–9. https://doi.org/10.1021/acs.nanolett.5b05303.
[401] Zelisko M, Hanlumyuang Y, Yang S, Liu Y, Lei C, Li J, et al. Anomalous piezoelectricity in two-dimensional graphene nitride nanosheets. Nat Commun 2014;5:1–7. https://doi.org/10.1038/ncomms5284.
[402] Yin B, Qu S. An ab initio investigation of flexoelectric effect in ultrathin $BaTiO_3$ nanotubes. J Appl Phys 2014;115:1–5. https://doi.org/10.1063/1.4866355.
[403] Brennan CJ, Ghosh R, Koul K, Banerjee SK, Lu N, Yu ET. Out-of-plane electromechanical response of monolayer molybdenum disulfide measured by piezo-response force microscopy. Nano Lett 2017;17:5464–71. https://doi.org/10.1021/acs.nanolett.7b02123.
[404] Chandratre S, Sharma P. Coaxing graphene to be piezoelectric. Appl Phys Lett 2012;100. https://doi.org/10.1063/1.3676084.
[405] Duerloo KAN, Reed EJ. Flexural electromechanical coupling: a nanoscale emergent property of boron nitride bilayers. Nano Lett 2013;13:1681–6. https://doi.org/10.1021/nl4001635.
[406] Ilina MV, Blinov YF, Ilin OI, Rudyk NN, Ageev OA. Piezoelectric effect in non-uniform strained carbon nanotubes. IOP Conf Ser Mater Sci Eng 2017;256. https://doi.org/10.1088/1757-899X/256/1/012024.
[407] Jin H-J, Yoon WY, Jo W. Virtual out-of-plane piezoelectric response in MoS_2 layers controlled by ferroelectric polarization. ACS Appl Mater Interfaces 2018;10:1334–9. https://doi.org/10.1021/acsami.7b14001.
[408] Kundalwal SI, Meguid SA, Weng GJ. Strain gradient polarization in graphene. Carbon N Y 2017;117:462–72. https://doi.org/10.1016/j.carbon.2017.03.013.
[409] Narvaez J, Vasquez-Sancho F, Catalan G. Enhanced flexoelectric-like response in oxide semiconductors. Nature 2016;538:219–21. https://doi.org/10.1038/nature19761.
[410] Vales-Castro P, Roleder K, Zhao L, Li J-FF, Kajewski D, Catalan G. Flexoelectricity in antiferroelectrics. Appl Phys Lett 2018;113:132903. https://doi.org/10.1063/1.5044724.
[411] Vasquez F, Abdollahi A, Damjanovic D, Catalan G, Rica C, Vasquez-Sancho F, et al. Flexoelectricity in bones. 1705316 Adv Mater2018. https://doi.org/10.1002/adma.201705316.
[412] Kang H, Hou Z, Qin QH. Experimental study of time response of bending deformation of bone cantilevers in an electric field. J Mech Behav Biomed Mater 2018;77:192–8. https://doi.org/10.1016/j.jmbbm.2017.09.017.
[413] Kalinin SV, Jesse S, Liu W, Balandin AA. Evidence for possible flexoelectricity in tobacco mosaic viruses used as nanotemplates. Appl Phys Lett 2006;88:10–3. https://doi.org/10.1063/1.2194008.
[414] Breneman KD, Brownell WE, Rabbitt RD. Hair cell bundles: flexoelectric motors of the inner ear. PLoS ONE 2009;4. https://doi.org/10.1371/journal.pone.0005201.
[415] Breger L, Furukawa T, Fukada E. Bending piezoelectricity in polyvinylidene fluoride. Jpn J Appl Phys 1976;15:2239–40. https://doi.org/10.1143/JJAP.15.2239.
[416] Baskaran S, He X, Chen Q, Fu JY. Experimental studies on the direct flexoelectric effect in α -phase polyvinylidene fluoride films. Appl Phys Lett 2011;98. https://doi.org/10.1063/1.3599520.
[417] Baskaran S, He X, Wang Y, Fu JY. Strain gradient induced electric polarization in -phase polyvinylidene fluoride films under bending conditions. J Appl Phys 2012;111. https://doi.org/10.1063/1.3673817.
[418] Poddar S, Ducharme S. Temperature dependence of flexoelectric response in ferroelectric and relaxor polymer thin films. J Appl Phys 2014;116. https://doi.org/10.1063/1.4895988.
[419] Poddar S, Foreman K, Adenwalla S, Ducharme S. Finite-size scaling of flexoelectricity in Langmuir-Blodgett polymer thin films. Appl Phys Lett 2016;108:012908. https://doi.org/10.1063/1.4939687.
[420] Zhou Y, Liu J, Hu X, Chu B, Chen S, Salem D. Flexoelectric effect in PVDF-based polymers. IEEE Trans Dielectr Electr Insul 2017;24:727–31. https://doi.org/10.1109/TDEI.2017.006273.
[421] Kang S, Kim S, Jeon S, Jang WS, Seol D, Kim YMY, et al. Atomic-scale symmetry breaking for out-of-plane piezoelectricity in two-dimensional transition metal dichalcogenides. Nano Energy 2019;58:57–62. https://doi.org/10.1016/j.nanoen.2019.01.025.
[422] Hu G, Wu JJZ, Ma C, Liang Z, Liu W, Liu M, et al. Controlling the Dirac point voltage of graphene by mechanically bending the ferroelectric gate of a graphene field effect transistor. Mater Horizons 2019;6:302–10. https://doi.org/10.1039/c8mh01499j.